

Modelling multicomponent solute transport in structured soils

Promotor: Prof. dr W.H. van Riemsdijk,
Hoogleraar in de Bodemscheikunde en Chemische
Bodemkwaliteit, Wageningen Universiteit

Co-promotor: Dr. ir. J.C.L. Meeussen,
Wetenschappelijk medewerker, Energieonderzoek Centrum
Nederland (ECN), Petten

Samenstelling promotiecommissie:
Prof. dr. P.C. de Ruiter, Universiteit Utrecht
Prof. dr. ir. S.E.A.T.M. van der Zee, Wageningen Universiteit
Dr. J. Griffioen, NITG-TNO, Utrecht
Prof. W. Davison, Universiteit van Lancaster, Engeland

Dit onderzoek is uitgevoerd binnen de onderzoekschool WIMEK/SENSE.

Modelling multicomponent solute transport in structured soils

Wendy van Beinum

Proefschrift
ter verkrijging van de graad van doctor
op gezag van de rector magnificus
van Wageningen Universiteit,
Prof. dr. M.J. Kropff,
in het openbaar te verdedigen
op vrijdag 5 januari 2007
des namiddags te half twee in de Aula.

van Beinum, W.

Modelling multicomponent solute transport in structured soils.

PhD-thesis Wageningen University, Wageningen, the Netherlands 2007. - With references. - With summary in English and Dutch.

ISBN 90-8504-570-3

Abstract

Van Beinum, W., 2007. **Modelling multicomponent solute transport in structured soils.** PhD-thesis, Wageningen University. Wageningen, The Netherlands, 176 p.

The risks for soil contaminants to spread into the environment and to reach ground and surface water are determined by a combination of physical and chemical processes. In this thesis the combined effects of multicomponent chemistry, diffusion-limited sorption and reactive transport are studied by process-based modelling and experimental studies. Transport processes were studied in experiments with physically and chemically well-defined column systems. The chemical complexity of the experimental system was gradually increased from inert to adsorbing substances and the process descriptions in the transport model were adjusted accordingly. First, nitrate transport through a column filled with spherical alginate-gel beads was simulated with a two-region model that accounts for ion diffusion into the stagnant water inside the gel. Then the model was extended for transport of protons that interact with alginate gel by an ion-exchange mechanism. Subsequently, the model was extended with a surface complexation model (CD-MUSIC) to describe transport of interacting substances, sulphate and chromate transport through a column with goethite immobilised in polyacrylamide gel beads. The results show that a combination of multicomponent chemistry, diffusion-limited sorption and transport can be modelled by combining mechanistic process descriptions. The effects of diffusion-limited sorption and multicomponent chemistry on transport are discussed.

A novel modelling approach was developed to simulate the effect of the electrostatic potential on diffusion through micro-porous mineral particles. The internal surfaces of a mineral aggregate are charged and this can have a drastic effect on the concentrations of ions in the pore space. The Donnan-diffusion model describes diffusion as a function of the local concentration inside the pores (i.e. the Donnan concentration) and the electrostatic potential using the Nerst-Planck diffusion equation. The influence of electrostatics on diffusion and sorption was demonstrated for strontium adsorption inside hydrous ferric oxide particles. The model was then used to describe strontium transport in a column filled with hydrous ferric oxide particles. This thesis demonstrates that mechanistic modelling provides valuable insights into the processes that are involved in multicomponent transport in soil systems.

Contents

1. Introduction	11
1.1. <i>Solute transport in soil</i>	13
1.2. <i>Transport models</i>	14
1.2.1. The homogeneous convection-dispersion equation (CDE)	14
1.2.2. Transport in structured soil	15
1.2.3. The mobile-immobile transport model	17
1.2.4. Two-region and diffusion models	17
1.3. <i>Sorption and transport</i>	19
1.4. <i>Controlled experiments</i>	23
1.5. <i>Numerical modelling in ORCHESTRA</i>	23
1.6. <i>Outline thesis</i>	25
2. Transport of ions in physically heterogeneous systems; convection and diffusion in a column filled with alginate gel beads, predicted by a two-region model	27
2.1. <i>Introduction</i>	29
2.2. <i>Diffusion of solutes in spherical beads</i>	32
2.2.1. Preparation of gel beads	32
2.2.2. Diffusion experiments	32
2.2.3. Diffusion model	33
2.3. <i>Transport processes in a column with gel beads</i>	35
2.3.1. Column experiments	35
2.3.2. Transport model	35
2.4. <i>Results and discussion</i>	37
2.4.1. Diffusion experiments and modelling	37
2.4.2. Column experiments and modelling	38
2.5. <i>Conclusions</i>	42
3. Modelling transport of protons and calcium ions in an alginate gel bead system: The effects of physical nonequilibrium and nonlinear competitive sorption	43
3.1. <i>Introduction</i>	45
3.2. <i>Material and methods</i>	47
3.2.1. Preparation of the beads	47
3.2.2. Flow experiments	49
3.2.3. Sorption model	49
3.2.4. Transport Model	52
3.3. <i>Results</i>	54

4. Competitive sorption and diffusion of chromate and sulphate in a flow system with goethite in gel beads	63
4.1. <i>Introduction</i>	65
4.2. <i>Material and methods</i>	66
4.2.1. Preparation of the goethite-gel beads	67
4.2.2. Sorption model	69
4.2.3. Experiments	70
4.2.4. Transport model	74
4.3. <i>Results and discussion</i>	75
4.3.1. Sorption isotherms	75
4.3.2. Tracer experiments	77
4.3.3. Breakthrough curves of sulphate and chromate	79
4.3.4. Competition between sulphate and chromate	83
4.4. <i>Conclusions</i>	85
5. Sorption kinetics of strontium in porous hydrous ferric oxide aggregates. I. The Donnan diffusion model	87
5.1. <i>Introduction</i>	89
5.2. <i>Methods</i>	92
5.2.1. Surface complexation model	92
5.2.2. Donnan electrostatic model	95
5.2.3. Donnan diffusion model	96
5.2.4. Free pore diffusion model	100
5.2.5. Comparison of apparent diffusion rates	101
5.2.6. Simplified approximations for apparent diffusion coefficients	103
5.3. <i>Results</i>	104
5.3.1. Equilibrium sorption and pore concentrations	104
5.3.2. Diffusion simulations	106
5.3.3. Effects of pH on pore diffusion	109
5.4. <i>Conclusions</i>	111
6. Sorption kinetics of strontium in porous hydrous ferric oxide aggregates. II. Comparison of experimental results and model predictions	113
6.1. <i>Introduction</i>	115
6.2. <i>Materials and Methods</i>	116
6.2.1. Hydrous ferric oxide	116
6.2.2. Proton and Sr sorption to HFO	117
6.2.3. Surface complexation modeling	118
6.2.4. Column experiments	120

6.2.5. Column geometry and hydrodynamic parameters	122
6.2.6. The Donnan diffusion model	125
6.3. <i>Results</i>	127
6.3.1. Proton and Strontium sorption	127
6.3.2. Pore accessibility of the HFO aggregates	130
6.3.3. Strontium breakthrough curves	132
6.4. <i>Discussion</i>	137
6.5. <i>Conclusion</i>	140
7. Epilogue	141
7.1. <i>Modelling solute transport in soils</i>	143
7.2. <i>Well-defined experimental systems</i>	144
7.3. <i>Solute transport in multicomponent systems</i>	145
7.4. <i>The Donnan-diffusion model</i>	145
7.5. <i>Conclusions</i>	146
8. References	149
Appendix 1. Proton sorption by calcium alginate beads	161
Appendix 2. Derivation of multicomponent diffusion equation	163
Summary	165
Samenvatting	169
Curriculum Vitae	173
Publications	173
Final word	175

1. Introduction

Nomenclature

α	mass transfer coefficient	s^{-1}
θ	water content of the soil (volume fraction)	-
θ_{im}	volume fraction of immobile pore water	-
θ_m	volume fraction of mobile pore water	-
ρ	bulk density of the soil	$kg\ m^{-3}$
C	dissolved concentration in soil solution	$mol\ m^{-3}$
C_{im}	dissolved concentration in immobile region	$mol\ m^{-3}$
C_m	dissolved concentration in mobile region	$mol\ m^{-3}$
D	dispersion-diffusion coefficient	m^2s^{-1}
D_e	effective diffusion coefficient	m^2s^{-1}
D_m	dispersion-diffusion coefficient in mobile region	m^2s^{-1}
f	fraction of soil associated with the mobile region	-
K_d	linear sorption coefficient	m^3kg^{-1}
K_F	Freundlich sorption coefficient	$(mol\ kg^{-1})(mol\ L^{-1})^{-n}$
K_L	Langmuir sorption coefficient	m^3kg^{-1}
n	Freundlich exponent	-
r	radial distance	m
R	retardation coefficient	-
S	adsorbed concentration in soil	$mol\ kg^{-1}$
S_{im}	adsorbed concentration in immobile region	$mol\ kg^{-1}$
S_m	adsorbed concentration in mobile region	$mol\ kg^{-1}$
S_{max}	maximum sorption capacity	$mol\ kg^{-1}$
t	time	s
v_m	average flow velocity in the mobile pore region	$m\ s^{-1}$
v_p	average flow velocity in the pores	$m\ s^{-1}$
x	distance	m

1.1. Solute transport in soil

The environmental impacts of soil contaminants are strongly affected by the mobility of the contaminants in soil. Transport processes can lead to spreading of soil contaminants into the wider environment via several different routes such as volatilisation, erosion or ground water flow. For inorganic contaminants and a large group of organic contaminants, the main transport route within soil is dissolution and subsequent movement with water. Leaching of water down the soil profile enables transport of dissolved chemicals (solutes) towards ground and surface water and may lead to contamination of surface waters and drinking water supplies. Therefore, a high mobility of contaminants in the environment is generally undesirable. Gaining a better understanding of the processes involved in contaminant transport allows more accurate estimations of potential contaminant concentrations in surface water and groundwater. This knowledge can be used to improve development of soil protection legislation and to underpin soil quality standards. Better understanding of transport processes can also help to evaluate potential soil remediation scenarios.

Many contaminants are mobile in the soil environment because they are soluble in water. In soil and other porous media, the distribution of chemicals between the mobile water phase and the stationary solid phase determines the relative mobility of substances. This distribution is determined by interaction of dissolved substances with the soil solid matrix. Chemical sorption is an important interaction process and is therefore one of the main factors that control the mobility of chemicals in soils. Substances that are strongly bound by soil solid particles are much less mobile and therefore have a greatly reduced potential to spread into the environment or to reach ground or surface water.

Chemical interactions between dissolved substances and the solid phase are generally multi-component processes that are affected by the concentration of the chemical in solution, the soil pH and the presence of other chemicals. The chemical composition of the solution affects the surface chemistry and sorption behaviour of soil particles. This may result in either enhanced sorption through collaboration or poorer adsorption due to competition between substances. Therefore, the sorption behaviour of a substance is not simply a function of the concentration of this single substance (component), but of the complete set of substances that makes up the soil solution (multi-component).

1. Introduction

Simple empirical sorption models that do not take into account these interaction processes, for example models that describe sorption as a linear function of the concentration in solution, will not be able to accurately describe transport of reactive solutes in soil for a wide range of conditions. Such sorption models are only valid for conditions in which the relationship was established, and lack predictive value for other conditions. Also, because purely empirical models are not based on a mechanistic theory, it is difficult to use empirical models to contribute to the understanding of mechanisms for chemical sorption and the potentially controlling factors for transport. More mechanistic complexation models that account for the multi-component nature of sorption mechanisms have made significant progress over recent years. Sorption studies on specific soil constituents have shown that these models possess good predictive value under varying conditions.

This thesis focuses on the modelling of chemical sorption and transport, using the latest mechanistic surface complexation models. The aim is to test the performance of mechanistic sorption models in combination with transport modelling to predict multi-component transport of substances. Mechanistic sorption models and transport models are combined and validated against measurements from controlled transport experiments.

1.2. Transport models

Transport processes in soil occur at different spatial scales. At the scale of individual particles and the pores between them (the micro-scale), transport processes take place over very short distances where diffusion is the dominating transport process. Diffusion is important for instance for the transport of nutrients towards micro-organisms or plant roots, or diffusion into soil aggregates and sorbent particles. At the scale of a soil profile (the macro-scale), transport takes place over greater distances where convection and dispersion become relatively more important. This is the case for chemicals that leach from the soil surface to the groundwater. In macro-scale models, the soil is usually assumed to be a homogeneous mixture of soil and pore space. Under this assumption water flows through the soil at an equal and uniform flow rate, and dissolved chemicals (solutes) can interact directly with soil particles.

1.2.1. The homogeneous convection-dispersion equation (CDE)

The most common model that describes solute transport by convection and dispersion is the convection-dispersion equation (CDE). This equation describes

the change in concentration at any point along the flow path as a function of time (Equation 1.1). The left hand side of the equation expresses the change in the total concentration of chemical (mol m^{-3}), which is the sum of the dissolved and adsorbed concentrations. The right hand side of the equation expresses the contributions of convection and dispersion to the change in total concentration.

$$\theta \frac{\partial C}{\partial t} + \rho \frac{\partial S}{\partial t} = -\theta v_p \frac{\partial C}{\partial x} + \theta D \frac{\partial^2 C}{\partial x^2} \quad [1.1]$$

in which C is the concentration in solution (mol m^{-3}) and S is the amount adsorbed (mol kg^{-1}) as a function of time (t) and distance (x). D is the effective dispersion coefficient ($\text{m}^2 \text{s}^{-1}$), v_p is the flow rate in the pores (m s^{-1}) and θ is the water-filled soil porosity. The effective dispersion coefficient describes the broadening of the concentration front by molecular diffusion and hydrological dispersion. Diffusion is the spreading of the front caused by the concentration gradient and dispersion is a mixing effect caused by flow around the soil particles. At higher flow rates, the effect of diffusion becomes negligible and the concentration front is affected by hydrological dispersion only.

1.2.2. Transport in structured soil

The classical CDE model assumes a uniform flow rate through the pores and a homogeneous pore space. Sorption is assumed instantaneous at equilibrium with the concentration in the flowing water. In reality however, soils are not homogenous but structured with a complex network of macro-, meso- and micropores. Water flow is faster through the larger water-filled pores. During heavy rainfall, water flows down the soil profile via preferential flow paths, such as root and worm channels, macropores and cracks. In this way, solutes can be transported rapidly down the soil profile and bypass the bulk of the soil. Water inside smaller pores, for example inside aggregates or soil peds, is less mobile or immobile. Chemicals inside these immobile regions are protected from leaching. The exchange of solutes between the immobile water and the flowing water is controlled by diffusion. This phenomenon is referred to as physical nonequilibrium or transport nonequilibrium. It has been observed in aggregated soils, macroporous and fractured porous media, at the field scale, in undisturbed soil cores and in packed columns (reviews by Brusseau and Rao, 1990; Brusseau, 1994).

Transport models that consider the soil as homogeneous are often not able to describe transport in structured soils. For many soils, the transport of a chemical through the soil is faster than would be predicted by a homogeneous transport

1. Introduction

model. The moment of breakthrough, which is the moment the chemical reaches a certain depth in the profile, or a drain, or the outlet of a soil column, is earlier than expected. In addition, the complete leaching takes much longer than expected. This is evident by the ‘tailing’ of the leached concentration.

Figure 1.1 shows examples of so-called breakthrough curves for a nonreactive solute, which is a solute that does not adsorb onto the soil. A breakthrough curve shows the concentration in the soil solution at a certain travelled distance or depth, plotted against time or leached volume. In Figure 1.1 the concentration is plotted against the total number of pore volumes that has been leached. A nonreactive chemical would appear as soon as the pore volume of the soil is replaced once by the infiltrating solution, which is after one pore volume on the x-axis. The breakthrough curve is symmetrical when flow is homogenous. Dispersion causes the front to be sloped but the front stays symmetrical around one pore volume. Nonequilibrium transport on the other hand is characterised by an early breakthrough and tailing. The first breakthrough of the chemical occurs when the mobile water in the larger pores has been replaced. This is followed by a tail, which is caused by the delay due to diffusion into the stagnant water. The intensity of the effect depends on the flow rate, as shown in Figure 1.1. Tailing is more extensive at higher flow rates than at low flow rates because more time is available

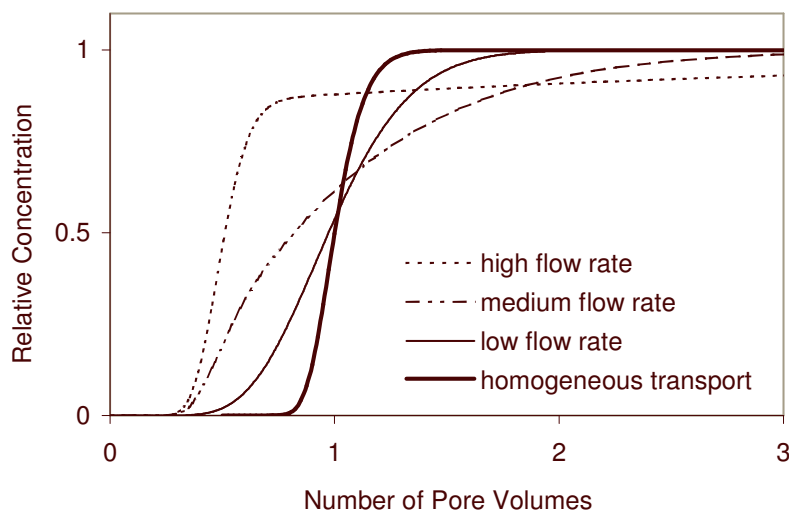


Figure 1.1. Typical nonequilibrium breakthrough curves at different flow rates, together with an equilibrium breakthrough curve for homogeneous transport. The nonequilibrium effect is stronger at higher flow rates.

for diffusion into the immobile water at low flow rates. At very low flow rates, transport becomes effectively homogeneous.

1.2.3. The mobile-immobile transport model

A mobile-immobile transport model is often used to describe nonequilibrium transport in soil. The total pore volume of the soil is divided into a mobile and an immobile pore region, with mobile and immobile (stagnant) water. Solutes are transported by convection with the water flow in the mobile region and diffusive mass-transfer between the mobile and immobile regions. The approach of mobile and immobile regions was proposed by Deans (1963), and further developed by Coats and Smith (1964), Passioura (1971) and Van Genuchten and Wierenga (1976). Solute transport of a nonreactive solute is described by convection and dispersion in the mobile region:

$$\theta_{im} \frac{\partial C_{im}}{\partial t} + \theta_m \frac{\partial C_m}{\partial t} = -\theta_m v_m \frac{\partial C_m}{\partial x} + \theta_m D_m \frac{\partial^2 C_m}{\partial x^2} \quad [1.2]$$

where θ_m and θ_{im} are volume fractions of the soil taken by the mobile and immobile pore water, and C_{im} and C_m are the solute concentrations in the immobile and mobile region respectively (mol m^{-3}), v_m is the pore water velocity in the mobile region (m s^{-1}) and D_m is the dispersion coefficient for transport in the mobile region ($\text{m}^2 \text{s}^{-1}$). Mass-transfer between the mobile and immobile region is described by:

$$\frac{\theta_{im}}{\theta} \frac{\partial C_{im}}{\partial t} = \alpha (C_{im} - C_m) \quad [1.3]$$

where α is the mass transfer coefficient between the mobile and immobile region (s^{-1}). The two-region model is the simplest description of a nonuniform flow system. In this model, the variation in pore size and flow rates is reduced to two distinct regions, a mobile and immobile region. Despite its simplicity the model has been proven a very successful tool for describing nonideal transport in aggregated soils and cracked clay soils (Brusseau and Rao, 1990). However, the model assumes that all of the stagnant phase is well mixed and equally accessible for solutes in the mobile phase. It does not account for concentration gradients within the aggregates and how these change with time and loading of the particles.

1.2.4. Two-region and diffusion models

A more mechanistic approach is to model diffusion into and within the immobile water region explicitly according to Ficks law. The immobile water is likely

1. Introduction

situated inside aggregates or soil peds and therefore solutes would diffuse through the aggregate pores to reach the interior of the soil ped or aggregate. Rao et al (1980a) used the mobile-immobile model to describe transport through a column with aggregates, whereby diffusion into the aggregates was described by radial diffusion. The model assumes that the aggregates are spherical and uniform in size and composition. Diffusion is calculated from Fick's second law of diffusion:

$$\frac{\partial C_{im}}{\partial t} = D_e \left(\frac{\partial^2 C_{im}}{\partial r^2} + \frac{2}{r} \frac{\partial C_{im}}{\partial r} \right) \quad [1.4]$$

in which D_e is the effective diffusion coefficient (m^2s^{-1}), r is the radial distance from the centre of the sphere.

Several relationships have been developed between the different models. In systems with a lesser degree of nonequilibrium (i.e. where diffusion is relatively fast compared to flow, so the system is close to equilibrium), the breakthrough curves are symmetrical and can be described by the CDE model (Equation 1.1). The enhanced dispersion can be described by the use of a lumped dispersion coefficient (D) that accounts for hydrodynamic dispersion and the additional effect of diffusion into the immobile water. Passioura (1971) derived the following relationship:

$$D = \frac{\theta_m}{\theta} D_m + \frac{\theta_{im}}{\theta} \frac{a^2 v_m^2}{15 D_e} \quad [1.5]$$

in which D_m is the hydrodynamic dispersion coefficient in the mobile region (m^2s^{-1}) and a is the radius of the spherical aggregates (m). Similar relationships have been derived by Van Genuchten and Dalton (1986) and Parker and Valocchi (1986) for rectangular and cylindrical geometry. This relationship shows that fitting the CDE (Equation 1.1) to a nonequilibrium breakthrough curve would largely overestimate the hydrodynamic dispersion in the system. This was for example observed by De Smedt and Wierenga (1984), Ma and Selim (1995) and Koch and Fluhler (1993).

The relationship between the diffusion coefficient (Equation 1.4) and the mass transfer coefficient α (Equation 1.3) for diffusion into a sphere was derived by Parker and Valocchi (1986):

$$\alpha = \frac{15 D_e \theta_{im}}{a^2} \quad [1.6]$$

The relationship is valid for systems that are not too far from equilibrium. Over the full diffusion period, α is time dependent. Rao et al. (1980a) derived a time-averaged estimate for α similar to Equation 1.6, in which the constant 15 is replaced by a variable depending on the residence time in the column or soil profile.

One drawback of the mass-transfer model is that the parameter α , derived from the aggregate dimensions, does not always give a good prediction of the breakthrough curves. The parameter has been found to increase with flow rate (e.g. De Smedt and Wierenga, 1984). Also the definition of the mobile and immobile fraction of a system is arbitrary. Several suggestions for how to estimate the mobile fraction have been made, such as using the moisture tension curves (e.g. Jarvis et al., 1991), or by resin casting of the macro-pores (Singh et al., 1991). However, when curve fitting is used, the immobile fraction that best fits the breakthrough curves seems to vary with the flow rate. Nevertheless, the mobile-immobile model has proven to be a valuable tool for modelling nonideal transport. In contrast with more complex models, the model only needs two additional parameters over the classical CDE. In many cases, models with additional parameters did not improve the description of the breakthrough curves and often the mobile-immobile model was superior over other model approaches.

1.3. Sorption and transport

The effect of sorption on transport can be taken into account in different ways. In the simplest case, sorption is assumed linear. The sorption isotherm is linear if the ratio between the adsorbed and dissolved concentrations is constant, i.e. independent of the concentration. Sorption is then described with the sorption constant K_d .

$$S = K_d C \quad [1.7]$$

Under the assumption of linear adsorption, sorption can be accounted for in the CDE. The amount of adsorption (S) can be substituted by $K_d C$, and the CDE (Equation 1.1) can be rewritten as:

$$(\theta + \rho K_d) \frac{\partial C}{\partial t} = -\theta v_p \frac{\partial C}{\partial x} + \theta D \frac{\partial^2 C}{\partial x^2} \quad [1.8]$$

The rate at which the concentration front moves through the soil is then retarded in comparison with the flow rate of water and of nonreactive solutes. This retardation delay is expressed by the retardation factor:

1. Introduction

$$R = \frac{\theta + \rho K_d}{\theta} = 1 + \frac{\rho}{\theta} K_d \quad [1.9]$$

Chemical sorption in soil is usually not linear with concentration but relatively higher ratios are adsorbed at lower concentrations than at higher concentrations, resulting in a so-called convex sorption isotherm. Most commonly used sorption models are the Freundlich and the Langmuir equation. The Freundlich equation describes a convex sorption isotherm for Freundlich exponents (n) smaller than zero:

$$S = K_F C^n \quad [1.10]$$

When only a limited amount of sorption sites is available for sorption, sorption approaches a sorption maximum (S_{max}). This behavior is described by a Langmuir equation:

$$S = S_{max} \frac{K_L C}{1 + K_L C} \quad [1.11]$$

In case of non-linear adsorption, retardation is not constant but concentration dependent. At low concentrations, relatively more sorption takes place with a small increase in concentration than at a high concentration because the sorption curve is steeper at low concentrations. Therefore low concentrations are more retarded than high concentrations. This behaviour causes concentration fronts that are self-sharpening during adsorption, but increasingly diffuse during desorption. In case of adsorption, the concentration front remains sharp because any solute that advances the concentration front will be more strongly retarded than the concentration front itself. The retardation factor of the sorption front can be calculated by replacing the K_d in Equation 1.9 by the ratio $\Delta S/\Delta C$, the ratio between the increase in sorption and increase in concentration in the soil column. For the desorption front we cannot identify a constant retardation factor. Because the lower concentrations are more retarded, the elution front will become increasingly diffuse during transport. The breakthrough curve will show tailing as the lower concentrations that leach out towards the end are most strongly retarded.

The mobile-immobile model (Equations 1.2 and 1.3) can be extended to describe mobile-immobile transport of reactive solutes. S_m and S_{im} are included to describe the sorbed concentrations in the mobile and immobile regions of the soil. An additional parameter is introduced to describe the fraction of soil associated with the mobile region (f). The modified transport equation becomes:

$$\theta_{im} \frac{\partial C_{im}}{\partial t} + \theta_m \frac{\partial C_m}{\partial t} + f \rho \frac{\partial S_m}{\partial t} + (1-f) \rho \frac{\partial S_{im}}{\partial t} = -\theta v_m \frac{\partial C_m}{\partial x} + \theta D_m \frac{\partial^2 C_m}{\partial x^2} \quad [1.12]$$

$$\theta_{im} \frac{\partial C_{im}}{\partial t} + (1-f) \rho \frac{\partial S_{im}}{\partial t} = \alpha (C_{im} - C_m) \quad [1.13]$$

Analytical solutions for Equations 1.12 and 1.13 have been derived by Van Genuchten and Wierenga (1976) and De Smedt and Wierenga (1984) for different initial and boundary conditions. Analytical solutions are however only available for linear sorption isotherms and for few specific cases of nonlinear isotherms. When sorption models are more complex, it is no longer possible to solve transport equations analytically.

When both transport processes and chemical interactions are considered, the system can easily become very complex. As discussed by Brusseau (1994), there are many factors that may cause nonideal transport behaviour of reactive chemicals. Additional to the physical causes of nonequilibrium transport (structural heterogeneity and variable flow), transport of reactive chemicals may also be influenced by nonlinear sorption, multicomponent effects, transformation reactions, rate-limited sorption (sorption kinetics), and spatially variable sorption.

The effect of nonlinear sorption was already mentioned earlier: a concave sorption isotherm causes a sharpening of the intrusion curve and a tailing of the elution curve. This will alter the tailing caused by nonequilibrium transport. The tailing caused by nonequilibrium will be suppressed for the infiltration curve but intensified for the elution curve. Natural soil systems are multicomponent systems in which the presence of other chemicals may influence the sorption and transport of the studied chemical. Multicomponent effects occur when chemicals compete for interaction with the same solid phase (competitive sorption), by enhanced interaction with solid phase (cooperative sorption), or by the formation of solution complexes that interact less with the solid phase (solubilisation). Studies of nonequilibrium transport with multicomponent chemistry are most abundant with respect ion-exchange in aggregated clay soils (Selim et al., 1987; Mansell et al., 1988; Schulin et al., 1989; Gaston and Selim 1990; Selim et al., 1992). The studies showed that the transport phenomena could be simulated well with an ion-exchange model incorporated into the mobile-immobile transport model.

Rate-limited sorption and desorption cause leaching behaviour that is very similar to what is observed in case of mobile-immobile transport. It is not possible to distinguish between transport nonequilibrium and sorption nonequilibrium just by

1. Introduction

examining the breakthrough curve of a solute. Ma and Selim (1997) point out that under steady state water flow and linear sorption, the two-region model (Equations 1.2 and 1.3) can be expressed in the same dimensionless form as the two-site chemical nonequilibrium model. Modelling can elucidate the underlying processes, but only if model parameters can be estimated or measured independently. In many cases it is necessary to use a nonreactive tracer or multiple tracers to allow distinction between physical and chemical forms of nonequilibrium. A nonreactive tracer can confirm nonequilibrium caused by mobile-immobile transport and may be used to derive parameters for the mobile-immobile transport model. Transport of reactive solutes can then be simulated with the same parameters to confirm that mobile-immobile transport is the only reason for nonequilibrium transport. Nonreactive tracers can however only confirm physical nonequilibrium, not to rule out physical nonequilibrium for all other chemicals. Diffusion of reactive solutes is retarded because of sorption and it takes longer for a reactive solute than for a nonreactive tracer to reach equilibrium with the immobile phase. Therefore, if the breakthrough curve of a nonreactive solute does not exhibit physical nonequilibrium, transport of a strongly adsorbed chemical may still be affected. Especially if sorption occurs in porous sorbent particles that make up a small fraction of the soil, this may cause nonequilibrium transport of the reactive solutes, but will not affect transport of nonreactive solutes.

This thesis explores the combination of mobile-immobile transport with multicomponent chemistry. The CD-MUSIC model (Hiemstra and Van Riemsdijk, 1996) describes sorption on oxide and hydroxide mineral surfaces in soils. The model describes specific surface sites formed by the oxygen groups on the surface of the mineral (Hiemstra et al., 1989). These groups can be positively or negatively charged depending on the degree of protonation. Solutes can bind onto these sites in two different ways, by forming outersphere or innersphere complexes. In an innersphere complex the solute approaches the surface more closely and one of the solutes ligands is replaced by the surface oxygen (ligand sharing). The variable surface charge causes an electric potential in the vicinity of the surface that affects the ion concentrations near the surface. The electrostatic behaviour is implemented using the Basic Stern model that describes the charge and electrostatic potential of a surface plane, a Helmholtz plane further away from the surface, and a diffuse double layer that starts at the Helmholtz plane and stretches into the bulk solution. The CD-MUSIC approach accounts for the effect of pH and ionic strength of the solution on sorption, as well as for competition between solutes during adsorption. It is not possible to include these processes in analytical approaches to transport

modelling without simplifications that would weaken the predictive qualities of the model.

1.4. Controlled experiments

To validate a combination of diffusion and multicomponent adsorption it is essential to use an experimental system with well-defined chemical and physical properties. As was mentioned earlier, it is not possible to clarify transport mechanisms based on observed experimental phenomena, unless model parameters can be independently obtained. Early studies into nonequilibrium transport used flow systems with well-defined mobile and immobile regions, by packing columns with uniformly sized porous spheres or aggregates. For example, Rose and Passioura (1971) used porous and non-porous glass beads to examine transport in aggregated media. Rao et al. (1980) used columns with ceramic spheres from kaolinite clay to represent soil aggregates. Other studies used uniform aggregate size fractions that were separated from loamy or clay soil through sieving (Nkedi Kizza et al., 1982; Selim et al., 1987) or by manual selection of stable aggregates (Hatano et al., 1993). The advantage of these systems is that all model parameters can be measured separately, such as the diameter, volume and porosity of the spheres, and the mobile-immobile water fractions. Equilibrium sorption can be measured in separate batch experiments with non-aggregated material or after long equilibration times and diffusion in the spheres or aggregates can be tested with tracers in separate diffusion experiments. By extending the information about the system, the number of adjustable parameters in the model can be brought to a minimum.

In this thesis, we used a well-defined experimental system from gel beads. Spherical gel beads were made from open-structured hydrogel in which solutes can diffuse freely. Gel beads were packed in a column to create an idealised mobile-immobile system with immobile water inside the gel beads and mobile water in between the gel beads. The experimental system was extended by mixing synthetic ironoxide (goethite) with the gel to form a well-defined system for evaluating transport models with multicomponent chemistry.

1.5. Numerical modelling in ORCHESTRA

The transport models in this thesis were implemented in ORCHESTRA (Meeussen, 2003), a framework for chemical equilibrium and transport modelling. ORCHESTRA stands for Objects Representing CHEmical Speciation and TRANsport. A unique and useful feature of the programme is that the model

1. Introduction

definitions (the equations describing the chemistry and dynamic processes) are not defined within the source code of the executable, but can be given as input at run time. This makes it possible to store the model definitions in a database that can be accessed and altered by the user. The advantage is that the programme does not put any restriction on the choice of chemical models and transport equations, and new models can be implemented without adjustments of the source code.

Transport is calculated numerically by a mixing-cell transport algorithm. The soil system is divided into calculation cells, and transport between the cells is calculated at small time steps. Chemical equilibrium in each cell is calculated by iteration after every transport step. The advantage of a numerical method is that any combination of chemical models and transport equations can be solved, including the complex sorption models described above.

In ORCHESTRA, the number of calculation cells, their layout and the boundary conditions are user defined. The mobile-immobile flow system in this thesis was represented by a two-dimensional network of calculation cells (Fig. 1.2). One vertical row of cells represents the mobile water region. Convection is calculated in between these vertically connected cells. The additional cell at the top represents the feed solution that enters the system and the final cell at the bottom represents the outlet. These cells function as infinite source and sink for the system. Every mobile cell is connected to a row of ten horizontal cells that represent the immobile region. Diffusion into the immobile region is calculated horizontally. To calculate spherical diffusion, every horizontal row of immobile cells represents a sphere. Because spheres are symmetrical around their centre, radial diffusion can be solved as one-dimensional diffusion towards the sphere centre. The cell properties (volume, contact area between cells) are calculated for concentric layers with equal thickness from the geometry of a sphere.

Hydrological dispersion can be simulated directly, by calculating dispersion fluxes between the calculation cells for which convection is calculated, or indirectly, by using numerical dispersion. Numerical dispersion (or truncation error) is caused by using discrete calculation cells and average concentrations for each cell instead of a continuous gradient. Numerical dispersion gives a similar broadening of the breakthrough curves as hydrological dispersion and can therefore be used to our advantage. In mobile-immobile systems, the broadening of the curve caused by nonequilibrium effects is often much larger than the broadening caused by dispersion. In this thesis, hydrological dispersion was in most cases negligible because of the stronger nonequilibrium effects.

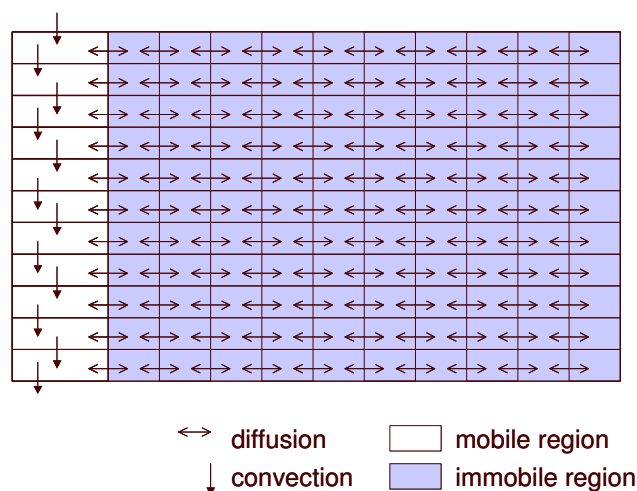


Figure 1.2. Diagram of the network of calculation cells that was used to simulate mobile-immobile transport with diffusion into spheres.

1.6. Outline thesis

Chapters 2 to 4 describe the development of a well-defined experimental system, to facilitate a detailed evaluation of the combination of multicomponent sorption and transport. The result is a technique in which sorptive materials are immobilised in spherical gel beads and used for evaluating multicomponent chemistry and transport processes.

Chapter 2 describes the development of the gel-beads system and the validation of a numerical mobile-immobile model. In Chapter 3 the combination of sorption and diffusion modelling is tested. The mobile-immobile model was extended to describe ion-exchange on the alginate gel, and used to predict transport of protons in a gel bead column. Chapter 4 considers competitive sorption of two anions on goethite. The CD-Music model was used to describe the pH dependent sorption of the anions on goethite. The combined modelling of competitive sorption and mobile-immobile transport was evaluated.

Chapter 5 and 6 present a novel diffusion model for diffusion and sorption of ions in charged microporous media. The model was developed to predict the influence of electrostatic surface effects on diffusion. The model is described and evaluated in comparison with a commonly used diffusion model in Chapter 5. In Chapter 6 the model was tested for strontium diffusion and sorption in columns with small microporous aggregates of hydrous ferric oxide (HFO).

2. Transport of ions in physically heterogeneous systems; convection and diffusion in a column filled with alginate gel beads, predicted by a two-region model

Wendy van Beinum, Johannes C.L. Meeussen, Anthony C. Edwards and
Willem H. van Riemsdijk

Water Research (2000), Vol. 34, No. 7, pp. 2043-2050.

2. Transport in physically heterogeneous systems

Nomenclature

a	bead radius	m
A	surface area between concentric cells in the model	m^2
C/C_0	(‘Relative concentration’) solute concentration relative to initial concentration and feed concentration	-
C_0	initial concentration in the column (in both regions)	mol m^{-3} or mol L^{-1}
C_f	solute concentration in the feed solution	mol m^{-3} or mol L^{-1}
C_g	solute concentration in the gel beads (batch system)	mol m^{-3} or mol L^{-1}
C_i	initial concentration in the gel beads (batch system)	mol m^{-3} or mol L^{-1}
C_m	solute concentration in the mobile solution	mol m^{-3} or mol L^{-1}
C_s	initial concentration in the bulk solution (batch system)	mol m^{-3} or mol L^{-1}
D	effective diffusion coefficient	$\text{m}^2 \text{s}^{-1}$
D^0	tracer or self-diffusion coefficient in water at infinite dilution	$\text{m}^2 \text{s}^{-1}$
J_D	mass flux caused by diffusion	$\text{mol m}^{-2} \text{s}^{-1}$
J_m	mass flux caused by convection	$\text{mol m}^{-2} \text{s}^{-1}$
L	column length	m
M.W.	molecular weight	-
m_D	diffusional mass transfer between cells	mol s^{-1}
m_m	convective mass transfer between cells	mol s^{-1}
M_t/M_∞	the released amount of solute divided by the amount released after infinite time	-
r	radial distance from bead centre	m
$S(x,t)$	source or sink term caused by diffusion into or out of the beads	$\text{mol m}^{-3} \text{s}^{-1}$
t	time	s
V/V_0	(‘Pore volumes’) cumulative number of pore volumes percolated through the column	-
V_0	total inner volume of the column	L
V_b	total volume of the beads in the column	L
v_m	flow velocity of the mobile solution in the column	m s^{-1}
V_m	total volume of the mobile solution in the column	L
x	depth in the column	m

2.1. Introduction

The mobility of solutes in soil is controlled by the movement of water through the soil and by interaction of the solute with the solid phase. Most soils are structured, they contain aggregates or pores with a range of sizes. In that case, the water movement cannot be described by one average flow velocity because soil water flows significantly faster in larger pores than in smaller pores. The soil water that is located in the small pores inside aggregates might even be considered effectively stagnant. Solute will migrate along with the movement of water through the large pores (convection), while diffusion into the stagnant solution causes retardation. This phenomenon is referred to as physical nonequilibrium or transport nonequilibrium (Brusseau and Rao, 1990). It causes an asymmetrical breakthrough curve for non-reactive chemicals: initial breakthrough occurs faster, and complete breakthrough takes much longer than would be expected in the case of a homogeneous soil. This effect, also named 'tailing', has been observed in transport studies with different types of structured media, such as: aggregated and fractured soils, soils with macro pores, root channels or earth worm channels, and soils with spatial variation in hydraulic conductivity (Brusseau and Rao, 1990).

There are different possible ways to describe this non-ideal behaviour in a transport model. An overview is given by Ma and Selim (1997). One of the most commonly used approaches is the two-region model, which is based on dividing the soil solution into a mobile and an immobile region. Transport takes place by convection and dispersion in the mobile region and by diffusion in the immobile region and across the interface between the two regions. This approach was also used by Rao et al. (1980), who successfully predicted solute transport in a column with porous ceramic beads. Although a two-region model simplifies the geometry of a soil considerably, it has been shown to give a good representation of the breakthrough of non-reactive solutes from an aggregated soil (Nkedi-Kizza et al., 1982). Rao et al. (1982) showed that the model can also be used for systems with non-spherical aggregates, and for a system with a range of aggregate sizes, using a weighted average radius. Two-region models have also been used to describe the transport of reactive solutes but to date, only relatively simple sorption models have been employed to describe the chemical behaviour of reactive solutes. With the development of more advanced multicomponent sorption models which describe the competitive interactions of solutes with soil components (Koopal et al., 1994; Hiemstra and Van Riemsdijk, 1996), it becomes appropriate to create a combined model capable of describing multicomponent transport in physically heterogeneous

2. Transport in physically heterogeneous systems

systems. The implementation of such an integrated model is made easier by a recently developed object oriented approach for computer transport modelling (Meeussen et al., 1996).

To enable experimental verification of this integrated transport model, a synthetic two-region flow system was developed in which a combination of physical and chemical processes can be simulated. The system consists of a column, filled with spherical alginate beads. The gel acts as a stagnant water phase in which solutes can only migrate by diffusion (see Figure 2.1). The physical properties of this system are defined by the dimensions of the column and beads, which can be determined independently. The two-region properties of this system are similar to the column filled with ceramic beads that was developed by Rao et al. (1980), but the gel system presented here offers significant advantages. Firstly, the alginate gel consists of more than 98% of water, so the pore water fraction can be assumed to be one, and there is no need to take a so-called tortuosity factor into account. Diffusion of small ions in the alginate gel is expected to be virtually equal to diffusion in pure water. This was shown to be the case for small proteins (M.W. $<2 \cdot 10^4$) by Tanaka et al. (1984). Diffusion in the gel can thus be predicted using reported diffusion coefficients for tracer diffusion in water (D^0) and does not require determination of effective diffusion coefficients in the beads from separate batch experiments. Furthermore, the technique to prepare Ca-alginate beads is fast and simple and beads can be formed with controlled and constant diameters. A further reason to use alginate gel beads is the application of alginate in related fields of research: Alginate beads are used for a range of different purposes, for example for the immobilisation of micro-organisms, for the uptake of heavy metals

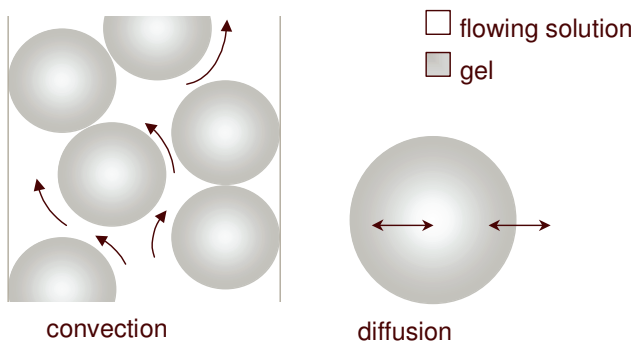


Figure 2.1. Transport processes in a column with gel beads: diffusion and convection.

from wastewater, or for the slow release of pesticides into soil. These applications reflect a wide range of possibilities given by the gel. Previous work has shown that the gel can be mixed with materials such as organic matter (Hatzinger and Alexander, 1997), clay minerals and oxides (Johnson and Pepperman, 1998). These materials are of major importance in soil chemistry and immobilisation in gel beads makes it possible to perform flow experiments with these soil components in columns. The chemical behaviour of most of these materials is studied intensively and described in sorption models. Flow experiments can be used to validate these chemical models in combination with the transport model. It is however also possible to perform reactive transport experiments with pure alginate beads, as alginate is capable of binding cations, such as protons and metal ions. The adsorption of Cu^{2+} -ions has for example been investigated by Jang et al. (1995). They showed that chemical interactions by alginate gel can be described by an extended Langmuir equation, that takes competition between ions into account. A column filled with pure alginate beads can therefore be used to test the incorporation of such an adsorption model in the transport model.

Before the system can be used for reactive transport experiments, the physical properties of the column with pure gel beads have to be verified. The main objectives of the present work are therefore,

- to test if the diffusion rate of non-reactive ions in the Ca-alginate gel is equal to that in pure water and if it can be predicted by a model describing Fickian diffusion in a sphere, and
- to test if the bead-filled column behaviour conforms an 'ideal' two-region system, in which solute transport can be described by convection in the mobile phase and diffusion in the gel phase.

The results of this study will also be of interest for other types of research that use the alginate gel beads in experimental work, for example research into the influence of nutrient availability on micro-organisms, or the immobilisation of heavy metals by alginate beads, cases in which diffusion could play a rate limiting role.

2. Transport in physically heterogeneous systems

2.2. Diffusion of solutes in spherical beads

2.2.1. Preparation of gel beads

An alginate solution (0.5%) was prepared by adding 0.5 g of sodium alginate (from *Macrocystis pyrifera*) to 100 mL demineralised water. The solution was stirred thoroughly and left overnight to avoid air bubbles. The gel beads were prepared according to Martinsen et al. (1989) by dripping the alginate solution into an aqueous solution of 0.2 M CaCl_2 . The gel drops solidify as soon as they enter the calcium chloride solution and form spherical beads. Each batch of beads was transferred to a fresh 0.2 M CaCl_2 solution, and allowed to stabilise for 24 hours. They were then washed with 10^{-3} M CaCl_2 solution and stored at 4°C. It was possible to adapt the bead size to a maximum diameter of approximately 4 mm by changing the size of the tubing end where the drops were formed. The size distribution of beads within a batch was found to be narrow, with a standard deviation of 0.07 mm for 4.32 mm beads. The average bead size for each experiment was calculated from the measured volume of the beads. The average bead diameters in the diffusion experiments with nitrate and phosphate respectively were approximately 4.32 and 4.06 mm. The alginate gel can slightly shrink or swell when the ionic strength or Ca^{2+} concentration change, therefore both were held constant during the experiments. The beads appeared perfectly spherical and homogeneous and were strong and stable under the experimental conditions applied.

2.2.2. Diffusion experiments

To study the diffusion of solutes in the alginate beads, the release of nitrate and phosphate from beads was measured in time. Nitrate or phosphate containing beads were added to a clean solution. The release of the solutes from the beads as a function of time was estimated from the increasing concentration in the solution. First the beads were equilibrated with either 0.01 M $\text{Ca}(\text{NO}_3)_2$ or $\text{Ca}(\text{H}_2\text{PO}_4)_2$ solution for five days, with the solution being replaced twice. Subsequently 100 beads were selected and excess solution was removed using absorbent paper. These beads were added to one litre 0.01 M CaCl_2 solution with solution samples taken every 20 seconds for at least 30 minutes. After sampling, the solution volume is still approximately 190 times larger than the bead volume, so the nitrate or phosphate concentration in the bulk solution remains very low. In the experiment with phosphate, both the chloride and the phosphate solutions used were brought to pH 4.4 by adding HCl solution. At this pH virtually all the phosphate exists in the

form H_2PO_4^- , which has a slightly different diffusion coefficient than HPO_4^{2-} (Li and Gregory, 1974). For the model calculations the diffusion coefficient of H_2PO_4^- was used. The concentrations of nitrate and phosphate in the samples were measured by spectrophotometric methods for analysing nitrate (Technicon Instruments, 1987) and for analysing phosphate (Murphy and Riley, 1962, modified) respectively.

2.2.3. Diffusion model

If we assume that the beads are perfectly spherical and physically homogeneous, radial diffusion of solutes in beads can be described using Fick's second diffusion law (Crank, 1956):

$$\frac{\partial C_g}{\partial t} = D \left(\frac{\partial^2 C_g}{\partial r^2} + \frac{2}{r} \frac{\partial C_g}{\partial r} \right) \quad [2.1]$$

where C_g stands for the solute concentration in mol m^{-3} , t is the time in seconds, r is the radial distance from the centre of the bead in meters and D is the apparent diffusion coefficient in m^2s^{-1} . The solution outside the beads is assumed to be perfectly mixed. Mass flow between a gel bead and the bulk solution is assumed to be controlled by diffusion only and assumed not to be restrained by the permeability of the bead surface or by a boundary layer. The system is defined by the following initial and boundary conditions:

$$C_g = C_i; \quad t = 0, 0 \leq r < a \quad [2.2]$$

$$C_g = C_s; \quad t = 0, r = a \quad [2.3]$$

$$C_g = C_g(r, t); \quad 0 \leq r \leq a, t \geq 0 \quad [2.4]$$

$$\frac{\partial C_g}{\partial r} = 0; \quad r = 0, t \geq 0 \quad [2.5]$$

where C_i is the uniform initial concentration in the gel beads, C_s is the initial concentration in the bulk solution and a is the bead radius.

Equation 2.1 was solved numerically by a mixing cell method. A gel bead was represented by ten cells, representing concentric layers of the gel bead. The mass flux between neighbouring cells, J_D ($\text{mol m}^{-2}\text{s}^{-1}$) is calculated according to Fick's first law:

2. Transport in physically heterogeneous systems

$$J_D = -D \frac{\Delta C_g}{\Delta r} \quad [2.6]$$

where ΔC_g is the concentration difference between the cells, and Δr is the distance between the cell centres. Mass exchange between two neighbouring cells (m_D in mol s^{-1}) was calculated by multiplying the flux with the contact area between the neighbouring layers (Equation 2.7). The contact surface area between the cells (A in m^2) was calculated from the bead radius.

$$m_D = J_D A \quad [2.7]$$

Mass exchange between gel bead and bulk solution was calculated in the same way as inside the gel beads, using Equations 2.6 and 2.7. Only in this case the concentration gradient was estimated from the concentration difference between the outer cell of the bead and the bulk solution, divided by $\frac{1}{2} \Delta r$, the distance from the centre of the outer cell to the boundary surface. The mass exchange between bead phase and solution phase was corrected for the total ratio bead volume/solution volume. At every time step, first all the potential mass changes were calculated for every cell in the system, before the mass totals were actually updated. This diffusion model could be simply coupled to the numerical convection model that is described later.

In the case of a constant concentration outside the beads, Equation 2.1 can also be solved semi-analytically with Equation 2.8, according to Crank (1956). Because the equation is only valid in case of a constant concentration outside the beads it can not be used for the column system described in this paper. It was only used here to verify the numerical diffusion model against a theoretical solution. Equation 2.8 gives the released mass of solute (M_t) as a fraction of the mass released after infinite time (M_∞) as a function of time. The term ‘ierfc’ is a function of the error function ‘erfc’ (Equation 2.9).

$$\frac{M_t}{M_\infty} = 6 \sqrt{\frac{Dt}{a^2}} \left(\frac{1}{\sqrt{\pi}} + 2 \sum_{n=1}^{\infty} \text{ierfc} \frac{na}{\sqrt{Dt}} \right) - \frac{3Dt}{a^2} \quad [2.8]$$

$$\text{ierfc } x = \frac{1}{\sqrt{\pi}} e^{-x^2} - x \text{erfc } x \quad [2.9]$$

2.3. Transport processes in a column with gel beads

2.3.1. Column experiments

The transport of solutes in the column with gel beads was studied by measuring the breakthrough curve of nitrate. After complete breakthrough, the column was flushed with a nitrate-free solution, and the nitrate-leaching curve was measured. The experiment was repeated, so that three different flow rates and two different bead sizes were tested.

The experimental system consists of a column with an inner diameter of 10.0 mm, and a total volume (V_0) of 10.0 mL, packed with alginate beads. The column length (L) is approximately 127 mm. The properties of the column are shown in Table 2.1. Note that the gel beads used in the column experiment were smaller than the ones in the batch experiments. The total volume of beads (V_b) was calculated from the number of beads and their individual volume. Solution was pumped through the column, causing an upward flow with a certain flow rate. The flow rate in the column was calculated from the measured volumetric flow rate and the column dimensions (Table 2.1). First the column was equilibrated with a nitrate-free solution (10^{-3} M CaCl_2), which was then replaced with a 10^{-3} M $\text{Ca}(\text{NO}_3)_2$ solution. The effluent was collected in fractions of approximately 1 mL at set time intervals. After complete equilibrium with this solution, the column was percolated with nitrate-free solution again, while taking samples. The concentration of nitrate in the samples was measured using spectrophotometric analysis (Technicon Instruments, 1987).

Table 2.1. Characteristics of the columns

no.	bead radius (mm)	total bead volume (mL)	mobile volume (mL)	volumetric flow rate (10^{-5} L s $^{-1}$)	flow velocity (10^{-3} m s $^{-1}$)
1	1.60	5.6	4.4	1.0	0.29
2	1.60	5.6	4.4	2.9	0.84
3	1.60	5.6	4.4	8.7	2.5
4	1.36	6.3	3.7	8.7	3.0

2.3.2. Transport model

To model the solute transport in the column, the solution in the system was divided into an immobile region, representing the gel beads, and a mobile region,

2. Transport in physically heterogeneous systems

representing the mobile solution surrounding the beads. Because the water fraction of the beads is approximately one, the volumes of both solutions together equal the total volume of the column ($V_m + V_b = V_0$).

Underlying assumptions for the model are:

- transport in mobile region takes place only by convection, and diffusion and dispersion in the mobile region can be neglected,
- the mobile solution is perfectly mixed at each depth in the column,
- the total surface of each bead is in direct contact with the mobile solution and mass exchange between the bead and the solution is diffusion controlled.

Convective transport in the mobile region can be described by the following transport equation:

$$\frac{\partial C_m}{\partial t} = -v_m \frac{\partial C_m}{\partial x} - S(x, t) \quad [2.10]$$

in which C_m is the concentration in the mobile phase, v_m is the average pore water velocity in the mobile region in m s^{-1} and $S(x, t)$ is the source or sink term caused by diffusion into or out of the gel beads, which follows from the solution of Equations 2.1 to 2.5. The system is subject to the following initial and boundary conditions:

$$C_m = C_0; \quad 0 \leq x \leq L, t = 0 \quad [2.11]$$

$$C_m = C_f; \quad x = 0, t > 0 \quad [2.12]$$

$$C_m = C_m(x, t); \quad 0 < x \leq L, t > 0 \quad [2.13]$$

in which L is the column length, C_0 is the initial concentration in the column and C_f is the concentration in the feed solution.

Convective transport (Equations 2.10-2.13) was solved numerically by representing the mobile solution in the column in 30 vertical cells. The radial diffusion model (Equations 2.1-2.5) was used at the same time to calculate the concentration in the gel bead phase at each depth and the fluxes in and out of the gel. This is solved in the same way as for the diffusion model, by representing the beads at every depth in the column by 10 concentric layers. The outer cell, representing the outer layer of the beads at a certain depth, is linked to the cell representing the mobile region at that depth. The mass flow m_m (mol s^{-1}) from one cell in the mobile region to the next, follows from the mass flux J_m ($\text{mol m}^{-2}\text{s}^{-1}$) in the direction of the water flow:

$$J_m = v_m C_m \quad [2.14]$$

$$m_m = v_m \frac{V_m}{L} C_m \quad [2.15]$$

The combined set of equations that describe the mass exchange in the system is equivalent to a so-called mixing cell model and was solved using a first order difference scheme in time. At every time step, first all the potential mass changes were calculated for every cell in the system, before the mass totals were actually updated. The simulations were carried out using a time step of 0.25 s. Increasing the number of time steps and nodes did not change the calculated results noticeably, indicating that the results are not significantly affected by numerical truncation errors. The input variables for the model are: the mobile volume in the column, the total bead volume, the flow rate, the radius of the beads and the diffusion coefficient of the solute.

2.4. Results and discussion

2.4.1. Diffusion experiments and modelling

The release of either nitrate or phosphate from the beads was calculated with both the analytical model (Equation 2.8) and the numerical model. Because of the large solution volume, the concentration in the bulk solution could be assumed constantly zero, which was essential for solving Equation 2.8. Input parameters for both models are the average bead size and the diffusion coefficients for nitrate and phosphate. Because diffusion of ions in alginate is assumed to be similar to diffusion in water, we used the diffusion coefficients in water: $1.90 \cdot 10^{-9} \text{ m}^2 \text{ s}^{-1}$ for nitrate and $0.85 \cdot 10^{-9} \text{ m}^2 \text{ s}^{-1}$ for phosphate (H_2PO_4^-) at 25°C (Li and Gregory, 1974). The actual temperature at which the experiment took place was around 23°C , as the solution was slightly warmed up by the automatic stirrer. The used diffusion coefficients are valid for infinite dilution and not corrected for the ionic strength.

The cumulative release of nitrate and phosphate from the gel beads, expressed as fraction of the maximal release, is plotted as a function of time in Figure 2.2. The maximal release of nitrate and phosphate was estimated from the last samples that were taken, at least 40 minutes after the beads were added to the reservoir. The results of numerical and analytical calculations were identical, which confirms that the numerical model is consistent with the diffusion theory according to Fick. From the results in Figure 2.2 it can be concluded that the models are able to predict the release of a solute from the beads by diffusion, provided the bead size and the

2. Transport in physically heterogeneous systems

diffusion coefficient of the solute are known. According to these results, the apparent diffusion coefficients for ions in alginate appear not to differ from those in water. The simulated diffusion rate is proportional to D/a^2 (s^{-1}), the ratio of the diffusion coefficient and the square of the bead radius. Both the diffusion coefficient and the bead radius varied for the nitrate and phosphate simulations, resulting in $D/a^2 = 3.5 \cdot 10^{-4} s^{-1}$ for nitrate and $2.1 \cdot 10^{-4} s^{-1}$ for phosphate. This difference is mainly caused by the different diffusion coefficients. Figure 2.2 shows that the simulation results are very sensitive for the value of the diffusion coefficient. Therefore it is important for transport predictions, to use the correct values for the different ions. The results show that the reported values for diffusion in water can properly be used to predict transport in the gel system.

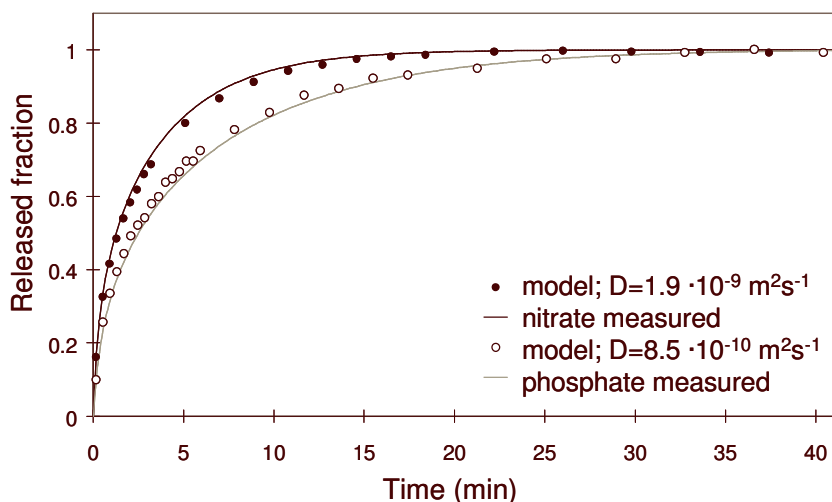


Figure 2.2. The release of nitrate and phosphate from alginate beads by diffusion: the measured fractions of nitrate and phosphate are plotted against time, together with the results of model calculations.

2.4.2. Column experiments and modelling

The parameters that were used for input in model calculations are shown in Table 2.1. For the calculation of nitrate diffusion in the gel column, the diffusion coefficient of nitrate in water at 18°C was used: $D^0 = 1.61 \cdot 10^{-9} m^2s^{-1}$ (Li and Gregory, 1974). The actual temperature at which the experiments took place was around 20°C.

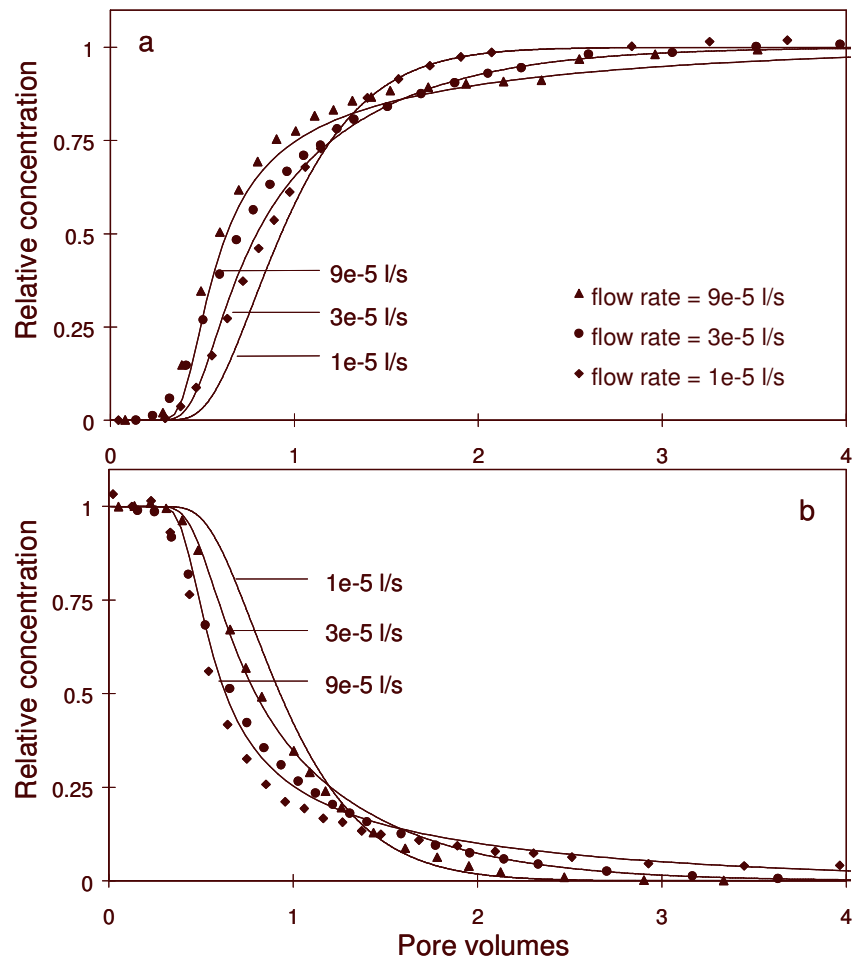


Figure 2.3. The breakthrough curves for nitrate flow through a column with alginate beads at different flow rates. Plotted are the relative concentrations measured in the effluent in case of nitrate input (a) and release (b), together with the results of model calculations.

The measured and calculated breakthrough curves at different flow rates are shown in Figure 2.3. Figure 2.3a shows the breakthrough curves for percolation with nitrate containing solution. Figure 2.3b shows the curves for the percolation of nitrate saturated columns with nitrate-free solution. The concentration in the

2. Transport in physically heterogeneous systems

effluent is expressed on the y-axis, relative to the concentration in the nitrate solution. The curves for nitrate leaching (Fig. 2.3b) are identical mirror images of the nitrate input curves (Fig. 2.3a), which indicates that diffusion into the beads and release from the beads are the same reversible process. The number of percolated column volumes (V/V_0) is given on the x-axis and stands for the total percolated solution volume (V) divided by the total volume of solution in the column (V_0), which includes the immobile solution in the gel. As expected for two-region systems, the breakthrough curves for the columns with alginate beads are not symmetrical: the initial breakthrough is fast, followed by a slow approach of the complete breakthrough. The first half of the breakthrough ($C/C_0=0.5$) is reached before the total volume of solution in the column is displaced once ($V/V_0=1$). At low flow rates, the solution remains longer in the column, so there is more time for diffusion into the beads. This causes the differences between the breakthrough curves at different flow rates. The shape of the breakthrough curve is determined by the ratio of flow rate and diffusion rate, the latter of which is determined by the diffusion coefficient of the solute and the bead radius. This ratio can be described with $(v_m/L)/(D/a^2)$, which also reflects the relative sensitivity of the simulations for the different parameters. For example, a three times smaller diffusion coefficient will give the same breakthrough curve as a three times larger flow rate (Fig. 2.3).

Figure 2.4 shows the breakthrough curves for two columns filled with different sized beads. The figures show that the model calculations give a good prediction of the breakthrough of nitrate from the column for different flow rates and for different sized beads. The small difference between the measured and the calculated curves might be due to heterogeneous flow in the column. Because the beads are relatively large compared to the inner diameter of the column, it is possible that flow near the glass surface of the column can be slightly faster than between the beads, due to the relatively large space between the beads and the glass surface. This causes a form of dispersion which is not simple to describe in a model. However, dispersion mainly affects the initial part of the breakthrough curve and becomes less significant after one pore volume, when diffusion into the beads becomes more important. Figure 2.3 shows that the model describes perfectly the tailing of the breakthrough curves, which is particularly of interest for studies on nonequilibrium solute transport.

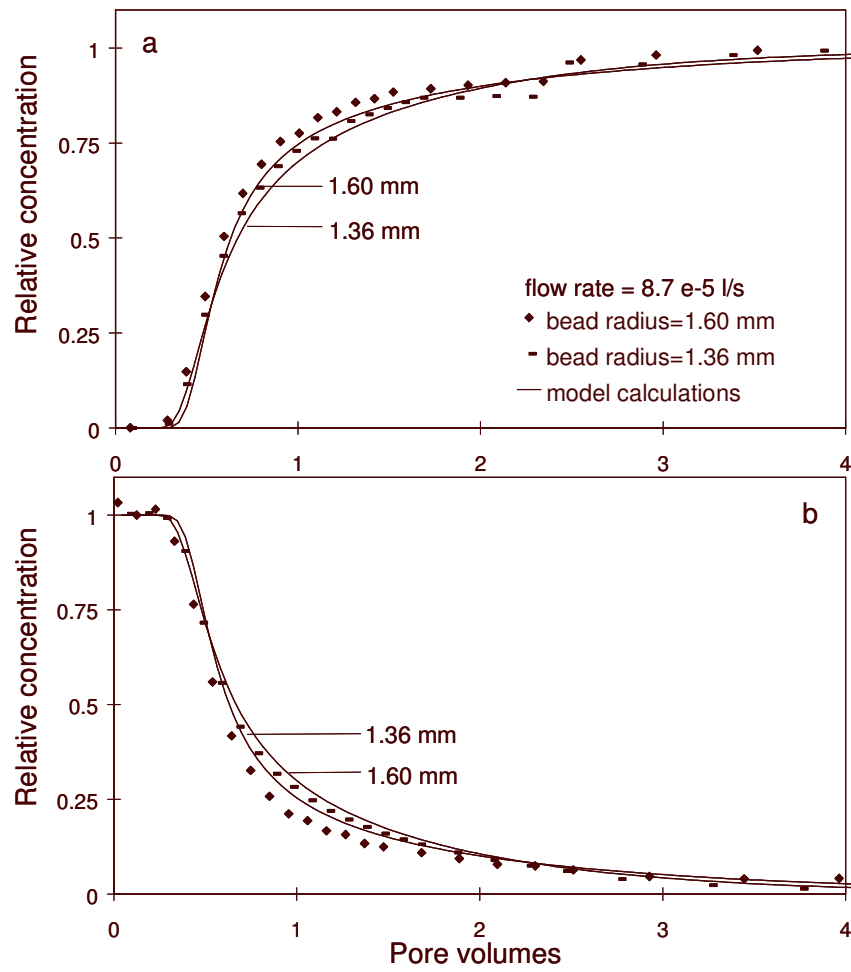


Figure 2.4. The breakthrough curves for nitrate flow through two columns filled with different sized alginate beads. Plotted are the relative concentrations measured in the effluent in case of nitrate input (a) and release (b), together with the results of model calculations.

2. Transport in physically heterogeneous systems

2.5. Conclusions

The main conclusions of this work are:

- the gel bead column can be used as an experimental model for a porous system in which physical transport nonequilibrium occurs,
- transport of ions through a gel bead column can be described with a two-region transport model with convection in the mobile phase and diffusion in the gel phase,
- for the ions studied in this work, the release of ions from spherical gel beads can be accurately predicted with Fick's law assuming radial diffusion, and using the diffusion coefficients for diffusion in pure water,
- transport in the gel bead column could be predicted from the following independent parameters: dimensions of the column, radius of the beads, flow rate and diffusion coefficients from literature.

Altogether, this study showed that the bead-filled column is a suitable tool for studies on nonequilibrium transport and to provide experimental data for model verification.

3. Modelling transport of protons and calcium ions in an alginate gel bead system: The effects of physical nonequilibrium and nonlinear competitive sorption

Wendy van Beinum, Johannes C.L. Meeussen and Willem H. van Riemsdijk

Environmental Science and Technology (2000), Vol.34, No.23, pp. 4902-4907.

3.1. Introduction

Migration of substances in soils is governed by a combination of physical and chemical processes. Being able to predict the resulting transport rates is potentially useful for estimating the impacts of contaminated soils on groundwater quality, or for estimating the required flushing times for soil clean up procedures. The modelling of solute transport requires a thorough understanding of the main processes involved. A complicating factor is the fact that soils are generally physically heterogeneous and exhibit spatial variation in hydraulic conductivity. This results in so-called nonideal transport behaviour: the water flow will be faster in the more permeable parts of the soil and slower in the less permeable parts. The flow in the less permeable parts can be so slow that the mass transfer in these parts becomes effectively limited by diffusion and we speak of physical nonequilibrium. During transport, the initial breakthrough of the solutes will take place earlier than in the case of homogenous flow, and the complete breakthrough will be reached very slowly (tailing). Different models have been developed to describe nonideal transport of solutes in heterogeneous systems. Extended reviews are given by Brusseau and Rao (1990), and Ma and Selim (1997). A common approach is the use of a two-region model (Van Genuchten and Wierenga, 1976; Rao et al., 1980), in which the flow region in the system is divided between a mobile part and an immobile part. The model assumes that solute transport in the mobile part takes place by convection, and in the immobile part by diffusion.

For reactive solutes, the interaction with the soil solid phase is an important factor controlling transport. The solute front can either exhibit sharpening or spreading, depending on the shape (linear, concave or convex) of the sorption curve (Appelo and Postma, 1999; Scheidegger et al., 1994). In case of nonequilibrium transport, the spreading caused by nonlinear sorption can add to the tailing caused by nonequilibrium. This has been shown for the transport of organic chemicals through a soil column (Spurlock et al., 1995). Transport of a solute in a natural soil can also be influenced by the interaction with ions that are naturally present in the soil solution, such as competition for sorption on the soil solid phase. The effects that can be expected in case of a combination of multicomponent chemistry and physical nonequilibrium are not fully resolved yet (Nkedi-Kizza et al., 1982; Brusseau, 1994).

A transport model in which chemical and physical processes are integrated, is a useful tool to examine these processes and the way they interact. A serious problem when testing advanced nonideal transport models for natural systems is the

3. Modelling transport of protons and calcium ions

difficulty in obtaining the necessary input parameters. It is therefore essential to use a well-defined experimental system. Previous experiments have used columns with ceramic spheres (Rao et al., 1980), with soil aggregates (Nkedi-Kizza et al., 1982) and with alginate gel beads (Chapter 2). All these systems can be described as two-region systems, in which the immobile part consists of, respectively, ceramic spheres, aggregates, or gel beads. For the work presented in this paper, a column with alginate beads was used. One of the advantages of using gel is that the gel is virtually all water (>98%), and that diffusion into the beads can simply be estimated with the diffusion coefficients for diffusion in water (Chapter 2). Another advantage is that the chemistry of the alginate gel is relatively well known.

In the present work we will demonstrate and discuss the processes that take place during proton transport in the gel column. As will be shown by the results of titrations and column experiments, proton sorption on calcium alginate is nonlinear and competes with the sorption of calcium ions. The bead-filled column, with its immobile water in the gel phase and its mobile water in the pores is a strongly simplified representation of an heterogeneous soil. Nevertheless, the column does have physical and chemical characteristics in common with natural soils. As shown in previous work (Chapter 2), solute flow through the column results in the same typical breakthrough as observed in heterogeneous soils, caused by diffusion into a stagnant water phase. Also, the reactivity of the gel is comparable to that of natural organic matter in soils. Humic matter is thought to have similar properties to polyelectrolyte gels because of the three-dimensional structure (Marinsky and Ephraim, 1986). Humic acids contain two kinds of sorption sites formed by the carboxylic groups and the phenolic groups (Milne et al., 1995). At neutral and low pH, the reactivity of the humic matter is mainly caused by the carboxylic groups, the same groups that determine the reactivity of the alginate gel. Nevertheless sorption on humic acids can not be described by a Langmuir or Gapon exchange model as we used here for the alginate. The main reason is that the chemistry of humic acids is very heterogeneous, which causes the sorption affinity is to be non-identical for all carboxylic sites, but distributed around an average (Kinniburgh et al., 1999). Sorption on alginate can be described by Langmuir sorption (Jang et al., 1995), which indicates that the sorption affinity distribution is very narrow. The site density (approx. 5 mol sites per kg alginate) is similar to the site density of humic substances in soils. The concentration of the alginate in the column (approx. 0.85% weight per column volume) is comparable to concentrations of humic matter in mineral soils which are typically in the range of 1-2% weight per volume.

The aims of this work are:

- to show that with sufficient understanding of both the chemical and the physical processes, transport of reactive substances can be accurately predicted from independently obtained physical and chemical parameters,
- to show the effects of nonlinear sorption and competition on transport in a physically heterogeneous system.

In order to achieve this, we will first describe the chemical interactions of protons with alginate gel with a sorption model. This chemical model will be incorporated in the two-region transport model to predict nonequilibrium transport of protons in the gel column. The model will be tested against the results of column experiments.

3.2. Material and methods

3.2.1. Preparation of the beads

Alginate solution (0.5%) was prepared by adding 0.5 g of sodium alginate (from *Macrocystis pyrifera*, Sigma Chemical Co.) to 100 mL demineralised water. The gel beads were prepared according to Martinsen et al. (1989) by dripping the alginate solution into an stirred aqueous solution of 0.2 M CaCl_2 . The gel drops solidify as soon as they enter the calcium chloride solution and form spherical beads. Then the beads were transferred to a fresh 0.2 M CaCl_2 solution, and allowed to stabilise for 24 hours. They were then washed and equilibrated with 10^{-3} M or 10^{-2} M CaCl_2 solution and stored at 4°C. The amount of gel that was used to prepare a batch of beads was measured and divided by the number of beads in the batch. The resulting average sodium alginate mass was approximately $1.60 \cdot 10^{-4}$ grams per bead or $8.09 \cdot 10^{-7}$ moles per bead (molar weight = 198). The alginate gel shrinks during the crosslinking by calcium ions (approximately 3 times). The final bead size depends on the concentration of CaCl_2 solution in which they are kept. The average size of the beads in a batch was estimated by measuring the volume of the batch. The measured bead volume was approximately 10.6 μL in 10^{-3} M CaCl_2 and 8.75 μL in 10^{-2} M CaCl_2 . This corresponds with bead diameters of 2.72 and 2.56 mm respectively.

3. Modelling transport of protons and calcium ions

Table 3.1. Column experiments

no.	initial solution		feed solution		total bead	mobile	bead	flow rate	pore flow	T
	CaCl ₂ -concentr.	pH	CaCl ₂ -concentr.	pH	volume	volume	diameter	(10 ⁻⁵ L s ⁻¹)	velocity	(°C)
	(mol L ⁻¹)		(mol L ⁻¹)		(mL)	(mL)	(mm)		(10 ⁻³ m s ⁻¹)	
1a	10 ⁻³	5.02	10 ⁻³	3.51	5.6	4.4	2.72	4.7	1.36	20-21
1b	10 ⁻³	3.49	10 ⁻³	5.00	5.6	4.4	2.72	4.7	1.36	21
2a	10 ⁻³	5.00	10 ⁻³	3.49	5.6	4.4	2.72	18.1	5.24	21
2b	10 ⁻³	3.48	10 ⁻³	5.02	5.6	4.4	2.72	18.1	5.24	21
3a	10 ⁻²	4.97	10 ⁻²	3.50	4.7	5.3	2.56	9.2	2.21	20
3b	10 ⁻²	3.50	10 ⁻²	5.01	4.7	5.3	2.56	13.5	3.24	18-19

3.2.2. Flow experiments

A column with an inner diameter of 10.0 mm, an inner volume of 10.0 mL, and a length of 127 mm, was packed with alginate beads. The properties of the columns are given in Table 3.1. The total volume of beads (V_b) was calculated from the number of beads and their individual volume. The bead diameter is relatively large in comparison to the inner diameter of the column, but from previous results (10) with even larger beads, we expect no problems for the flow behaviour.

Calcium chloride solutions were prepared at pH 5 and pH 3.5 by adding small amounts of HCl solution. First the gel column was equilibrated by slowly pumping CaCl_2 solution with pH 5 through the column overnight. After equilibration, the flow experiment was started by pumping the pH 3.5 feed solution through the column. The pH in the effluent was measured online with a pH combination glass electrode in a flow cell, and registered by a recorder. The temperature in the solutions was measured before and after the experiment. After the pH of the effluent had reached the pH of the feed solution, the column was slowly percolated with the same solution for another night to establish complete equilibrium. Then the process was repeated by pumping a pH 5 solution through the column initially at pH 3.5. The experiments were performed at two flow rates ($4.70 \cdot 10^{-5}$ and $18.1 \cdot 10^{-5} \text{ L s}^{-1}$) and at two CaCl_2 concentrations (10^{-3} M and 10^{-2} M).

The measured pH values were plotted against the number of pore volumes. To facilitate comparison between the curves, plots were also made of the relative proton concentrations.

3.2.3. Sorption model

Sodium alginate is a collective term for a group of copolymers containing 1,4-linked β -D-mannuronate and α -L-guluronate residues in varying proportions and sequential arrangements (Martinsen et al., 1989). Every uronate residue contains a negatively charged carboxylate group, which can interact with cations (Jang et al., 1995). Calcium alginate gel is formed by crosslinkage of the polymer chains by calcium ions. Because of their divalent charge, calcium ions can form bonds between two carboxylate groups on neighbouring strings. Proton sorption by alginate takes place by carboxylate groups binding a proton, which results in a zero charged carboxylic group.

To maintain electroneutrality in the gel, all the negative charge of the carboxylate groups is counterbalanced by the binding of positively charged ions. This can

3. Modelling transport of protons and calcium ions

either be by chemical binding on the carboxylic sites or by electrostatic binding. In the case of proton sorption by calcium alginate, all the negative charge of the calcium alginate gel is compensated by Ca^{2+} - and H^+ -ions. The contribution of electrostatic repulsion of negatively charged ions is assumed to be negligible. The cation sorption can be described as an ionexchange process, where protons and calcium ions compete for the same binding sites. For every two protons that are adsorbed, one Ca^{2+} ion has to be desorbed to maintain electroneutrality in the gel:



in which $\text{SCa}_{1/2}$ is a site compensated by a shared Ca^{2+} ion and SH is a protonated site. All carboxylic sites are assumed to be compensated by sorption of protons or calcium ions, so the total amount of sites per gram alginate equals the sum of bound ions:

$$S_t = \text{SH} + \text{SCa}_{1/2} \quad [3.2]$$

The stability constant K for the exchange reaction of Equation 3.1 is given by:

$$K = \frac{\{\text{SH}\} (\text{Ca}^{2+})^{1/2}}{\{\text{SCa}_{1/2}\} (\text{H}^+)} \quad [3.3]$$

where (Ca^{2+}) is the calcium activity and (H^+) is the proton activity in the solution entrapped by the gel structure. $\{\text{SH}\}$ and $\{\text{SCa}_{1/2}\}$ are the charge-equivalent fractions of the exchanger, which are assumed to represent the activities of the adsorbed phase. This model is known as the Gapon exchange model (Gapon, 1934). Combining Equations 3.2 and 3.3 gives:

$$\text{SH} = S_t \frac{K (\text{Ca})^{-1/2} (\text{H}^+)}{1 + K (\text{Ca})^{-1/2} (\text{H}^+)} \quad [3.4]$$

where SH and S_t are expressed in mol per gram alginate. Equation 3.4 reduces to a simple Langmuir equation, when the calcium activity in solution is constant.

For the simulation of proton sorption inside the alginate beads during flow experiments, Equations 3.2 and 3.3 were incorporated in the transport model. The sorption sites are assumed to be equally distributed throughout the gel. The input parameters needed for the calculations are S_t , the site density, and K, the ionexchange constant. The site density was assumed to be equal to the number of uronate residues in the gel. Assuming a 100% pure sodium alginate this results in $S_t = 5.05 \cdot 10^{-3} \text{ mol g}^{-1} \text{ Na-alginate}$. This value is in the same range as the site density given by Jang et al. (1997), who measured 4.36 mmol per gram Na-

alginate. The remaining difference could be caused by differences in the purity of the alginates. The K-value was obtained from titrations between pH 5 and 3.5 at different calcium concentrations between 0.001 and 0.01 mol L⁻¹ (see Appendix 1). The Gapon model gives a good description of the influence of calcium on the proton adsorption, using a fitted exchange constant of K=25 (Fig. 3.1). The model describes all curves well, except for the curve at 0.001 mol L⁻¹ calcium. However, the measurements for this curve are less reliable as they are relatively sensitive to small changes in calcium concentration and ionic strength. The activities of the ions in solution are calculated by multiplying their concentration with the activity coefficient (γ_i) calculated with the Davies equation:

$$\log \gamma_i = -0.51 z_i^2 \left(\frac{\sqrt{I}}{1 + \sqrt{I}} - 0.2I \right) \quad [3.5]$$

where I is the ionic strength, and z_i is the charge of the ion i .

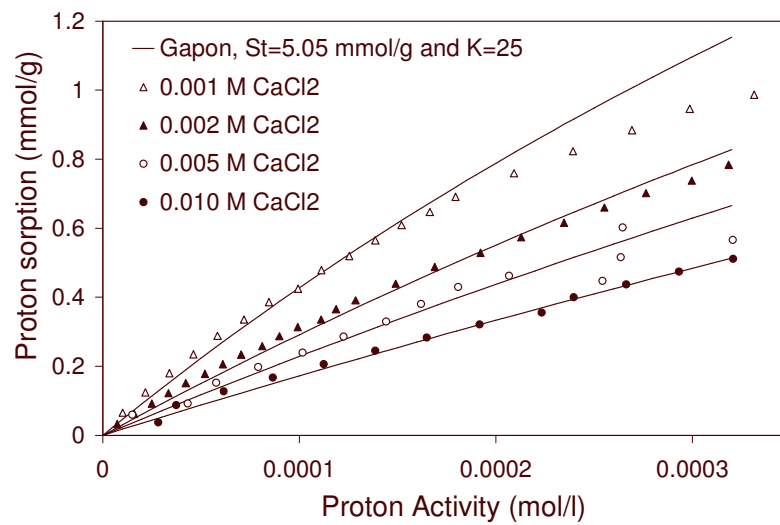


Figure 3.1. Measured proton sorption (mmol g⁻¹ alginate) at different CaCl₂ concentrations, plotted against the proton activity, together with the curves calculated with the ionexchange model.

3. Modelling transport of protons and calcium ions

3.2.4. Transport Model

To model the solute transport in the column, the solution in the system was divided into an immobile region, representing the gel beads, and a mobile region, representing the mobile solution surrounding the beads. Because the water fraction of the beads is approximately one, the volumes of both solutions together equal the total volume of the column ($V_m + V_b = V_0$). Underlying assumptions for the model are:

- transport in mobile region takes place by convection only; diffusion and dispersion in the mobile region can be neglected,
- the mobile solution is perfectly mixed at each depth in the column,
- the total surface of each bead is in direct contact with the mobile solution, in other words, there is no diffusive boundary layer outside the bead, and mass exchange between the bead and the mobile solution is purely diffusion controlled.
- mass transport inside the beads takes place by diffusion.

In our previous work we showed that non-reactive transport in a similar column experiment could be described without taking dispersion into account (Chapter 2). Therefore dispersion in the column is also assumed to be negligible in case of reactive transport. The dispersivity (α) caused by flow around the beads is expected to be approximately equal to the bead diameter (Appelo and Postma, 1999), which is small in relation to the column length (L/α is approx. 50).

Convective transport in the mobile region can be described by the following transport equation:

$$\frac{\partial C_{i,m}}{\partial t} = -v \frac{\partial C_{i,m}}{\partial x} - S_i(x, t) \quad [3.6]$$

in which $C_{i,m}$ is the concentration of ion i in the mobile phase, t is the time in seconds, x is the distance from the column inlet in meters, v is the average pore water velocity in the mobile region in m s^{-1} and $S_i(x, t)$ is the source or sink term caused by diffusion out of or into the gel beads. The system is subject to the following initial and boundary conditions:

$$C_{i,m} = C_{i,ini}; \quad 0 \leq x \leq L, t = 0 \quad [3.7]$$

$$C_{i,m} = C_{i,f}; \quad x = 0, t > 0 \quad [3.8]$$

3. Modelling transport of protons and calcium ions

$$C_{i,m} = C_{i,m}(x, t); \quad 0 < x \leq L, t > 0 \quad [3.9]$$

in which L is the column length, $C_{i,ini}$ is the initial concentration in the column and $C_{i,f}$ is the concentration in the feed solution.

Diffusion of ions in the beads is driven by their concentration gradient and the electrostatic gradient caused by surrounding ions. The resulting flux of an ion is therefore a function of the concentration gradients of all the ions in solution. Assuming that the movement of charged species is subject to maintaining electroneutrality, the following equation can be derived (Aguilella et al., 1987). The derivation is presented in Appendix 2.

$$J_i = -D_i \left(\frac{dC_i}{dr} - z_i C_i \frac{\sum_j D_j z_j \frac{dC_j}{dr}}{\sum_j D_j z_j^2 C_j} \right) \quad [4.10]$$

where J_i is the radial diffusional flux of ion i in $\text{mol m}^{-2}\text{s}^{-1}$, C_i is the concentration in mol m^{-3} , r is the radial distance from the centre of the bead in meter, D_i is the diffusion coefficient in m^2s^{-1} and z_i is the charge of the ion i . Between brackets is given the concentration gradient of ion i minus a factor representing the electrical force on ion i . The last factor is a function of the concentration gradients, charges and mobilities of all charged ions in the system. For the application of Equation 4.10 to simulate diffusion of protons into the beads, the concentration gradients of the Ca^{2+} and Cl^- ions have to be known as well. Therefore transport was simulated for all ions in the system simultaneously. The system is defined by the following initial and boundary conditions:

$$C_{i,g} = C_{i,ini}; \quad 0 \leq r < a, t = 0 \quad [3.11]$$

$$C_{i,g} = C_{i,m}; \quad r = a, t \geq 0 \quad [3.12]$$

$$C_{i,g} = C_{i,g}(r, t); \quad 0 \leq r \leq a, t > 0 \quad [3.13]$$

$$J_i = 0; \quad r = 0, t > 0 \quad [3.14]$$

where a is the bead radius, $C_{i,g}$ is the concentration of ion i in the gel bead, $C_{i,ini}$ is the uniform initial concentration and $C_{i,m}$ is the concentration in the mobile solution surrounding the beads. For the calculation of H^+ , Ca^{2+} and Cl^- diffusion, their diffusion coefficients in water at 20°C were used. These coefficients were derived by linear interpolation of the diffusion coefficients at 18 and 25°C (Li and Gregory,

3. Modelling transport of protons and calcium ions

1974), resulting in $8.49 \cdot 10^{-9}$, $1.80 \cdot 10^{-9}$ and $7.07 \cdot 10^{-10} \text{ m}^2\text{s}^{-1}$ for H^+ , Cl^- and Ca^{2+} respectively. The pH of the feed solution was assumed to be equal to the final pH that was measured in the effluent, although in reality there were small differences (less than 0.03 pH unit).

For the implementation of the transport model, we used the program ORCHESTRA (Meeussen et al., 1996). The equations for convection and diffusion (Equations 3.6-3.14) were solved numerically using a mixing cell method and a first order difference scheme in time (Chapter 2). Therefore the mobile volume was divided into 50 vertically connected cells, each one connected to 10 horizontally connected cells representing the gel volume. Mass transport between the cells was calculated for a time step of 1 second. The chemical equilibrium for the solution and solid phase was found by iteration after every mass transport calculation. The number of horizontal calculation cells was chosen so that the length of each cell approximately equals the bead diameter. In that case the truncation error caused by the numerical method should equal the hydrological dispersion caused by the flow around the beads (Appelo and Postma, 1999). But variation of the number of cells did not significantly alter the outcome of the calculations, which suggests that truncation errors are negligible.

For comparison with the two-region model, simulations were also performed assuming a homogeneous system, in which all the water in the column was considered mobile and in immediate contact with the sorption sites. To demonstrate the importance of multicomponent effects, transport in the columns was also simulated while ignoring the influence of calcium. In that case the Gapon exchange model (Equation 3.4) reduces to a Langmuir model, and the Ca-dependent electroneutral diffusion equation (Equation 3.10) reduces to Fick's law.

3.3. Results

The measured pH breakthrough curves (Fig. 3.2) show that proton transport through the column with the alginate beads is considerably retarded by sorption of protons in the column, as it takes around 100 pore volumes of feed solution before the final pH is reached. At the lower flow rate, only the first part of the curve was measured, due to problems with the data recorder. The curves show the effect of the flow rate on the breakthrough curve: at higher flow rate, the initial breakthrough takes less pore volumes, but it takes more volumes before complete equilibrium is reached. At a low flow rate, the solution remains in the column for a longer period, which gives more time for diffusion into the stagnant phase and to establish complete equilibrium. If the flow rate would be low enough, the systems

would effectively behave as a homogeneous system. These effects are similar to those observed for a nonreactive solute (Chapter 2). For reactive transport however, the effect of diffusion becomes much more important, because it takes longer for the solute concentration in the beads to establish equilibrium with the surrounding solution. This means that a transport system can appear homogeneous with respect to transport of nonreactive tracers, but would nevertheless exhibit nonequilibrium effects (i.e. appear heterogeneous) with respect to reactive transport. The transport of protons through the column with alginate beads could be predicted fairly well with the transport model, shown by the solid lines in Figure 3.2. Because essentially all nonequilibrium effects observed from the column can be explained by the calculated diffusion, we can exclude the possible influence of chemical nonequilibrium during proton transport, which would have added to the effects of diffusion. The dashed lines in Figure 3.2 show the results of the homogeneous simulation.

Expressing the same data in terms of relative proton concentration (Fig. 3.3) shows that the breakthrough from a high to a low pH (sorption) is different from the breakthrough curve for the low to high pH (desorption). This proves that sorption of protons is nonlinear, as the sorption and desorption curves would in theory be identical for non-reactive or linear sorbing solutes. It is interesting to note that this effect is also apparent in the simulated results, even though at first sight the modelled sorption isotherms in Figure 3.1 seem almost linear in this pH range. Because most inorganic ions exhibit nonlinear sorption behaviour in soil, this effect has to be taken into account for the prediction of contaminant transport in these systems. Assumption of a linear isotherm causes an overestimation of the nonideality for the breakthrough curve, but more importantly an underestimation of the tailing of an elution curve and consequently an underestimation of the volume of water needed for cleaning a soil by flushing.

Although the truncation errors caused by the numerical method are negligible for the simulations with diffusion, this is strictly speaking not the case for the homogeneous calculations in Figure 3.3. The homogeneous calculations are more sensitive to these errors, because of the sharp concentration front. Without this effect the homogeneous breakthrough curve for sorption in Figure 3.3 would resemble a perfect block front with sharp corners. This is not the case for the desorption curves, of which the shape is determined by nonlinear sorption.

3. Modelling transport of protons and calcium ions

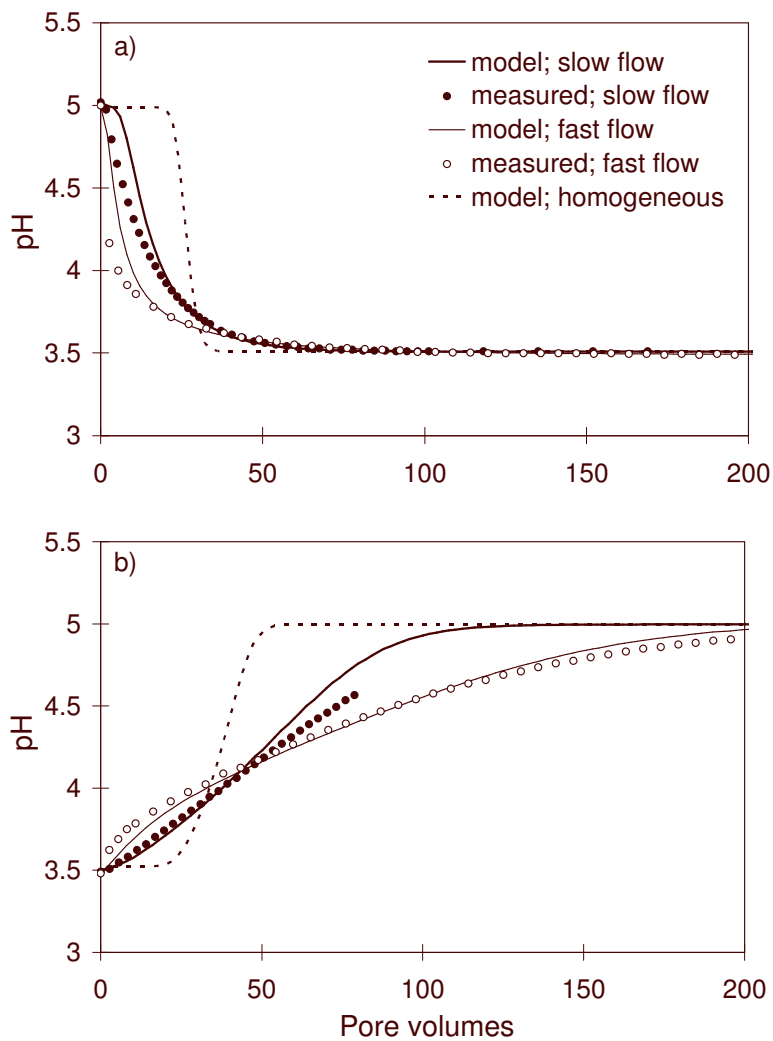


Figure 3.2. pH breakthrough curves in 10^{-3} M CaCl_2 , at two different flow rates ($4.7 \cdot 10^{-5}$ and $18.1 \cdot 10^{-5} \text{ L s}^{-1}$), together with the results of model calculations (solid lines). The dashed lines show the predicted pH breakthrough curves for a homogeneous system. (a) initial pH 5.0 and feed pH 3.5, (b) initial pH 3.5 and feed pH 5.0.

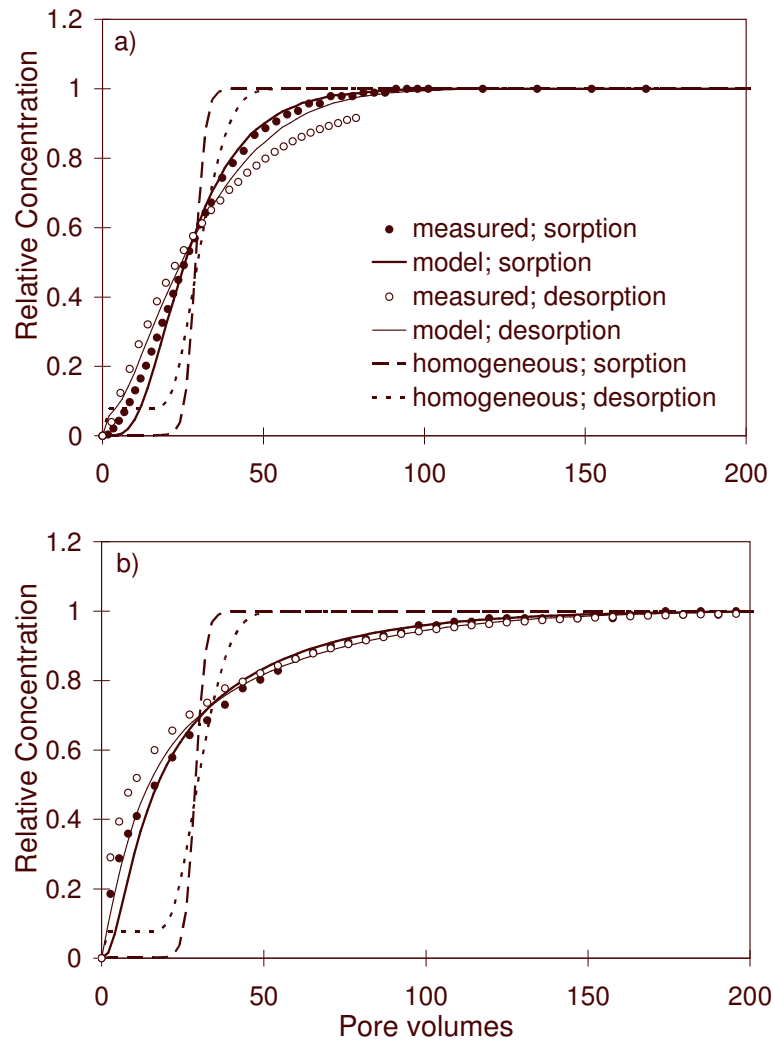


Figure 3.3. Breakthrough curves of the proton concentrations, expressed relatively to the initial proton concentration (relative concentration = 0) and the feed concentration (relative concentration = 1). (a) flow rate = $4.7 \cdot 10^{-5} \text{ l s}^{-1}$, (b) flow rate = $18.1 \cdot 10^{-5} \text{ l s}^{-1}$. The CaCl_2 concentration is 10^{-3} M . The dashed lines show the predicted pH breakthrough curve for a homogeneous system.

3. Modelling transport of protons and calcium ions

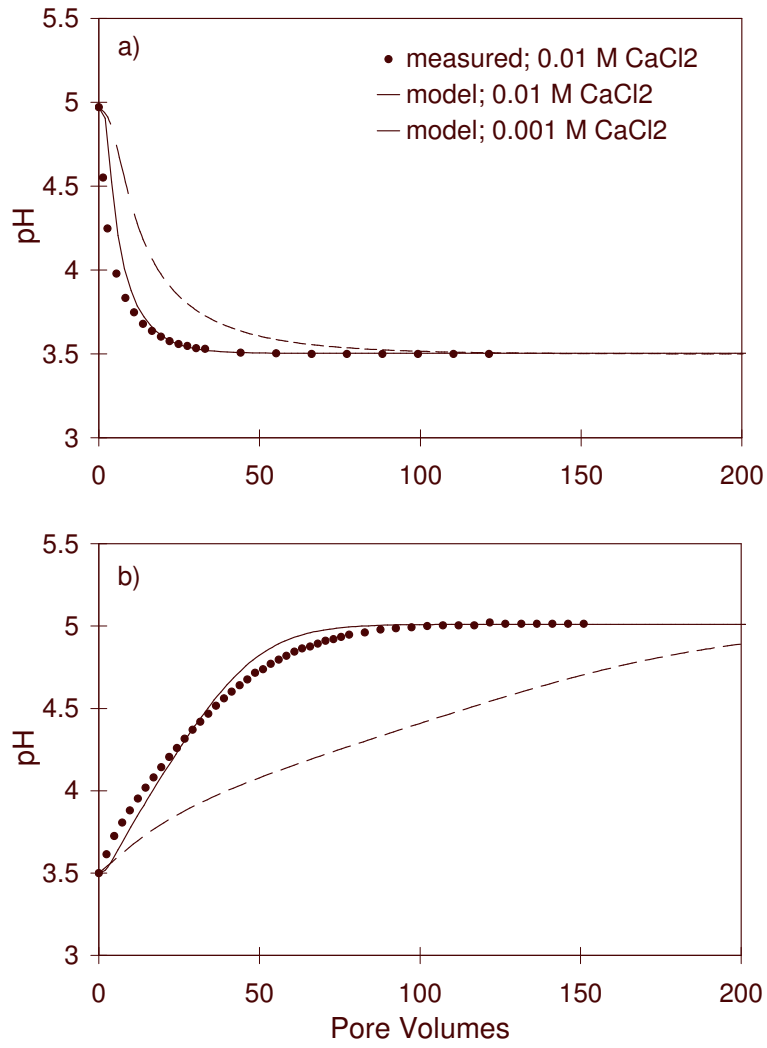


Figure 3.4. pH breakthrough curves in 10^{-2} M CaCl_2 . The measured pH values are plotted together with the results of model calculations for 10^{-3} and 10^{-2} M CaCl_2 . (a) initial pH 5.0 and feed pH 3.5, (b) initial pH 3.5 and feed pH 5.0.

The jump that can be seen in the desorption curves is caused by a small change in calcium concentration after slightly more than one pore volume. The influence of the changing calcium concentration on the other calculations will be discussed later. The breakthrough curves are also expected to be influenced by the ionic strength, which is also changing during proton transport. Model calculations with a constant ionic strength (not shown) showed that the variation in ionic strength has no noticeable effect on the proton breakthrough curves.

Figure 3.4 shows that the column experiments at 10^{-2} M CaCl_2 can also be predicted very well by the transport model. The sensitivity for the calcium concentration is illustrated by the model calculations at 10^{-3} and 10^{-2} M CaCl_2 . At 10^{-2} M CaCl_2 less proton sorption takes place, which causes higher proton transport rates and an earlier proton breakthrough. Proton sorption in turn, influences the calcium concentration by means of competition. Changes in proton concentration cause Ca^{2+} -desorption and cause local changes in calcium concentration. Especially inside the beads, the local Ca^{2+} concentration can deviate significantly from the initial concentration. This is shown by the simulated Ca concentration inside the beads during experiment 2a and b, in Figure 3.5.

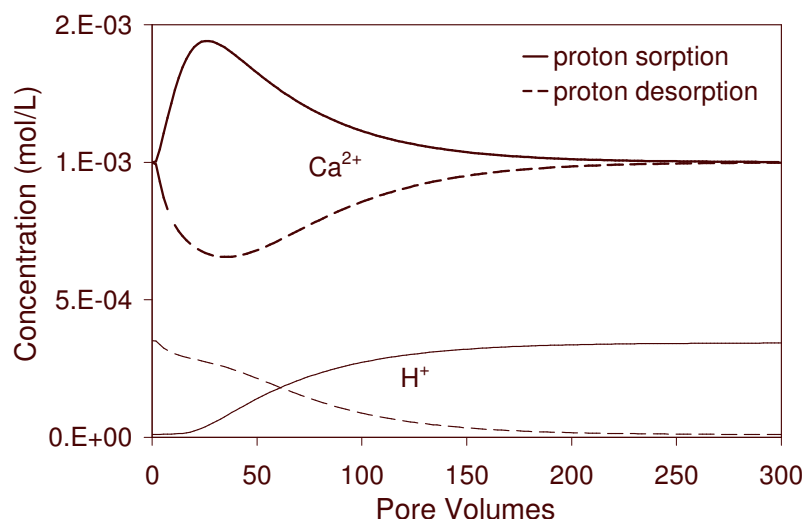


Figure 3.5. Simulated concentrations of protons and calcium ions in the centre of the beads near the column outlet. Ionexchange between protons and calcium ions cause a temporary increase in calcium concentration.

3. Modelling transport of protons and calcium ions

Figure 3.6 shows that multicomponent effects can cause an increased tailing of the desorption curves (Fig. 3.6b) at lower calcium concentrations. At 10^{-2} M CaCl_2 in Figure 3.6b, the effect is hardly noticeable because the relative change in calcium concentration during the proton front is smaller and therefore the proton sorption curve is almost a Langmuir curve. The effect and the significance in a multicomponent system will very much depend on the ion composition and concentrations.

The results show that the transport rate and tailing are the result of the interacting effects of physical nonequilibrium, the sorption isotherm and multicomponent effects, such as competitive sorption and coupled diffusion. Because all these processes can be expected to occur during transport in soils, they have to be taken into account when predicting reactive transport in these systems. Incorrect assumptions or approximations concerning the mechanisms in contaminant transport can cause a substantial error when predicting leaching times or concentrations.

This work also demonstrates that the relatively simple gel bead system can be used to examine multicomponent transport in heterogeneous systems. The system is complex enough to show effects of physical heterogeneity and nonlinear multicomponent chemistry, while at the same time the system is sufficiently well defined to allow representation in a numerical model. The computer model demonstrates that with sufficient understanding of chemical and physical properties of the system, transport processes can be accurately predicted. In this way the computer model can help to gain more understanding of the importance of different (interacting) processes that take place in natural systems and under which conditions they would become important. The chemical and physical properties of the model system can be modified according to the object of study. The chemistry can for example be modified by immobilising soil components, such as iron oxides or humic acids, in the gel beads, to integrate nonequilibrium transport and more complex sorption processes that take place in soils.

Supporting Information

The methods and results of the titrations to measure proton sorption by alginate beads are described in Appendix I. The derivation of the multicomponent ion diffusion equation is given in Appendix II.

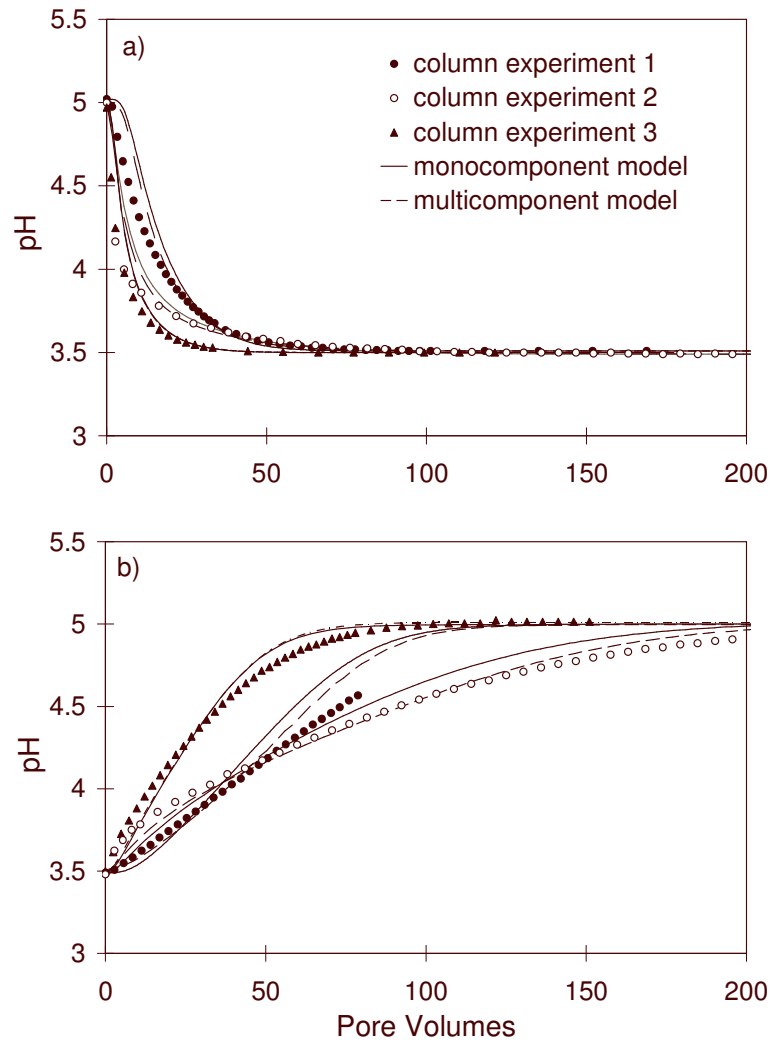


Figure 3.6. Simulation results assuming a monocomponent system, using a Langmuir sorption model and Fickian diffusion model (solid lines) compared with the results from the multicomponent model in which ionexchange and electroneutral diffusion takes place (dashed lines). (a) initial pH 5.0 and feed pH 3.5, (b) initial pH 3.5 and feed pH 5.0.

4. Competitive sorption and diffusion of chromate and sulphate in a flow system with goethite in gel beads

Wendy van Beinum, Johannes C.L. Meeussen and Willem H. van Riemsdijk

Journal of Contaminant Hydrology (2006), Vol. 86, pp. 262-278.

4.1. Introduction

Transport of chemicals in soil is of major importance for the potential leaching and spreading of contaminants from contaminated soil, the leaching of agricultural chemicals, as well as for the bio-availability of compounds, for example for uptake by plant roots. Solute transport is often influenced by non-equilibrium processes such as heterogeneous flow, diffusion into soil aggregates, intra-sorbent diffusion, or time dependent sorption (e.g. Brusseau, 1994). In most cases, a combination of chemical and physical processes is involved in non-equilibrium transport. The soil solution is a multicomponent medium in which different solutes coexist. Interaction between these solutes influences their sorption and mobility in soil.

Oxy-anions, such as selenate, arsenate and chromate, tend to bind strongly to the surfaces of oxide minerals in soil, such as hydrous ferric oxide and goethite (e.g. Waychunas et al., 1993; Manceau and Charlet, 1994; Fendorf et al., 1997). Competition between oxy-anions for sorption on the same surface may significantly reduce the amount of sorption. Zachara et al. (1987) and Villalobos et al. (2001) showed the influence of sulphate, silicate and carbonate on chromate sorption. Consequently, competition can significantly enhance the mobility of contaminants in soil, as was demonstrated by the influence of phosphate on arsenate leaching (Peryea and Kammereck, 1997). The effects of competition can be accounted for by mechanistic models that describe competitive sorption of ions onto available sites. Examples are surface complexation models such as the Diffuse Layer Model (Dzombak and Morel, 1990) and the CD-MUSIC model (Hiemstra et al., 1989; Hiemstra and Van Riemsdijk, 1996). These models describe the adsorption behaviour of variably charged surfaces of oxide minerals. They account for pH-dependent sorption, electrostatic interaction and competition between ions. Adsorption of anions will add negative charge to the surface and therefore decrease the affinity for sorption of additional anions. The CD-MUSIC model has been very successful in the description of sorption on goethite over a large range of conditions, including multicomponent sorption (e.g. Geelhoed et al., 1997; Hiemstra and Van Riemsdijk, 1999; and Rietra et al., 1999a) and the combination of sorption and transport (Meeussen et al., 1996, 1999).

The effect of physical non-equilibrium during transport can be described by mobile-immobile transport models (Ma and Selim, 1997). For example in aggregated soils, physical non-equilibrium is caused by transport with water flow through the macropores in between the aggregates and slow diffusion of solutes into and out of the aggregates. This was described by dividing the soil water into a

4. Competitive sorption of chromate and sulphate

mobile and an immobile water region (Van Genuchten and Wierenga, 1976). Two-region transport is described by convection in the mobile region and diffusion between the mobile and immobile region. This approach was extended by Rao et al. (1980) to describe spherical diffusion within aggregates in combination with convection in between the aggregates.

The aim of this work was to test the coupling of surface complexation modelling with transport and diffusion modelling. Our hypothesis is that reactive transport and competitive effects can be predicted by coupled mechanistic modelling, provided that the system is well defined and that parameters can be obtained from independent measurements. To allow for proper validation of the model, a model experimental system is required in which the chemical as well as the physical properties are well defined. For this purpose we developed a column filled with spherical gel beads (Chapter 2). The water inside the gel beads acts as an immobile water region through which transport of ions is only possible by diffusion. In this work we mixed goethite into the gel matrix of the gel beads to obtain a reactive matrix with known sorbing properties. Transport of chromate and sulphate through the column was measured and evaluated against model predictions.

4.2. Material and methods

To test the coupling of surface complexation modelling with transport and diffusion modelling a set of column experiments was performed. A well-defined flow system was build from a column filled with goethite-gel beads. Goethite is one of the most extensively studied iron oxides and the surface properties and sorption mechanisms on goethite are known in great detail from both spectroscopic studies and sorption experiments. The physical properties of the column with gel beads are sufficiently well defined to allow for accurate prediction of solute transport by a two-region transport model. The water inside the gel beads acts as an immobile water region through which transport of ions is only possible by diffusion. Transport down the column takes place by convection with the mobile water in between the gel beads. The two-region transport model was combined with the CD-MUSIC model to describe the surface chemistry of goethite. The model is based on a local equilibrium assumption (LEA), i.e. diffusion through the gel is the only time-limiting factor for sorption, and local sorption and desorption are instantaneous (i.e. chemical equilibrium). Numerical model simulations were used to predict the breakthrough of chromate and sulphate from the columns, as well as the pH changes resulting from anion sorption and desorption.

4.2.1. Preparation of the goethite-gel beads

Synthetic goethite was prepared based on the method of Atkinson (1967), by adding NaOH to a $\text{Fe}(\text{NO}_3)_3$ solution to a final pH 12, followed by ageing at 60°C. A solution of 30 g NaOH in 450 mL was added to 202 g of $\text{Fe}(\text{NO}_3)_3$ in 900 mL distilled water. The solution was shaken and left to nucleate for 50 hours. Then the pH was brought to pH 12 by adding 350 mL 2.5 M NaOH solution. The suspension was aged in Teflon® bottles at 60°C for four days, and shaken once a day. The goethite was dialysed for six days in dialysis tubes submerged in a large volume of distilled water. The water was refreshed after 1, 2 and 3 days. The surface area of the goethite was estimated by N_2 -BET (Beckman Coulter, SA3100) on two samples, which gave an average of $82.2 \text{ m}^2\text{g}^{-1}$. The suspension was stored in a Teflon® container for four months before it was used for the preparation of goethite-gel beads.

Earlier studies used gel beads made from alginate (Chapter 2 and 3), which contains carboxylate groups. As these groups would potentially interact with the goethite surface, it was decided to use the neutral polymer, polyacrylamide, instead. Goethite-gel beads were prepared by polymerisation of a mixture of acrylamide and goethite suspension. The mixture was prepared from 15 mL 40% acrylamide suspension (Biorad), 6 mL of a 2% AcrylAide crosslinker solution (DGT Ltd, Lancaster), 9 mL goethite suspension ($\sim 81 \text{ g L}^{-1}$) and 10 mL demineralised water (method adapted from Davison et al., 1994). Precautions should be taken to avoid any contact with the acrylamide, which is a known neurotoxin, and potentially carcinogenic and mutagenic. A metal tray was coated with a water repellent sheet (Whatman, Benchkote). A 1-cm layer of silicon oil (Fluca, Silicon oil AP 100, $d_{40}^{20} = 1.062$) was poured into the tray and heated on a hot plate to a constant temperature of approximately 50°C. Then 5 mL of the gel solution was mixed with 22 μL 10% persulphate solution and 10 μL TEMED (N,N,N',N'-tetramethylethylenediamine). All solutions were kept on ice to avoid early solidifying of the gel. Drops of the mixture (20 μL each) were carefully pipetted into the oil with a multi-pipette, just below the oil surface. As the density of the gel solution is not much different from the density of the oil, the drops float just above the bottom of the tray and maintain a spherical shape. Care was taken that the drops did not run into each other. This was repeated until the tray surface was fully covered by gel droplets. The gel beads were left in the oil for at least one hour to complete the solidification, scooped out and rinsed several times with demineralised water. They were left in demineralised water overnight to achieve full hydration. During hydration the beads increase in volume by approximately a

4. Competitive sorption of chromate and sulphate

factor 3. The beads were finally equilibrated with a 0.01 M NaCl solution and stored in polyethylene bottles before further use. After hydration and equilibration, the density of the gel was very similar to the density of water and the diameter of the gel beads was 4.6 mm.

The concentration of goethite in the gel beads was measured by dissolving the goethite from single goethite-gel beads in 10 mL solutions containing 0.26 M Na₃citrate, 0.11 M NaHCO₃, and 0.06 M Na₂S₂O₄. The Fe concentrations in the solutions were measured by inductive coupled plasma (ICP) (Applied Research Laboratories 3580 ICP-OES) and used to calculate the average goethite concentration in the beads. Averaged over ten beads, the measured goethite concentration was 4.44 g L⁻¹ with a standard deviation of 0.52 g L⁻¹.

Table 4.1. Input parameters for the CD-MUSIC model

surface parameters		
surface area	82.2	m ² g ⁻¹
capacitance	0.9	F m ⁻²
site density for site 1	3.45	mol m ⁻²
site density for site 2	2.7	mol m ⁻²
surface reactions	log K	$\Delta z_0, \Delta z_d$
$\text{FeOH}^{-1/2} + \text{H}^+ \leftrightarrow \text{FeOH}_2^{+1/2}$	9.2	1, 0
$\text{Fe}_3\text{O}^{-1/2} + \text{H}^+ \leftrightarrow \text{Fe}_3\text{OH}^{+1/2}$	9.2	1, 0
$\text{FeOH}^{-1/2} + \text{Na}^+ \leftrightarrow \text{FeOH}^{-1/2} - \text{Na}^+$	-1.0	0, 1
$\text{Fe}_3\text{O}^{-1/2} + \text{Na}^+ \leftrightarrow \text{Fe}_3\text{O}^{-1/2} - \text{Na}^+$	-1.0	0, 1
$\text{FeOH}_2^{+1/2} + \text{Cl}^- \leftrightarrow \text{FeOH}_2^{+1/2} - \text{Cl}^-$	-1.0	0, -1
$\text{Fe}_3\text{OH}^{+1/2} + \text{Cl}^- \leftrightarrow \text{Fe}_3\text{OH}^{+1/2} - \text{Cl}^-$	-1.0	0, -1
$\text{FeOH}^{-1/2} + \text{H}^+ + \text{SO}_4^{2-} \leftrightarrow \text{FeOSO}_3^{-3/2}$	10.27	0.65, -1.65
$2 \text{FeOH}^{-1/2} + 2 \text{H}^+ + \text{CrO}_4^{2-} \leftrightarrow (\text{FeO})_2 \text{CrO}_2^-$	21	1, -1
$2 \text{FeOH}^{-1/2} + 3 \text{H}^+ + \text{CrO}_4^{2-} \leftrightarrow (\text{FeO})_2 \text{CrOOH}$	24.9	1, 0

4.2.2. Sorption model

Sulphate adsorption on goethite was described according to Rietra et al. (1999b), using the CD-MUSIC model (Hiemstra and Van Riemsdijk, 1996) with a Basic Stern electrostatic model. The model parameters are given in Table 4.1. Chromate sorption was described by the same model. The sorption parameters were fitted to describe chromate sorption data published by Mesuere and Fish (1992), shown in Figure 4.1. Two types of bidentate surface complexes were used to describe chromate adsorption. One of these complexes is protonated (see Table 4.1). The distribution of the charge between the surface plane and the Helmholtz electrostatic plane was estimated from the Pauling rule, assuming that the charge of the Cr(VI) atom is contributed equally between the four ligands (Rietra et al., 1999a).

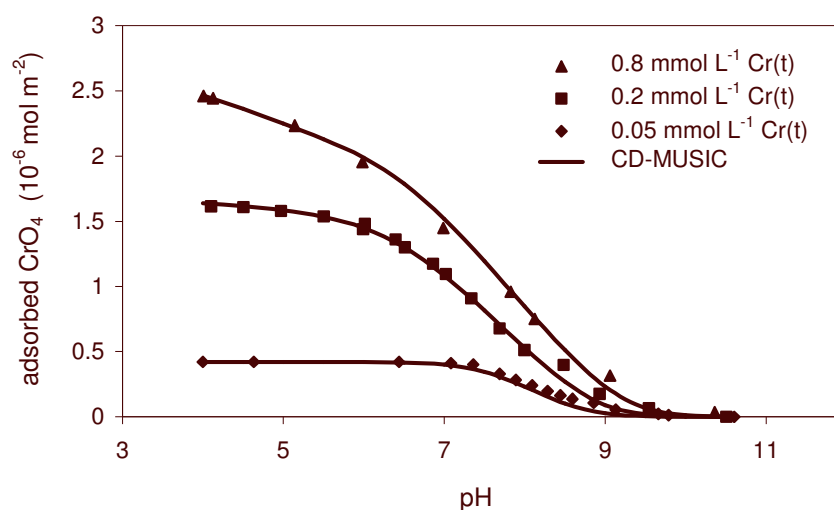


Figure 4.1. Chromate sorption edges measured by Mesuere and Fish (1992) and described by the fitted CD-MUSIC model (Table 4.1) for total chromate concentrations of 0.05, 0.2 and 0.8 mmol L⁻¹ in a 0.05 M KNO₃ electrolyte solution.

Table 4.2 shows the formation reactions of ionic complexes in solution and the formation constants that were used in the model. The activities of the ions in solution are calculated by multiplying their concentration with the activity coefficient (γ_i) calculated with the Davies equation:

$$\log \gamma_i = -0.51 z_i^2 \left(\frac{\sqrt{I}}{1 + \sqrt{I}} - 0.2I \right) \quad [4.1]$$

where I is the ionic strength, and z_i is the charge of the ion i .

4. Competitive sorption of chromate and sulphate

Table 4.2. Complexation of ions in solution

reactions	log K
$\text{SO}_4^{2-} + \text{Na}^+ \leftrightarrow \text{NaSO}_4^-$	0.7
$\text{SO}_4^{2-} + \text{H}^+ \leftrightarrow \text{HSO}_4^-$	1.98
$\text{SO}_4^{2-} + 2 \text{H}^+ \leftrightarrow \text{H}_2\text{SO}_4^0$	0.0
$\text{CrO}_4^{2-} + \text{Na}^+ \leftrightarrow \text{NaCrO}_4^-$	0.7
$\text{CrO}_4^{2-} + \text{H}^+ \leftrightarrow \text{HCrO}_4^-$	6.51
$\text{CrO}_4^{2-} + 2 \text{H}^+ \leftrightarrow \text{H}_2\text{CrO}_4^0$	5.65
$2 \text{CrO}_4^{2-} + 2 \text{H}^+ \leftrightarrow \text{Cr}_2\text{O}_7^{2-}$	14.56

4.2.3. Experiments

Goethite-gel beads from the same batch were reused for different equilibrium and column experiments during a two-year period. After each experiment with chromate or sulphate, the beads were packed in a column and leached with a 0.01 M NaCl solution at pH 9 for approximately 48 hours (~30 pore volumes) to desorb sulphate and chromate. After that the beads were re-equilibrated with 0.01 M NaCl at pH 4 by leaching for another 48 hours. All feed solutions were continuously purged with nitrogen gas to keep the CO_2 concentration low. Sulphate and chloride concentrations in effluent samples were analysed by ion chromatography (Dionex 600), and chromate concentrations were analysed by inductive coupled plasma (ICP) (Applied Research Laboratories 3580 ICP-OES; Thermo Jarrel Ash IRIS ICP-OES; or Agilent 7500i ICP-MS). All experiments were performed once, the results are therefore from single experiments (no replicates).

4.2.3.1. Sorption Isotherms

The sorption parameters used in this paper are taken from literature or derived from published sorption data. We assume that these parameters are valid for the goethite prepared for this work, and furthermore that the behaviour of the goethite is not affected by polyacrylamide. To test these assumptions, the sorption isotherms for sulphate and chromate were measured. Gel beads were initially equilibrated with a low- CO_2 , 0.01 M NaCl solution at pH 4. A series of 10 mL polyethylene tubes was prepared, with either 2 mL or 10 mL solutions, containing 0.01 M NaCl at pH 4, and a range in sulphate ($0\text{--}10^{-3}$ M) and chromate ($0\text{--}5 \cdot 10^{-4}$ M) concentrations. Ten goethite-gel beads were added (~0.5 mL containing 2.2 mg goethite) to each tube,

4. Competitive sorption of chromate and sulphate

and equilibrated on an orbital shaker for three days at a room temperature between 23 and 25°C. After equilibration, the sulphate and chromate concentrations in the solutions were sampled and analysed. The measurements were repeated for chromate sorption in a constant sulphate concentration (10^{-3} M) and for sulphate in a constant chromate concentration (10^{-4} M). The concentration of chromate was ten times smaller than the sulphate concentration to account for stronger chromate binding and to attain comparable concentrations of anions adsorbed on the goethite surface. The gel beads were first equilibrated in the appropriate sulphate or chromate concentration before the second solute was added. The influence of the second solute on the concentration of the first solute was assumed negligible. After equilibration for three days, the concentrations of the second solute were measured and the amount of sorption per gram goethite was calculated. To estimate the total solution volume, we assumed that the gel contains 1 mL water per gram.

4.2.3.2. *Tracer experiments with chloride*

Diffusion in the goethite-gel beads was tested using chloride as a non-reactive tracer. The diffusion rate out of the beads is measured and compared with the theoretical diffusion rate in water. At high chloride concentrations, the amount of chloride sorption is negligible, so the release of chloride from the gel beads is controlled by diffusion only. The goethite-gel beads were initially equilibrated with a low-CO₂, 0.1 M NaCl solution and 10^{-4} M HCl (~pH 4). One litre of batch solution was prepared containing 0.1 M NaNO₃ and 10^{-4} M HCl. One hundred beads were added to the batch solution in a large beaker, and the system was stirred by a magnetic stirrer. Before adding the beads, any excess solution was taken off with filter paper and the total bead weight was measured. Samples were taken from the batch solution manually several times during the first hour and once more after two hours. The solution temperature during the experiments varied between 17 and 19 °C. The chloride concentration in the samples was analysed by ion chromatography. The concentrations were used to calculate the cumulative release of chloride from the beads. The final concentration was estimated by taking the average of the two samples taken after 2 hours. The experiment was repeated without nitrate in the batch solution, to test whether counter-diffusion of nitrate ions has any effect on diffusion from the beads. Chloride was also used as a tracer to test the flow through the gel-bead column as described in the following paragraph.

4. Competitive sorption of chromate and sulphate

4.2.3.3. Column experiments

A borosilicate chromatography column with flow adapter (Sigma C4919) was filled with goethite-gel beads (4.6 mm diameter) and electrolyte solution. The inner diameter of the column was 2.5 cm and the length of the column bed was approximately 11.2 cm. After packing the column contained approximately 60% goethite-gel beads and 40% water-filled pore volume. The gel beads were equilibrated with electrolyte solution by pumping CO₂-free electrolyte solution through the column for approximately 20 hours. Feed solution was then pumped into the column at a constant flow rate using a peristaltic pump (Watson-Marlow 205U/CA). The CO₂ concentration in the feed solutions was kept at a minimum by purging with N₂ gas during the column experiments. All solutions were made up at pH 4 by adding 10⁻⁴ mol L⁻¹ HCl, unless stated otherwise. The effluent from the column was sampled with a fraction collector.

Table 4.3 gives an overview of the column experiments. For the tracer study (exp. 1-3), the column was equilibrated with 0.01 M NaCl, and then leached with 0.1 M NaCl solution at a low flow rate of 1·10⁻⁵ L s⁻¹ (exp. 1). The experiment was repeated at a flow rate of 4·10⁻⁵ L s⁻¹ (exp. 2). In another experiment the column was equilibrated with 0.012 M NaCl and leached with 0.01 M NaNO₃ solution for 2.5 hours at a flow rate of 7·10⁻⁵ L s⁻¹ (exp. 3a). Then nitrate solution was leached from the column with 0.01 M NaCl solution at the same flow rate (exp. 3b). Leaching of sulphate and chromate was measured in separate column experiments and in experiments with competition between the two ions. The columns were leached with chromate or sulphate at a flow rate of 1·10⁻⁵ L s⁻¹ for approximately 24 hours, after which full equilibration was expected. The chromate or sulphate was then leached from the column by pumping electrolyte solution into the column. For most experiments, the effluent was sampled during both parts of the experiment. The effluent pH was monitored online, using a flat surface electrode in a 200 µL flow-through cell. Sulphate leaching was repeated with different sulphate concentrations and two pH values (0.055 mmol L⁻¹ SO₄ at pH 5 (exp. 4) and 0.20 and 0.51 mmol L⁻¹ SO₄ at pH 4 (exp. 5 and 6)). Chromate leaching was performed with 0.1 mmol L⁻¹ CrO₄ at pH 4 (exp. 7). The concentration of chromate was lower than of sulphate to achieve similar levels of sorption and retardation.

For the column experiments with competition between chromate and sulphate, the column was first equilibrated with one of the two components. For the first experiment, the gel-bead column was equilibrated with 0.06 mmol L⁻¹ sulphate solution with the required electrolyte concentration. The column was then leached with the same sulphate concentration, but with added chromate (0.1 mmol L⁻¹).

4. Competitive sorption of chromate and sulphate

Table 4.3. Column experiments

no.	anions	concentr. in column (mmol L ⁻¹)	concentr. in feed (mmol L ⁻¹)	pH	flow rate (L s ⁻¹)	beads	V_b^a (mL)	V_m^a (mL)	T (°C)
1	Cl	10	100	4.0	$9.8 \cdot 10^{-6}$	650	33.6	19.1	18
2	Cl	10	100	4.0	$3.8 \cdot 10^{-5}$	650	33.6	18.9	17
3a	Cl	12	0	4.0	$7.3 \cdot 10^{-5}$	650	33.6	23.4	20
3b	Cl	0	10	4.0	$7.0 \cdot 10^{-5}$	650	33.6	21.1	20
4a	SO ₄	0	0.0545	5.0	$9.7 \cdot 10^{-6}$	645	33.3	22.8	17-18
5a	SO ₄	0	0.0202	4.0	$1.0 \cdot 10^{-5}$	650	33.6	20.4	19-20
5b	SO ₄	0.0202	0	3.9	$1.0 \cdot 10^{-5}$	650	33.6	20.4	19-21
6a	SO ₄	0	0.505	4.0	$9.2 \cdot 10^{-6}$	645	33.3	23.6	18-20
6b	SO ₄	0.505	0	4.0	$9.2 \cdot 10^{-6}$	645	33.3	23.6	18-20
7a	CrO ₄	0	0.101	4.0	$9.5 \cdot 10^{-6}$	650	33.6	18.4	17-20
7b	CrO ₄	0.101	0	4.0	$9.5 \cdot 10^{-6}$	650	33.6	18.4	18-20
8	CrO ₄	0	0.104	4.0	$9.6 \cdot 10^{-6}$	634	32.7	24.7	21-23
	SO ₄	0.069	0.063						
9	CrO ₄	0	0.110	4.0	$4.7 \cdot 10^{-5}$	634	32.7	25.3	21
	SO ₄	0.068	0.062						
10	SO ₄	0	1.04	4.0	$1.0 \cdot 10^{-5}$	650	33.6	21.7	19-21
	CrO ₄	0.021	0.021						
11	SO ₄	0	1.03	4.0	$8.0 \cdot 10^{-5}$	650	33.6	19.2	19
	CrO ₄	0.021	0.021						

^{a)} V_b is the bead volume and V_m is the mobile water volume in the column; The total volume of the column bed is the sum of V_m and V_b

4. Competitive sorption of chromate and sulphate

Both sulphate and chromate were analysed in the samples. The experiment was performed with a flow rate of $1 \cdot 10^{-5} \text{ L s}^{-1}$ (exp. 8) and repeated at $5 \cdot 10^{-5} \text{ L s}^{-1}$ (exp. 9). In a similar experiment, the column was first equilibrated with $2 \cdot 10^{-5} \text{ M}$ chromate solution, and then leached with the same solution also containing $1 \cdot 10^{-3} \text{ M}$ sulphate. The experiment was performed with a flow rate of $1 \cdot 10^{-5} \text{ L s}^{-1}$ (exp. 10) and repeated with $8 \cdot 10^{-5} \text{ L s}^{-1}$ (exp. 11). The concentrations of chromate and sulphate in the competition experiments were selected to achieve a strong effect of competition. The effect is expected to be stronger if the concentration of the inflowing ion is higher than the concentration of the initially present anion. If the competition experiments were done with similar concentrations of chromate and sulphate, then we would expect desorption of all sulphate when chromate is added, but no chromate desorption when sulphate is added.

4.2.4. Transport model

A two-region model was used to simulate solute transport in the column. The solution in the column is divided into an immobile region, representing the water in the gel beads, and a mobile region, representing the flowing solution surrounding the beads. We assume that the water fraction of the beads equals one, so that the volume of water in the gel beads (V_b) plus the volume of mobile solution in between the beads (V_m) equal the total internal volume of the column. Convection with the water flow down the column, and diffusion into the gel beads are calculated numerically. The mobile volume was divided into 20 vertically connected calculation cells (or nodes), each one connected to 10 horizontally connected cells representing concentric layers of a sphere. A more detailed description of the model can be found in Chapter 2. The model was implemented in ORCHESTRA (Meeussen, 2003), a framework for modelling chemical speciation and transport. Transport is calculated for small time steps and chemical speciation (in solution and at the goethite surface) is calculated by an iteration procedure after each mass transport calculation.

Diffusion was calculated for chromate, sulphate and protons simultaneously. The concentrations of the electrolyte ions were assumed constant. The electrostatic coupling of diffusion of charged ions was not included. Since the electrolyte concentration is high compared to the sulphate and chromate concentrations, it can be assumed that electroneutrality in the system during sulphate or chromate diffusion is maintained by the electrolyte without influencing the diffusion of sulphate and chromate.

4. Competitive sorption of chromate and sulphate

Diffusion was calculated using the diffusion coefficients for diffusion in water at 20°C. These coefficients were derived by linear interpolation of the diffusion coefficients at 18 and 25°C (Li and Gregory, 1974), resulting in $8.49 \cdot 10^{-9}$, $1.80 \cdot 10^{-9}$ and $7.07 \cdot 10^{-10} \text{ m}^2\text{s}^{-1}$ for H^+ , Cl^- and Ca^{2+} respectively. These diffusion coefficients were corrected by a factor for diffusion through the polyacrylamide gel, based on the results of the tracer diffusion experiments. The model does not include hydrological dispersion. The hydrological dispersion length in the column is expected to be similar to the diameter of the gel beads (Appelo and Postma, 1999). The estimated Peclet number is 24, based on the ratio between the dispersion length and the length of the column. However, the influence of hydrological dispersion on the shape of the breakthrough curve is insignificant in comparison to the dispersive effect caused by diffusion into the gel beads.

4.3. Results and discussion

4.3.1. Sorption isotherms

The measured sorption isotherms for chromate and sulphate with and without competition are shown in Figure 4.2. Figure 4.2a shows two sets of data for sulphate sorption without chromate. One set of sorption data (data 1) was measured up to 0.1 mmol L^{-1} sulphate. The experiment was repeated with higher sulphate concentrations (up to 1 mmol L^{-1}) to include the higher sulphate concentrations used in the flow experiments (data 2). Both data sets were used to compare with the model predictions. The model predictions were calculated for a goethite concentration of $4.44 \text{ g per litre gel volume}$ and the sorption parameters in Table 4.1. The dashed lines show the model predictions in the case of no competition. The model predicts slightly more adsorption than measured. Note that this model was determined completely independently and assumes no goethite-gel interaction. The description of the chemical model for both sulphate and chromate sorption can be improved by reducing the surface area of goethite by 20% (solid lines in Figure 4.2).

A possible reason for a less reactive surface could be the presence of the polyacrylamide gel. It has been shown that polyacrylamide interacts with aluminosilicate by forming hydrogen bonds with surface hydroxide groups (Pefferkorn, 1999). The polymer is likely to interact in a similar way with the goethite surface. Furthermore, polyacrylamide can contain impurities in the form of carboxylic groups, formed by hydrolysis of amino groups. The carboxylic groups have a high affinity for binding on positively charged surfaces and could therefore occupy part

4. Competitive sorption of chromate and sulphate

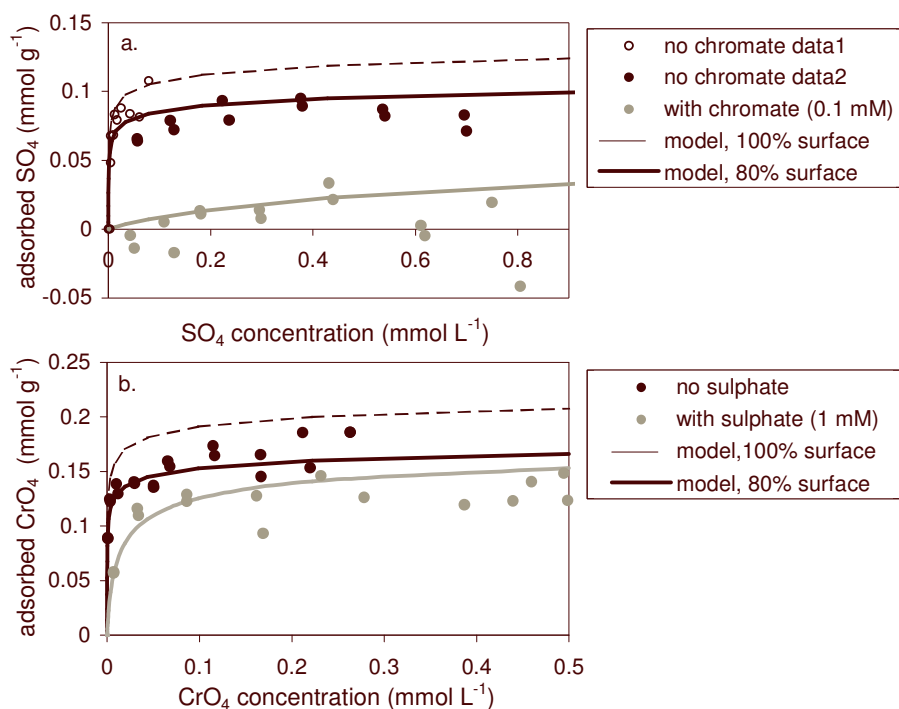


Figure 4.2. Adsorption isotherms for (a) sulphate and (b) chromate with competition (grey dots) and without competition (black dots). The sorption measurements for chromate were repeated at higher concentrations (data 2). The CD-MUSIC model with independent sorption parameters (dashed line) overestimates sorption of the individual ions (no competition). A better description was attained if only 80% of the surface was assumed available for adsorption (solid black and grey lines).

of the surface sites (Pefferkorn, 1999). Ideally, the interaction between polymer and goethite would be included in the model to account for competition between the polymer and the adsorbing anions. However, we lack information about the type and strength of interaction to produce a reliable description. For simplicity, we therefore assume that the amount of interaction is constant and can be described by a 20% reduction of the reacting surface area.

The effect of competition between sulphate and chromate is predicted fairly well with a 20% reduction of the surface area. The presence of chromate significantly reduced sulphate adsorption (Fig. 4.2a). The small amount of sulphate adsorption was negligible compared to the concentration in solution (<6%) and given the high

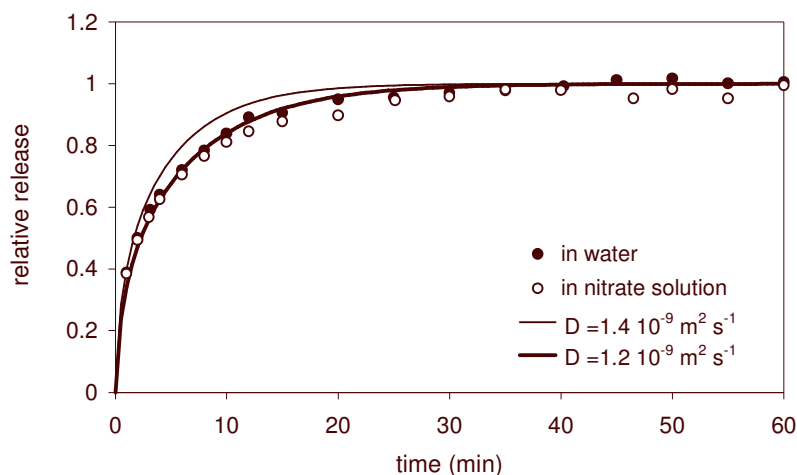


Figure 4.3 Chloride diffusion out of the goethite-gel beads into millipore water (solid dots) and into a solution of sodium nitrate (open dots), together with theoretical curves calculated from the diffusion coefficient in water (thin line) and the fitted diffusion coefficient (thick line).

variance within the measurements. This resulted in highly variable sorption (including negative values), but confirms the high competitive impact of chromate on sulphate sorption. Chromate sorption (Fig. 4.2b) is clearly less when 1 mM sulphate is present, in both the model and the measured data.

4.3.2. Tracer experiments

Figure 4.3 shows the results of chloride diffusion out of the goethite-gel beads. The cumulative release is plotted relative to the maximum release from the beads, estimated from the final samples taken after 2 hours. The batch volume decreased from 1 litre to 800 mL during the sampling, but the diffusion rate was not affected because the bulk concentration remained low compared to the initial concentration in the beads. There was no significant difference between diffusion into water and diffusion into nitrate solution. This indicates that the chloride diffusion rate is not affected by nitrate counter-diffusion. Both curves are described by a diffusion coefficient of $1.2 \cdot 10^{-9} \text{ m}^2 \text{ s}^{-1}$ (thick line). This is slightly lower than the diffusion coefficient of NaCl, which is $1.4 \cdot 10^{-9} \text{ m}^2 \text{ s}^{-1}$ (thin line), the average of Na^+ and Cl^- self-diffusion coefficients in water at 18°C (Li and Gregory, 1974).

The average diffusion coefficient for NO_3^- and Cl^- counter-diffusion would be even higher ($1.7 \cdot 10^{-9} \text{ m}^2 \text{ s}^{-1}$). These results suggest that diffusion in the gel is somewhat

4. Competitive sorption of chromate and sulphate

slower than diffusion in water. If we take diffusion of NaCl as a reference, then diffusion in the goethite-gel can be described by correcting the diffusion coefficient in water by a factor of 0.85. In previous work we found that the diffusion rate in alginate gel beads was similar to the diffusion rate in water. However, the polyacrylamide gel used here has a slightly higher polymer concentration than the alginate gel used in the previous work. The lower diffusion rate may be caused by tortuosity arising from the polymer structure or the goethite particles within the gel. Also, the viscosity of water inside the gel beads may be influenced by the polymer or the goethite surface.

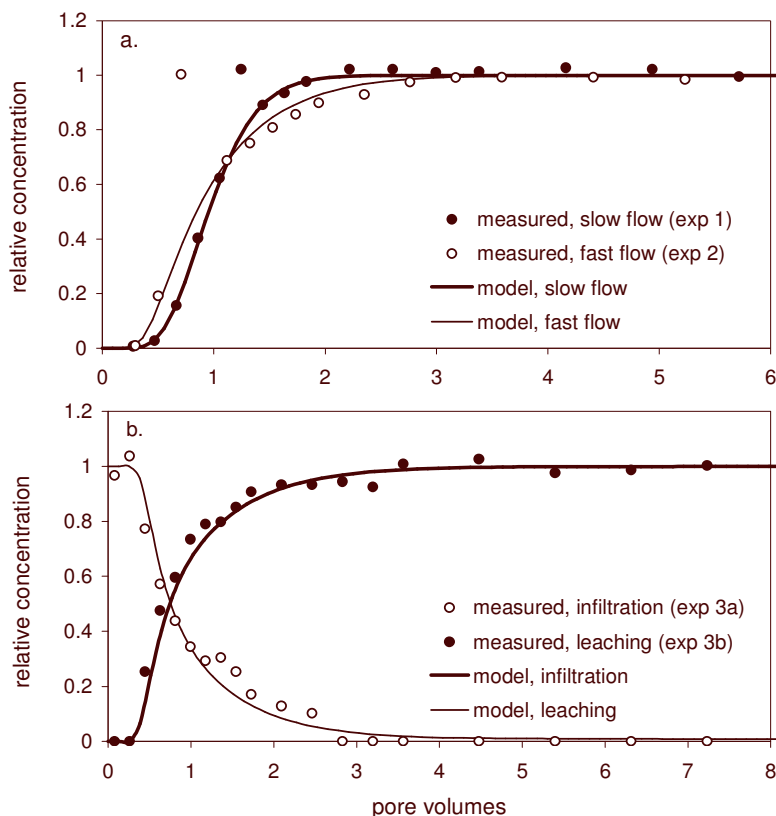


Figure 4.4. Chloride breakthrough curves from (a) infiltration at low ($1 \cdot 10^{-5} \text{ L s}^{-1}$) and high ($4 \cdot 10^{-5} \text{ L s}^{-1}$) flow rate, and (b) infiltration and leaching at a high flow rate ($9 \cdot 10^{-5} \text{ L s}^{-1}$). Concentrations are relative to the initial chloride concentration and the chloride concentration in the feed solution.

Figure 4.4. shows the results for chloride infiltration and chloride leaching from the column with goethite-gel beads, at different flow rates (exp. 1-3). Transport through the column was simulated with the transport model using the diffusion coefficient for chloride that was measured in the previous batch experiments (correction factor 0.85). The model simulations show good similarity with the measured results for chloride infiltration into the column at all flow rates as well as for chloride leaching out of the column. The results show that transport of a non-reactive ion in the gel-bead column can be predicted after a slight adjustment of the diffusion rate in water.

4.3.3. Breakthrough curves of sulphate and chromate

Sulphate and chromate infiltration and leaching from the columns was predicted with the transport model using the diffusion correction factor that was obtained from the tracer diffusion study (85% of the diffusion coefficients in water). In accordance with the results of the separate sorption experiments, 80% of the goethite surface was assumed reactive. Figure 4.5 shows the breakthrough curves for different sulphate concentrations (0.05, 0.2 and 0.5 mmol L⁻¹; exp. 4-6), together with the modelled breakthrough curves. Comparing the infiltration curves (left-hand side of Figure 4.5) shows that the retardation of the sulphate breakthrough curves (black dots) depends on the sulphate concentration in the feed solution. There is more retardation of the lowest concentration (exp. 4a) because of nonlinear sorption. Note that the results of the three experiments are plotted on different scales.

The model predictions give a reasonable prediction of the time of breakthrough. However, the measured curves are less sharp than the simulations, and they do not show the two-step increase as predicted by the model. The pH measurements (open dots in Figure 4.5) show a temporary increase in pH during the sulphate breakthrough, but not as large as the model calculations predict. The pH increases because sulphate adsorption is accompanied by the adsorption of protons. Meeussen et al. (1999) showed with a column of goethite-coated sand that the sulphate breakthrough front exhibits two steps for certain sulphate concentrations and pH values. The pH increases during the first step of the breakthrough. After a while the pH drops back to its initial value, accompanied by the second step. This effect on the breakthrough of sulphate was not observed in the measurements presented here because the pH change was too small. The two-step breakthrough curve would only show if the temporary pH change is large enough to decrease the affinity for sulphate sorption and reduce the retention time for the first sulphate

4. Competitive sorption of chromate and sulphate

front. The leaching curves of sulphate (right-hand side of Figure 4.5) do not show the same concentration dependence and pH changes as the infiltration curves. The reason is that not much sulphate desorbs during the leaching. The drop in sulphate concentration after one pore volume is mainly caused by the replacement of sulphate solution in the column by sulphate-free solution and is not retarded by desorption. Figure 4.2 shows that at a lot of sulphate is still adsorbed at low sulphate concentrations. Desorption slowly becomes more significant at low concentrations, and causes the tailing that is clear in the leaching curve of exp. 5b. Because sulphate desorption is gradual, it does not influence the effluent pH.

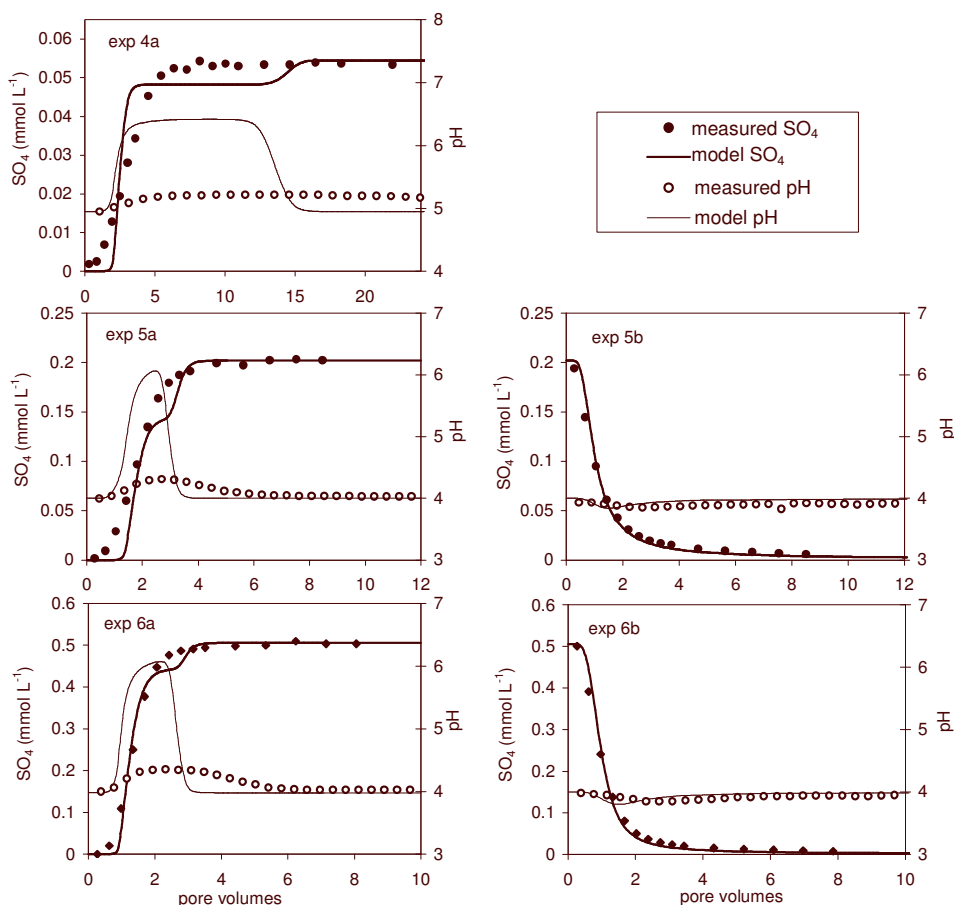


Figure 4.5. Measured and modelled breakthrough curves for sulphate infiltration (left) and leaching (right) of different sulphate concentrations (0.02, 0.05 and 0.5 mmol L^{-1} ; exp. 4-6).

Figure 4.6 shows the breakthrough curves for chromate infiltration and leaching. The pH did not change significantly, because the chromate concentration is low, and therefore only a small amount of protons adsorb during chromate infiltration. Breakthrough during infiltration (exp. 7a) takes place approximately at the same time as predicted by the model, however, again, the curve is less steep than the model predicts. The chromate leaching curve (exp. 7b) shows a faster decline of the chromate concentration during the first pore volumes than predicted by the model. This indicates that there is less chromate desorption during this period than the model predicts. However the tailing of the curve at higher pore volumes is predicted well.

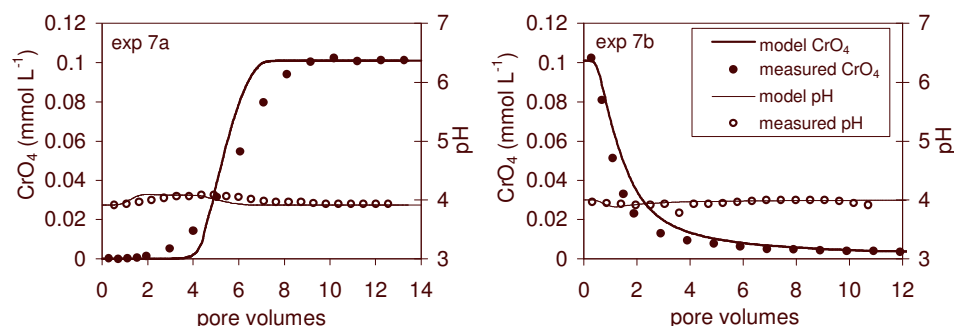


Figure 4.6. Breakthrough curves for chromate infiltration and leaching (exp. 7), measured data and curves predicted by the transport model. The pH of the effluent changes upon sulphate infiltration.

To investigate why the changes in pH during sulphate infiltration were not as large as predicted, we calculated the acidity of the leachate (H^+ minus the OH^- concentration) from the measured pH. The results are plotted in Figure 4.7. Although the measured pH peaks in Figure 4.5 are not as large as the model predicts, the total amount of protons that is taken up during sulphate adsorption is very similar to the amount predicted by the model. The modelled curve drops lower than the measured curve, but the measured curve stretches over a longer period. The area enclosed by the curves corresponds to the amount of protons that is adsorbed during the sulphate leaching, and is very similar for the modelled and measured curves. This shows that the amount of protons involved in the sorption process during sulphate and chromate transport is described correctly by the model. The spreading of the proton curves is possibly due to pH buffering by the polyacrylamide or by impurities in the form of acrylic acid. Acrylic acid has a pK_a of 4.26 (Swift, 2002), and will therefore buffer strongly around pH 4.

4. Competitive sorption of chromate and sulphate

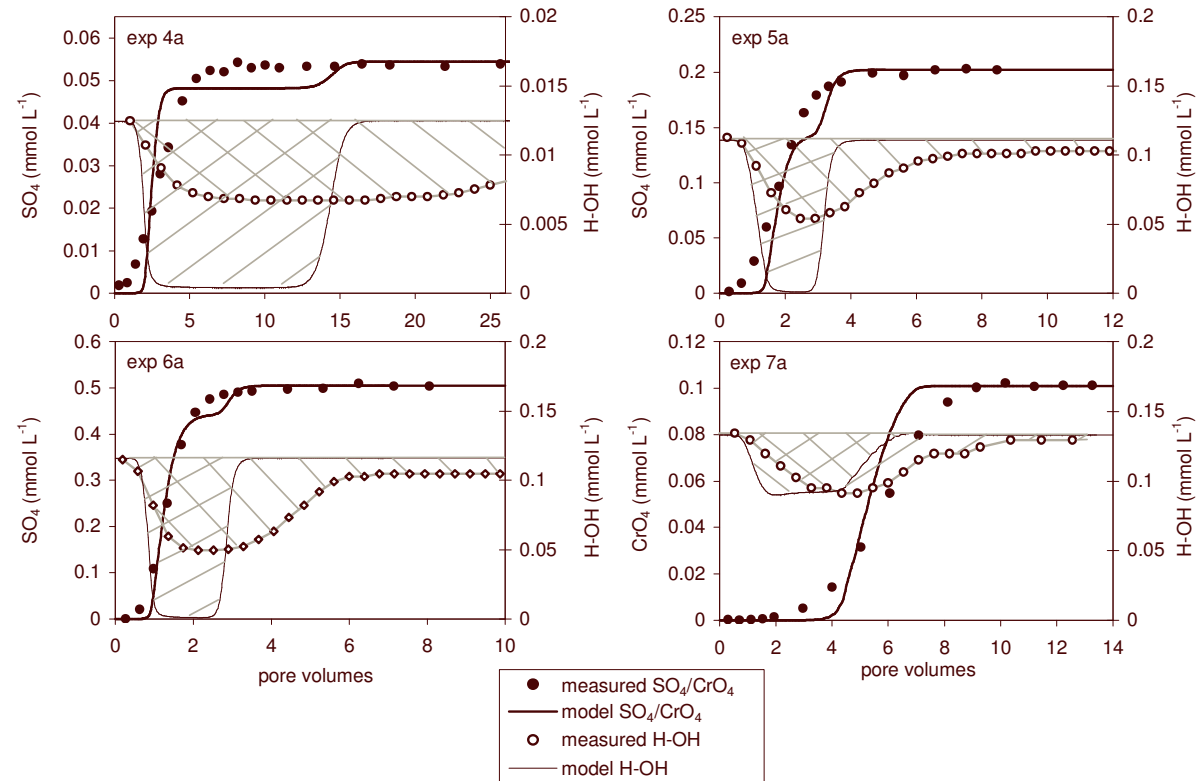


Figure 4.7. Breakthrough curves from sulphate (exp 4a, 5a, 6a) and chromate infiltration (exp. 7a), and the simultaneous change in proton concentration (H^+/OH^- concentration) calculated from the measured pH (open dots). The amount of protons involved in the pH change is indicated by the marked areas. The surface area described by the simulated proton curves (thin lines) is similar to the area described by the measured proton curves.

Buffering would suppress a change in pH, but would not affect the proton balance. In other words, the amount of protons that would be taken up by the system before the pH comes back to its initial value would be still be the same. The results in Figure 4.7 correspond to what would be observed in the case of proton buffering.

4.3.4. Competition between sulphate and chromate

Figure 4.8a shows the infiltration curves for chromate into a column initially equilibrated with sulphate. The chromate breakthrough curve at a low flow rate compares to the chromate breakthrough curve in Figure 4.6, only the curve has shifted slightly to the left, with its half-way point shifted from 6 to 4.5 pore volumes. This shows that competition with sulphate reduced the adsorption of chromate in the column. The results for the different flow rates in Figure 4.8a show the influence of diffusion into the gel beads. The curve at a higher flow rate shows a stronger effect of physical non-equilibrium, which is evident by an early breakthrough followed by tailing. The effect is more pronounced at higher flow rates because there is less time for diffusion during the shorter residence time in the column.

Figure 4.8b shows the response of sulphate to chromate infiltration. Adsorption of chromate causes sulphate desorption and a temporary increase of sulphate in the effluent. If we compare the sulphate curves at different flow rates we see that the peak is largest in case of slow flow, and flattened and spread over several pore volumes in case of fast flow. The effect of competition is less evident in the case of non-equilibrium transport than in a system closer to equilibrium.

Figure 4.9a shows the breakthrough curves for sulphate in a column at a constant chromate concentration. The sulphate breakthrough curves show no significant retardation and the average breakthrough even seems to occur slightly earlier than one pore volume. The model predicts no retardation either. This does not mean that no adsorption takes place, but sorption is small compared to the high concentration of sulphate. The effect of chromate on the retardation of sulphate is therefore also not visible.

Figure 4.9b shows the response of chromate to the sulphate breakthrough. According to the model predictions, the chromate concentration in the effluent would increase significantly during the sulphate breakthrough, from 20 to 70 $\mu\text{mol L}^{-1}$ at a low flow rate and from 20 to 50 $\mu\text{mol L}^{-1}$ at a high flow rate. However, the measured concentrations do not exceed 30 $\mu\text{mol L}^{-1}$.

4. Competitive sorption of chromate and sulphate

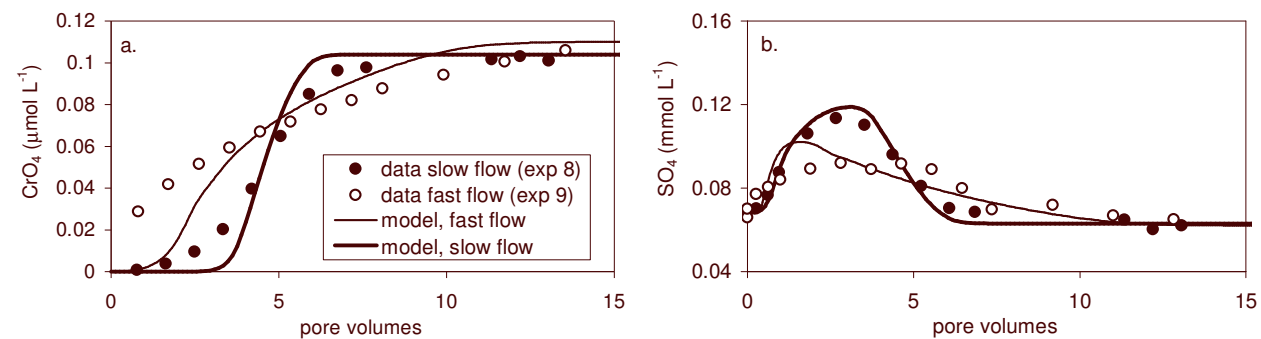


Figure 4.8. Chromate breakthrough curves (a), and the response in the sulphate concentration (b), at high ($4.7 \cdot 10^{-5} \text{ L s}^{-1}$) and low ($9.6 \cdot 10^{-6} \text{ L s}^{-1}$) flow rates (data from exp. 8-9).

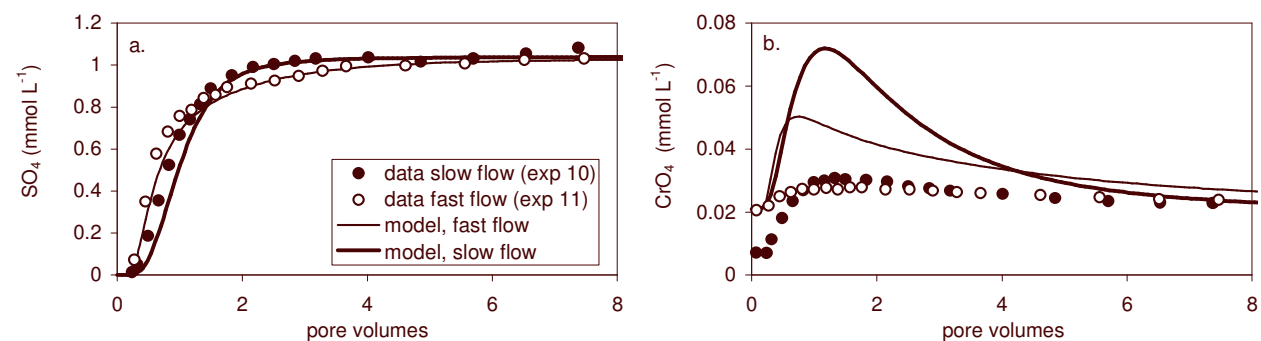


Figure 4.9. Sulphate breakthrough curves (a), and the response in the chromate concentration (b), at high ($8.0 \cdot 10^{-5} \text{ L s}^{-1}$) and low ($1.0 \cdot 10^{-5} \text{ L s}^{-1}$) flow rates (data from exp. 10-11).

The chromate concentration at a low flow rate also starts lower than expected, even though the column had been equilibrated at a low flow rate with a $20 \mu\text{mol L}^{-1}$ chromate solution for 14 pore volumes, before the start of the sulphate leaching. The reason for a lower concentration at the beginning of the experiment is not clear. The increase in concentration within one pore volume is probably mainly caused by the breakthrough of the higher concentration in the feed solution, and only very little by sulphate-chromate exchange.

It is surprising that the model predicts the competition effect well for chromate infiltration into a system with sulphate, but not for sulphate infiltration into a system with chromate. It seems as if sulphate adsorption is not strong enough to compete with the already bound chromate. This is contradictory, however, with the competitive effects that were measured in the separate sorption experiments (Fig. 4.2b). Those results suggest that chromate adsorption would decrease by 20 to 50% in 1 mM sulphate. It is possible that the exchange of bound chromate for sulphate is slow. It was shown for arsenate sorption on goethite that, although adsorption is relatively fast, desorption in the presence of phosphate (O'Reilly, 2001) and adsorption in the presence of silicate (Waltham and Eick, 2002) can be much slower, depending on the relative affinity for either of the competing anions. Sorption of chromate on goethite is very similar to arsenate adsorption (Fendorf et al., 1997), therefore desorption behaviour is expected to be similar. As the affinity of the surface is greater for chromate than for sulphate, it may well be that the exchange of adsorbed chromate against added sulphate is slower than between sulphate and added chromate. Then chromate release takes place over a longer period, and the change in concentration is hardly noticeable.

4.4. Conclusions

The synthetic flow system with gel beads proved a useful tool for the validation of transport modelling. We demonstrated that polyacrylamide gel can be used for the preparation of spherical gel beads and for immobilising goethite inside the gel. Sorption and diffusion were only slightly affected by the immobilisation in gel beads. The same method could be used to immobilise other materials, which opens up possibilities for column experiments with a variety of materials, such as minerals and organic sorbents found in soil.

The coupling of a transport model with spherical diffusion and a surface complexation model was successful in simulating the leaching of sulphate and chromate from a column with goethite in gel beads. The CD-MUSIC model

4. Competitive sorption of chromate and sulphate

described the effect of competition on the adsorption of chromate and sulphate on goethite in a batch system, although the measured surface area had to be reduced by 20%, possibly due to interactions between the gel and the mineral surface. The leaching of sulphate did not have the same effect on the pH in the leachate as was expected from modelling and as was observed on goethite-coated sand in an earlier study (Meeussen et al., 1996). The amount of protons that were involved was the same as predicted, but spread over a longer period due to pH buffering. A possible explanation for this buffering is the possible presence of carboxylic groups on the polyacrylamide structure.

The effect of competition between chromate and sulphate was predicted very well in a system where chromate was leached into a column equilibrated with sulphate. The sulphate release peak caused by chromate adsorption was predicted remarkably well at both flow rates. On the other hand, when sulphate was infiltrated in a column initially equilibrated with chromate, the measured chromate release was negligibly small. This is surprising because chromate sorption was significantly reduced in the batch sorption experiments with added sulphate. This could mean that the exchange process is fast for chromate adsorption and sulphate desorption, but slow for sulphate adsorption and chromate desorption. The more strongly bound chromate ions do not desorb within the short residence time in the column.

An interesting result from the sulphate release curves is the effect of physical non-equilibrium on the response peak. At a high flow rate, when the extent of non-equilibrium is the greatest, the sulphate peak is flattened and spread over a longer period than at a low flow rate. As a consequence, models that do not take physical non-equilibrium into account could overestimate the leaching concentration of the desorbed ions. This could have consequences, for example, for leaching from a contaminated soil as a response to the addition of other ions (for example by atmospheric deposition or human additions). Although the total amount that is released is the same, in a system with physical non-equilibrium this is expected to spread over a longer period and cause leaching at much lower concentrations.

5. Sorption kinetics of strontium in porous hydrous ferric oxide aggregates. I. The Donnan diffusion model

Wendy van Beinum, Annette Hofmann, Johannes C. L. Meeussen
and Ruben Kretzschmar

Journal of Colloid and Interface Science (2005), Vol. 283, pp. 18-28.

5. Sorption kinetics I. The Donnan diffusion model

Nomenclature

ε_0	dielectric constant in vacuum	$\text{C J}^{-1} \text{m}^{-1}$
ε_1	relative dielectric constant	-
τ^{-2}	tortuosity correction factor	-
ρ_a	aggregate bulk density	g m^{-3}
σ_0	total charge located on the 0-plane	C m^{-2}
σ_{DL}	total charge located in the diffuse layer	C m^{-2}
σ_D	total charge located in the Donnan phase	C m^{-2}
σ_d	total charge located on the d-plane	C m^{-2}
θ_a	aggregate porosity	-
ψ_D	electical potential in the Donnan phase	V
$\psi_{D,o}$	electical potential in the Donnan phase of the outer fraction of the aggregates	V
a	radius of the diffusion limited inner centre of the aggregates	m
A	surface area	$\text{m}^2 \text{g}^{-1}$
$C_{0,i}$	constant solution concentration outside the aggregates	mol m^{-3}
$C_{D,i}$	dissolved concentration in the Donnan phase	mol m^{-3}
$C_{D,o,i}$	dissolved concentration in the Donnan phase of the outer fraction of the aggregates	mol m^{-3}
C_i	concentration in solution	mol m^{-3}
$C_{p,i}$	dissolved concentration in the pore solution	mol m^{-3}
C_s	capacitance of the Stern layer	F m^{-2}
D_i^0	diffusion coefficient in water	$\text{m}^2 \text{s}^{-1}$
f	outer aggregate fraction for instantaneous access and sorption	-
F	Faraday constant	C mol^{-1}
F_i	diffusion flux for ion i	mol m^{-2}
K_i	surface complexation constant for ion i	-
M	cumulative mass taken up by aggregate	mol
M_{max}	maximum uptake by aggregate	mol
R	gas constant	$\text{J mol}^{-1} \text{K}^{-1}$
r	radial distance from aggregate centre	m
r_0	aggregate radius	m
S_i	adsorbed amount	$\text{mol g}^{-1} \text{HFO}$
$S_{o,i}$	adsorbed amount in the outer aggregate	$\text{mol g}^{-1} \text{HFO}$
T	temperature	K

Nomenclature (continued)

t	time	s
x	distance	m
z_0	charge distributed to the 0-plane	-
z_1	charge distributed to the d-plane	-
z_i	equivalent charge of the ion i	-

5.1. Introduction

Hydrous ferric oxide (HFO) is a common iron oxide mineral in aquatic and soil environments. Along with other oxides, such as aluminum hydroxide and goethite, it has the capacity to adsorb a wide range of trace elements including metal cations and oxyanions (Dzombak and Morel, 1990). Sorption controls the mobility and availability of contaminants in soils, and is important for risk assessment. Contaminant transport models are often based on equilibrium description of sorption processes. However, in many cases, a strong time-dependence of sorption has been observed (Sparks, 2000). A common observation is that sorption by hydroxides takes place in two steps: a fast initial step, and a slow subsequent sorption step that may continue for days to months (Barrow et al., 1989; Bérubé et al., 1967; Strawn et al., 1998; Fuller and Davis, 1993; Scheinost et al., 2001; Willett et al., 1988; Axe and Anderson, 1995, 1997; Trivedi and Axe, 1999, 2001a). The first step is attributed to fast sorption on the external surfaces of the oxide particles. The second step has been attributed to (i) intra-particle diffusion and sorption onto interior sites, (ii) slow redistribution of surface complexes (for example from monodentate to bidentate sites) (Sparks, 2000; Lützenkirchen, 2001) or (iii) surface precipitation (Sparks, 2000). For sorption by HFO, diffusion appears to be the dominating kinetic process (Fuller and Davis, 1993; Scheinost et al., 2001; Willett et al., 1988; Axe and Anderson, 1995, 1997; Trivedi and Axe, 1999, 2001a) due to the microporous structure of the mineral. Diffusion of ions in HFO has been explained as aqueous diffusion through pores (Fuller and Davis, 1993) and as surface diffusion where the adsorbed ions move along the internal surfaces (Scheinost et al., 2001; Axe and Anderson, 1997).

Axe and coworkers (Axe and Anderson, 1997; Trivedi and Axe, 2000, 2001a) reason that when pores are small compared to the size of the ion, an ion inside the pore never escapes the electrostatic force of the surface. To describe migration of cations into microporous hydrous oxides, they applied a surface diffusion model in

5. Sorption kinetics I. The Donnan diffusion model

which the ions move along the surface by hopping between sorption sites. Analogous with earlier models that describe gas diffusion in sorbents (Kärger and Ruthven, 1992), they relate the diffusion coefficient to the activation energy that is needed to free adsorbed ions from the surface. The surface diffusion model assumes that aqueous diffusion through the pores is negligible. This assumption is reasonable for microporous minerals in which the pores are smaller than approximately 2 nm and most of the pore space is occupied by hydration water. In larger pores, where unbound water is available, we consider that the use of a pore diffusion model is justified, and that the low diffusion rates of cations are explained by the electrical potential caused by the surface charge of the hydrous oxide. In this study we focus on diffusion in pores larger than 2 nm. These pores are well presented in the HFO aggregates that are used for demonstration in this and in the next chapter (Chapter 6).

Large HFO aggregates (diameter 0.23 mm) were produced by freezing and thawing of HFO suspension (Chapter 6). In these aggregates the pores range from 0.5 to 15 nm, however, pores smaller than 2 nm only make up 8% of the total pore volume (Hofmann et al., 2004). In these aggregates we model the diffusion by aqueous diffusion through the pores, constrained by electrostatic effects. The rate at which ions migrate deeper into the aggregate via the pore solution is directly related to the equilibrium concentration in the pore solution. Therefore, if an ion is repulsed from the pore solution, it will take much longer before equilibrium sorption is accomplished. Sato et al. (1995) developed a model for smectites in which they adjusted the diffusion rate according to the electrostatic repulsion or attraction of ions. The negatively charged surface of smectite causes faster diffusion of cations and slower diffusion of anions. The model was successfully tested for diffusion of several anions and cations (Sato et al., 1995; Kato et al., 1995; Ochs et al., 1998, 2001). The repulsion or attraction of ions was calculated using the Gouy-Chapman description of a diffuse layer. The average ion concentration in the pore space between two smectite surfaces was corrected for the two diffuse layers of both surfaces. This approach is not suitable for heteromorphous pores as found in HFO because it assumes a flat surface and an infinite bulk solution. The diffuse layers that develop in the small pore spaces in HFO are distorted by the surface curvature of the unit crystallites. Also, significant overlap occurs due to the proximity of the surrounding pore walls (Fig. 5.1b). Moreover, the surface charge of HFO is in many cases so high that the total repulsion predicted by the diffuse layer model would exceed the charge of the available ions in the small pore volume. For overlapping diffuse layers, it is more appropriate to use a Donnan model to describe the electrical potential in the pores

(Seke et al., 2000). The Donnan model assumes an equal electrical potential throughout the pore (Fig. 5.1c).

In this paper we introduce a new approach to modeling the electrostatic effect on ion diffusion in small heteromorphous pores. We use the Donnan model to calculate the electrical potential and the concentration of ions in the pores. The Donnan volume equals the pore space available for diffusion. Diffusion of ions within the pores is calculated from the concentration and electrostatic gradients in the Donnan phase, and from the diffusion coefficients reported for diffusion in water. This approach is demonstrated for Sr diffusion and adsorption in HFO aggregates at a range of pH values. Because iron oxides have a pH dependent surface charge, pH is a key factor that influences sorption and diffusion. The diffusion rates that are predicted by our Donnan diffusion model are compared with those predicted by a pore diffusion model in which no electrostatic effects are considered.

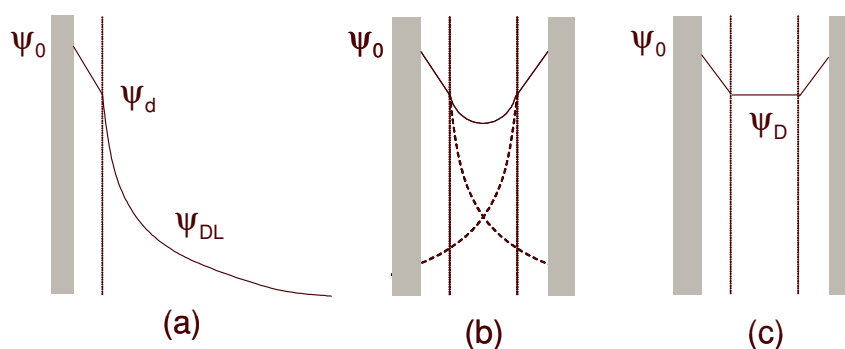


Figure 5.1. Schematic representation of the electrical potential; a) for the Basic Stern model with unlimited space for a diffuse layer, b) for overlapping diffuse layers within limited space, and c) for the Donnan model; where ψ_0 = surface potential, ψ_d = potential at head of the diffuse layer, ψ_{DL} = potential in the diffuse layer and ψ_D = Donnan potential. The figures are for illustration of the theory and are not meant to give a realistic picture of the potential distribution in the aggregate pores.

5. Sorption kinetics I. The Donnan diffusion model

5.2. Methods

The following sections describe the development of the Donnan diffusion model. The model is derived from a surface complexation model for HFO described in the first section. The parameters for the surface complexation model were determined in sorption experiments independently of the diffusion experiments (Chapter 6). These sorption measurements were carried out with the same HFO but with well dispersed mineral instead of aggregates to ensure equilibrium sorption. The derived surface complexation model is used here to predict diffusion into large porous HFO aggregates. The electrical potential inside the aggregates pore space is described by a Donnan electrostatic model. Strontium diffusion into the porous HFO aggregates is predicted by diffusion of the ions through the aggregate pores, taking into account the local concentration of the ions in the Donnan phase, the forces on the charged ions caused by a potential gradient, and sorption on the HFO internal surfaces. All parameters needed to predict Sr diffusion in the aggregates were derived independently. Sorption on HFO varies strongly with pH, therefore diffusion is simulated for a range of pH values. The results of the Donnan diffusion model are compared with the results from a free pore diffusion model in which the effect of electrical potential on diffusion through the pores is neglected. To allow comparison between the two models, the uptake rates predicted by the models are quantified by an apparent diffusion coefficient for every simulation. The apparent diffusion coefficient is a measure for the macroscopic uptake rate without any description of a specific diffusion mechanism. This parameter can be estimated analytically from the ratio between sorption and pore concentration without the need for a diffusion model, but only after simplification. These analytical estimates are further derived in the following method sections and compared with the results of the diffusion model in the results section.

5.2.1. Surface complexation model

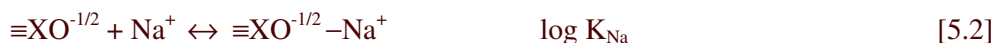
To model the electrostatic constraint on pore diffusion, it is essential to use an appropriate description of the surface charge and potential at the HFO surface. To describe the HFO surface chemistry we use the CD-MUSIC model developed by Hiemstra and Van Riemsdijk (Hiemstra et al., 1989; Hiemstra and Van Riemsdijk, 1996), a surface complexation model for oxides, where the description of the reactive sites is based on the atomic structure along crystallographic planes. For goethite, they define singly ($\text{FeOH}^{-1/2}$), doubly (Fe_2OH^0) and triply coordinated ($\text{Fe}_3\text{O}^{-1/2}$) surface oxygens. The doubly coordinated oxygens are assumed to be zero

charged and stable within normal pH ranges, and do not contribute to the surface charge in the model. Singly and triply coordinated oxygens have a similar charge. For goethite, the same protonation constant is used for both sites, equal to the pristine point of zero charge (PPZC) of goethite.

Hydrous ferric oxide has a poorly ordered crystallographic structure containing hydroxyl groups and water in its lattice. In analogy with goethite, we assume the following reaction with a $\log K_H$ that equals the PPZC for HFO:



in which XO represents either a singly or a triply coordinated surface oxygen. Part of the surface charge is neutralized by the formation of ion pairs with electrolyte ions:



The model parameters were determined experimentally on well dispersed HFO (Chapter 6). For this material, the electric double layer at the surface is described by a Basic Stern model (Westall and Hohl, 1980) with an unrestricted diffuse layer (Fig. 5.1a). The equations used are shown in Table 5.1. The CD-MUSIC model describes the contribution of adsorbed ions to the charges on the different electrostatic planes. Adsorbed protons contribute to the surface charge at the 0-plane, and the ions that form ion pairs are treated as point charges in the d-plane. The Stern-layer in between the two planes is considered charge free, with a capacitance C_s . The sum of charge in both planes is counterbalanced by ions in the diffuse layer. The model parameters were determined by acid base titration (Chapter 6) and are summarized in Table 5.2. Sr adsorption is described by monodentate binding on negatively charged sites.



The fitting of the model parameters (Chapter 6) implied a charge distribution with 34% of the Sr^{2+} charge allocated to the surface and 66% allocated to the d-plane.

5. Sorption kinetics I. The Donnan diffusion model

Table 5.1. Electrostatic models

model	charge balance ^{a)}	relationship between charge and potential ^{a)}
Basic Stern (for non-aggregated HFO)	$\sigma_0 + \sigma_d + \sigma_{DL} = 0$	$\sigma_0 = C_S (\psi_0 - \psi_d)$ $\sigma_{DL} = \pm \sqrt{2000 \epsilon_0 \epsilon_1 RT} \sqrt{\sum C_i (e^{-z_i \psi_d F / RT} - 1)}$
adapted Basic Stern with Donnan phase (for aggregates)	$\sigma_0 + \sigma_d + \sigma_D = 0$	$\sigma_0 = C_S (\psi_0 - \psi_d)$ $\sigma_D = \frac{\theta_a}{A \rho_a} \sum_i z_i F C_i e^{-z_i \psi_d F / RT}$

^{a)} See Nomenclature list for explanation of the symbols

Table 5.2. Surface complexation parameters for HFO determined in Chapter 6

parameter	value
surface area	600 m ² g ⁻¹
site density	4.0 nm ⁻²
capacitance C_S	1.07 F m ⁻²
log K_H	8.7
log K_{Na}	-1.5
log K_{NO_3}	-1.5
log K_{Sr}	4.47
z_0, z_1	0.68, 1.32

5.2.2. Donnan electrostatic model

The same surface chemistry model as described above is used for the porous HFO aggregates, only the diffuse layer model was replaced by a Donnan model (Fig. 5.1c). The Donnan model is based on the following assumptions:

- the Donnan volume is constant and equals the total pore volume minus the volume of the Stern layer
- the electrical potential in the Donnan phase is constant with distance from the d-plane
- the sum of charges at the surface, the d-plane and in the Donnan phase is zero
- the boundary where the electrical potential changes from Donnan potential to zero potential, lies at the external surface of the aggregate

The equations for the Donnan model are shown in Table 5.1. It is difficult to estimate the pore volume occupied by the Stern layer. For a surface area of 600 m²g⁻¹ with a Stern layer thickness of 0.6 nm, in an aggregate with a porosity of 0.75, the Stern layer would take approximately 48% of the pore volume. The simulations are performed for the maximum Donnan volume possible (i.e. the total pore volume), and for half this value, to estimate the sensitivity for the Donnan volume.

In surface complexation models, the intrinsic surface complexation constants (log K values) are corrected for columbic effects that originate from the electrostatic charge at the surface. These constants reflect the energy involved in

5. Sorption kinetics I. The Donnan diffusion model

sorption of ions that are already located at the surface. The energy involved in the positioning of an ion at the surface is accounted for by the electrostatic model, which can be the description of a diffuse layer or a Donnan model, depending on the geometry of the system. The intrinsic surface complexation constants are in theory independent on the geometry of the system. Therefore, in theory, these constants should be the same for the dispersed particles as for the aggregated particles, despite the change of geometry, the overlapping of diffuse layers and the substitution of the diffuse layer by a Donnan volume. Under this assumption, we used the sorption parameters as estimated from acid-base titration and sorption curves measured on well-dispersed HFO (Chapter 6). The electrical potentials in the models are treated as unknowns and are solved by iteration using the equations for the charge balance and for the relationships between the concentrations and potentials (Table 5.1).

5.2.3. Donnan diffusion model

The HFO aggregates are assumed spherical, with identical radius (r_0) and a homogeneous distribution of pore space and reactive surface. Part of the reactive surfaces is assumed to be external (fraction f) and therefore immediately accessible for Sr sorption. Likewise, the Donnan volume is divided into an immediately accessible fraction (f) and diffusion limited fraction ($1-f$). The effective radius of the diffusion limited centre (a) is calculated to represent the diffusion limited volume of the aggregates:

$$\frac{4}{3}\pi a^3 = (1-f) \frac{4}{3}\pi r_0^3 \quad [5.5]$$

Diffusion into the aggregate is described by diffusion in the Donnan phase. The driving forces for diffusion of an ion are its concentration gradient and the electrical potential gradient in the Donnan phase. The diffusion flux (F_i) of ion i is described by the Nernst-Planck equation, adjusted for a porous system by multiplying the diffusion coefficient in water with the porosity and tortuosity correction:

$$F_i(x,t) = -\theta_a \tau^{-2} D_i^0 \left(\frac{dC_{D,i}(x,t)}{dx} + z_i C_{D,i} \frac{F}{RT} \frac{d\Psi_D(x,t)}{dx} \right) \quad [5.6]$$

where F_i is the diffusion flux of ion i in $\text{mol m}^{-2}\text{s}^{-1}$ and C_D is the concentration in the Donnan phase in mol m^{-3} . See the Nomenclature list for the definitions of the other symbols. The diffusion coefficients for diffusion in water (D_i^0) for the different ions are shown in Table 5.3. In the model, diffusion into the diffusion

limited centre of the aggregates ($0 \leq r < a$) is calculated assuming radial symmetry, under which assumption the radial geometry reduces to a one dimensional system. The mass balance equation for the diffusion limited aggregate centre ($0 \leq r < a$) is given by:

$$\begin{aligned} \theta_a \frac{\partial C_{D,i}(r,t)}{\partial t} + \rho_a \frac{\partial S_i(r,t)}{\partial t} = \\ \theta_a \tau^{-2} D_i^0 \left\{ \left(\frac{\partial^2 C_{D,i}(r,t)}{\partial r^2} + \frac{2}{r} \frac{\partial C_{D,i}(r,t)}{\partial r} \right) \right. \\ \left. + z_i C_{D,i} \frac{F}{RT} \left(\frac{\partial^2 \psi_D(r,t)}{\partial r^2} + \frac{2}{r} \frac{\partial \psi_D(r,t)}{\partial r} \right) \right\} \end{aligned} \quad [5.7]$$

The model is solved numerically for the following boundary conditions:

- radial symmetry, therefore no gradients across the centre of the spheres,

$$\frac{\partial C_{D,i}(r,t)}{\partial r} = 0; \quad \frac{\partial \psi_D(r,t)}{\partial r} = 0 \quad \text{for } r = 0 \text{ and } t > 0 \quad [5.8]$$
- the Donnan concentration of the outer fraction of the aggregates is in equilibrium with the constant solution concentration outside the aggregates (C_0),

$$C_{D,i}(r,t) = C_{o,i} \exp \left(- \frac{z_i F}{RT} \psi_{D,o} \right) \quad \text{for } r = a \text{ and } t > 0 \quad [5.9]$$

The bulk solution concentration (C_0) outside the aggregates is assumed to be constant and is not part of the mathematical model. The total concentration of Sr (including sorption) associated with the outer and inner fractions of the aggregates are described by:

$$\text{Outer Sr concentration}(r = a) = f (\theta_a C_{D,o,i} + \rho_a S_{o,i}) \quad [5.10]$$

$$\text{Internal Sr concentration}(0 \leq r < a) = (1 - f) \{ \theta_a C_{D,i}(r,t) + \rho_a S_i(r,t) \} \quad [5.11]$$

5. Sorption kinetics I. The Donnan diffusion model

Table 5.3. Parameter input values for the simulations determined by curve

parameter	value	units	reference
aggregate dry bulk density (ρ_a)	1.0	kg L ⁻¹	Hofmann et al., 2004 ^{a)}
aggregate diameter (r_0)	$2.35 \cdot 10^{-4}$	m	Hofmann et al., 2004
fraction of external sorption sites (f)	0.55		Chapter 6 ^{b)}
porosity (θ)	0.73		Hofmann et al., 2004
D^0 for Sr ²⁺	$7.1 \cdot 10^{-10}$	m ² s ⁻¹	Li and Gregory, 1974 ^{c)}
D^0 for H ⁺	$8.5 \cdot 10^{-9}$	m ² s ⁻¹	Li and Gregory, 1974 ^{c)}
D^0 for OH ⁻	$4.7 \cdot 10^{-9}$	m ² s ⁻¹	Li and Gregory, 1974 ^{c)}
tortuosity factor (τ^{-2})	0.5		approximation
initial Sr concentration in batch	$1 \cdot 10^{-4}$	mol L ⁻¹	
electrolyte concentration (NaNO ₃)	0.01	mol L ⁻¹	

^{a)} Calculated from wet density (1.8 kg L⁻¹) and porosity (0.73)

^{b)} External site fraction at pH 7 estimated from outer pore volume fraction and pore size distribution (Fig. 6.5b in Chapter 6)

^{c)} Diffusion coefficients at 20°C found by linear interpolation of the values reported at 18 and 25°C

A finite difference scheme is used for the numerical calculations. A sphere with radius a is divided into ten discrete concentric layers of equal thickness, each layer being represented by a calculation cell with its own volume and surface area. Earlier work showed that ten calculation cells (representing ten concentric layers) are sufficient to give an accurate solution for spherical diffusion (Chapter 2). Diffusion is calculated by mass transfer between the calculation cells for small time steps. The length of the time steps is adjusted for every simulation, depending on the pH and the chemical conditions. Between the mass transfer steps, the new chemical equilibrium in every calculation cell is calculated by an iteration process. The numerical model is implemented using the computer program ORCHESTRA, an object-oriented framework for implementing chemical equilibrium and transport models (Meeussen, 2000, 2003). Using a numerical approach has several advantages over analytical solutions. First, in a numerical model, it is possible to calculate diffusion in combination with complex sorption models, whilst analytical solutions are restricted to simpler models. Second, with a numerical model it is possible to calculate simultaneous diffusion of several interacting ions. For example, for Sr diffusion, adsorption of Sr will cause desorption of protons and therefore a proton gradient in the opposite direction. These local pH changes can have significant effects on the Sr diffusion rate. In the Donnan diffusion model, the diffusion of Sr ions, protons and hydroxyl ions are calculated simultaneously from their local concentrations in the Donnan phase. The concentration of electrolyte ions in the pores is much higher than of the other ions. Therefore we assume that sorption and desorption of Sr cannot alter the equilibrium situation of the electrolyte ions. We assume that the Donnan concentrations of these ions in the pores are in equilibrium with the 0.01 M bulk solution concentration at any time.

Input for the model is given in Table 5.3. Model comparisons are based on a batch system with HFO aggregates and a constant outside concentration of 10^{-4} mol L⁻¹ Sr. The aggregate physical characteristics are taken from Chapter 6. The diffusion coefficients for Sr²⁺, H⁺ and OH⁻ at 20°C are estimated by linear interpolation of the diffusion coefficients in water at 18 and 25°C (Li and Gregory, 1974). The tortuosity correction factor (τ^{-2}) is estimated assuming homogeneous packing of spherical micro-particles in the aggregates. Assuming that a ratio between the effective path length and the shortest distance (τ) is 1.4, the tortuosity correction factor equals 0.5 (Appelo and Postma, 1999). Diffusion and sorption in the aggregates is simulated for a range of pH values between pH 4 and 10.

5. Sorption kinetics I. The Donnan diffusion model

5.2.4. Free pore diffusion model

For comparison, Sr diffusion in the HFO aggregates was also simulated using a pore diffusion model that does not take the electrostatic influence on diffusion into account. Diffusion is solved similar to the description given above, for the same spherical aggregates with equal properties. In this case diffusion in the pores is not influenced by the electrical potential. The entire pore space is available for free diffusion with the same diffusion rate as in water (D^0 , Table 5.3), and after equilibrium is reached, the pore concentration equals the concentration in the bulk solution. Diffusion in the pores is calculated from the concentration gradient in the pore solution:

$$F_i(x, t) = -\theta_a \tau^{-2} D_i^0 \frac{dC_{p,i}(x, t)}{dx} \quad [5.12]$$

where C_p is the concentration in the pore solution in mol m^{-3} . Sr sorption is calculated with the same surface complexation model described above, but using a Gouy-Chapman description of a diffuse layer instead of a Donnan phase. In the model this diffuse layer, however, does not take up any pore space, and is not considered in the mass balances of the ions.

$$\theta_a \frac{\partial C_{p,i}(r, t)}{\partial t} + \rho_a \frac{\partial S_i(r, t)}{\partial t} = \theta_a \tau^{-2} D_i^0 \left(\frac{\partial^2 C_{p,i}(r, t)}{\partial r^2} + \frac{2}{r} \frac{\partial C_{p,i}(r, t)}{\partial r} \right) \quad [5.13]$$

The model is solved numerically in ORCHESTRA with the following boundary conditions:

radial symmetry, therefore no gradients across the centre of the spheres,

$$\frac{\partial C_{p,i}(r, t)}{\partial r} = 0 \quad \text{for } r = 0 \text{ and } t > 0 \quad [5.14]$$

the pore concentration of the outer fraction of the aggregates is in equilibrium with the constant solution concentration outside the aggregates (C_0),

$$C_{p,i}(r, t) = C_{o,i} \quad \text{for } r = a \text{ and } t > 0 \quad [5.15]$$

Pore diffusion simulations were performed for a range of pH values from pH 4 to 10. The pH was set constant in the first set of simulations. In an additional set of simulations, the pH allowed to vary due to H^+ sorption and desorption and H^+/OH^- diffusion.

5.2.5. Comparison of apparent diffusion rates

The results of the numerical model simulations for some pH values are shown in Figures 5.2 and 5.3. The curves show the cumulative uptake of Sr by the aggregates plotted against time. Figure 5.2 shows simulation results of the Donnan diffusion model, and Figure 5.3 results of the free pore diffusion model. To allow quantitative comparison between the results of the two models, apparent diffusion coefficients (D_a) were fitted to the resulting curves. The apparent diffusion coefficient gives a macroscopic measure of the uptake rate into the aggregates. It reflects the overall uptake rate without specifying the diffusion mechanism.

Diffusion as a function of the apparent diffusion coefficient is described by

$$\frac{\partial C_i(r,t)}{\partial t} = D_a \left(\frac{\partial^2 C_i(r,t)}{\partial r^2} + \frac{2}{r} \frac{\partial C_i(r,t)}{\partial r} \right) \quad [5.16]$$

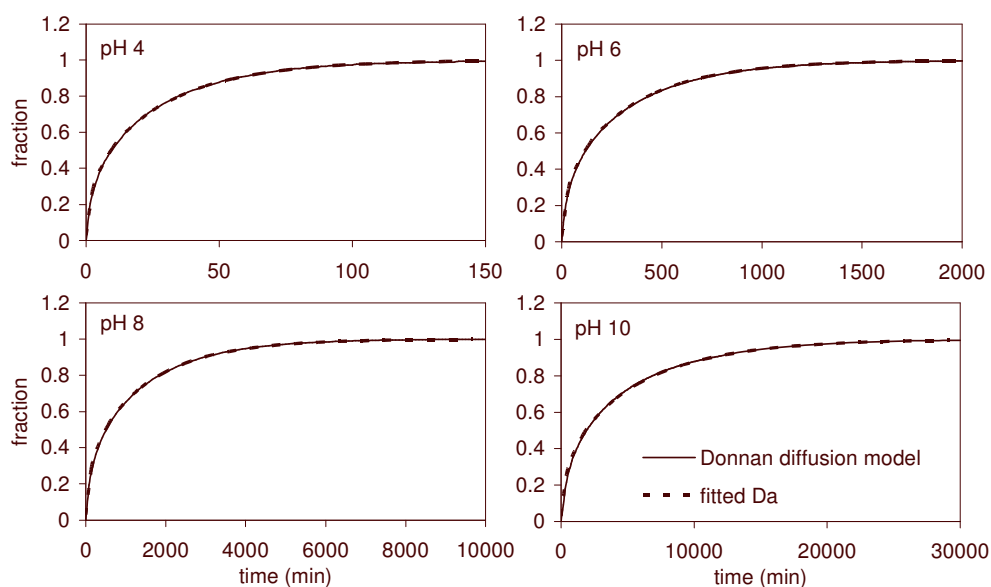


Figure 5.2. Simulations of Sr sorption to HFO aggregates with all calculations performed in a constant bulk solution of 10^{-4} M Sr and 0.01 M NaNO_3 . Simulations with the Donnan diffusion model are shown for pH 4, 6, 8, and 10 (solid lines). The dashed lines are found by fitting the apparent diffusion coefficient D_a in Equation 5.20 to the simulation results.

5. Sorption kinetics I. The Donnan diffusion model

This equation can be solved semi-analytically if the apparent diffusion coefficient is constant during the diffusion process, and subject to the following boundary conditions:

$$C_i(r, t) = 0 \quad t = 0, 0 \leq r < a \quad (\text{initial concentration}) \quad [5.17]$$

$$C_i(r, t) = C_{0,i} \quad r = a, t \geq 0 \quad (\text{constant bulk concentration}) \quad [5.18]$$

$$\frac{\partial C_i(r, t)}{\partial r} = 0; \quad r = 0, t \geq 0 \quad (\text{radial symmetry}) \quad [5.19]$$

The cumulative uptake as a function of time $M(t)$ can then be described by (Crank, 1956):

$$\frac{M(t)}{M_{\max}} = 1 - \frac{6}{\pi^2} \sum_{n=1}^{\infty} \frac{1}{n^2} \exp\left(-\frac{D_a n^2 \pi^2 t}{a^2}\right) \quad [5.20]$$

The maximum uptake M_{\max} is calculated from the final concentration in the pores and the equilibrium amount of sorption. The apparent diffusion coefficient is model dependent and is used here to quantify the model differences.

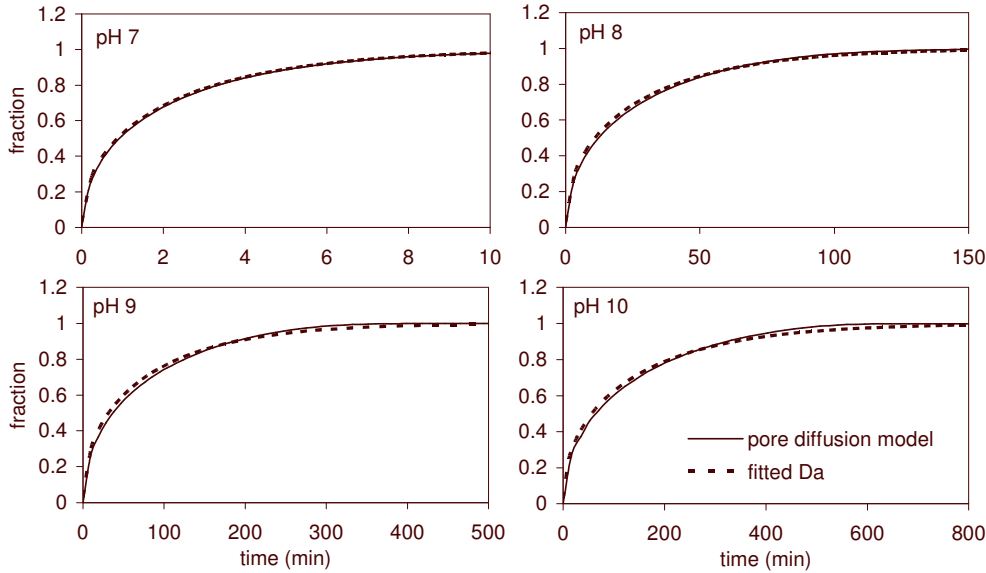


Figure 5.3. Simulations with the free pore diffusion model for pH 7, 8, 9 and 10 (solid lines). The dashed lines are found by fitting the apparent diffusion coefficient D_a in Equation 5.20 to the simulation results.

5.2.6. Simplified approximations for apparent diffusion coefficients

The combination of sorption and diffusion can be estimated with analytical solutions only with a number of simplifications. The effect of sorption can be solved if a linear sorption isotherm is assumed. It is not possible to include the effect of proton desorption and local pH changes on Sr sorption; the pH has to be assumed constant. Also the contribution of an electrostatic potential gradient to diffusion in the Donnan phase cannot be taken into account. Still, if used with caution, this approach can be useful to estimate the diffusion rate. It is of particular use to investigate how the diffusion rate is influenced by the amount of sorption and the concentration in the Donnan phase. The apparent diffusion coefficient is derived from the transport equation for diffusion as follows. The transport equation for diffusion into an aggregate is:

$$\theta_a \frac{\partial C_i(r,t)}{\partial t} + \rho_a \frac{\partial S_i(r,t)}{\partial t} = D_i^0 \theta_a \tau^{-2} \left(\frac{\partial^2 C_i(r,t)}{\partial r^2} + \frac{2}{r} \frac{\partial C_i(r,t)}{\partial r} \right) \quad [5.21]$$

This equation can be rewritten as:

$$\frac{\partial C_i(r,t)}{\partial t} = \frac{\theta_a}{\left(\theta_a + \rho_a \frac{\partial S_i(r,t)}{\partial C_i(r,t)} \right)} \tau^{-2} D_i^0 \left(\frac{\partial^2 C_i(r,t)}{\partial r^2} + \frac{2}{r} \frac{\partial C_i(r,t)}{\partial r} \right) \quad [5.22]$$

Under conditions of linear sorption, the ratio between the sorbed amount and the solution concentration ($\partial S_i / \partial C_i$) is a constant, equal to the distribution coefficient $K_{d,i}$ (L g⁻¹). Combination of Equations 5.16 and 5.22 gives:

$$D_{a,i} = \frac{\theta_a}{\theta_a + \rho_a \frac{dS_i}{dC_i}} \tau^{-2} D_i^0 \quad [5.23]$$

When Donnan diffusion is considered, the solution concentration C is replaced by the Donnan concentration C_D .

$$D_{a,i} = \frac{\theta_a}{\theta_a + \rho_a \frac{dS_i}{dC_{D,i}}} \tau^{-2} D_i^0 \quad [5.24]$$

The Donnan concentration and the adsorbed amount S_i in this equation are obtained by separate calculation using the surface complexation model (with Donnan volume) for equilibrium sorption. To estimate the diffusion rate in the simulations

5. Sorption kinetics I. The Donnan diffusion model

with a smaller Donnan volume (half the porosity), the value θ_a in Equation 5.24 was halved.

5.3. Results

5.3.1. Equilibrium sorption and pore concentrations

Before considering the diffusion results, the surface charge, Sr sorption and pore concentrations in the models are discussed. Figure 5.4 shows the equilibrium pore and surface concentrations of Sr calculated with the surface complexation model with either a diffuse layer (DL) or a Donnan model. All are calculated in equilibrium with 10^{-4} M Sr and plotted as a function of pH. Figure 5.4a shows the surface charge on the 0-plane. The point of zero charge (PZC) is lower than it would be in a pure electrolyte system, because of the presence of Sr in the system. Figure 5.4b shows the net surface charge, which is the sum of the charges on the surface planes (0-plane and d-plane). In equilibrium with the Sr solution, the net charge is always positive, with a minimum around pH 8. At low pH, the positive charge is a result of the protonation of the surface, and at high pH it is caused by the adsorption of Sr ions. The diffuse layer model describes less change in surface charge over the pH range than the Donnan model. Over the whole pH range, the net surface charges vary by up to 20% between the different models. Notably, the surface charge is smaller for a smaller Donnan volume. This is because there is less space for counter-ions to compensate the surface charge and therefore surface protonation and Sr sorption are lower.

Figure 5.4c shows the Sr concentrations in the pores (on a logarithmic scale). In the free pore diffusion model, the pore concentration is not influenced by electrostatic surface forces, so the equilibrium concentration in the pore is the same as the concentration outside the aggregate (10^{-4} M). The pore concentrations calculated by the Donnan model are much lower. Over the whole pH range considered, the positively charged Sr ions are repulsed from the pore space because the surfaces are positively charged. The extent of repulsion depends on the surface charge and on the Donnan volume. In a smaller Donnan volume, the electrical potential ought to be higher to achieve overall neutrality and, therefore, the Sr concentration in the pores is lower. Sr sorption is very similar between the models as shown by Figure 5.4d (logarithmic scale). The largest differences between the DL model and the Donnan models occur at low pH values where sorption is low. From pH 6 and higher, the differences between the models are smaller than a factor 2. There is less sorption in the model with the smaller Donnan volume than with a maximum

volume because of the higher surface potential and lower Sr concentrations present in a smaller Donnan volume.

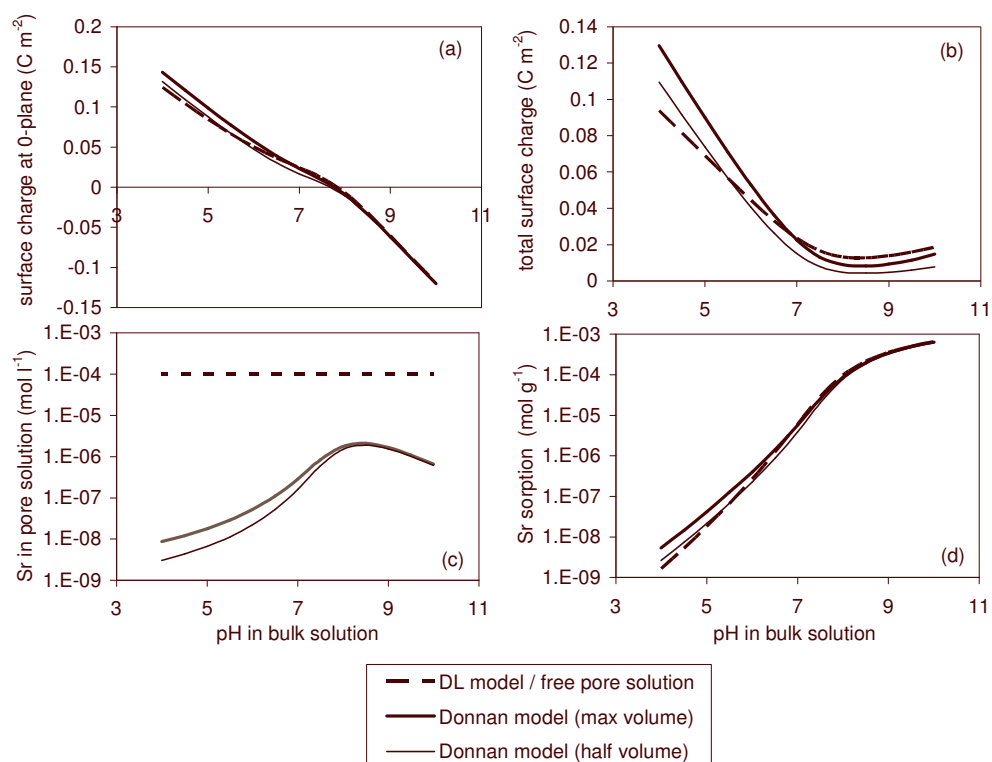


Figure 5.4. a) The surface charge on the 0-plane (in presence of Sr^{2+}) calculated by the surface complexation model with either a diffuse layer (DL) or a Donnan volume; b) the total surface charge (sum of 0-plane and d-plane); c) the pore concentrations used by the specified models; d) equilibrium Sr sorption; all calculated in equilibrium with $10^{-4} M Sr^{2+}$ and $0.01 M NaNO_3$ in the bulk solution.

5. Sorption kinetics I. The Donnan diffusion model

5.3.2. Diffusion simulations

The results of the numerical model simulations for some pH values are shown in Figure 5.2 and 5.3. Figure 5.2 shows simulation results of the Donnan diffusion model and Figure 5.3 results of the free pore diffusion model. To allow quantitative comparison between the results of the two models, apparent diffusion coefficients (D_a) were fitted to the resulting curves. The dashed lines in Figures 5.2 and 5.3 show the curves that were fitted by adjusting the value of D_a in Equation 5.20. In some cases it was not possible to describe the uptake curve accurately with a single apparent diffusion coefficient, because of the variation of the apparent diffusion rate with time. This is for example the case for pore diffusion model at pH 9, where the simulated curve and the fitted curve are slightly different. However, the best-fit apparent diffusion coefficients serve here only as an indication for the diffusion rates predicted by the different models.

The apparent diffusion coefficients were plotted in Figure 5.5 to allow comparison between the different models for the pH range from pH 4 to 10. The symbols in Figure 5.5 show the fitted D_a values. The lines present the D_a values that were estimated with Equations 5.23 and 5.24, based on some simplifications, one of which is the assumption of a linear sorption isotherm (constant dS/dC_i). The simplified approximations give a good estimate of D_a for $\text{pH} \leq 7$. At a higher pH, the sorption isotherm deviates slightly from linearity, and Equation 5.23 gave less accurate estimates. This is demonstrated in Figure 5.6, where the pore diffusion curves at constant pH values of 7, 8 and 9 are compared with the curves obtained with Equation 5.23. A good agreement is found at pH 7, but at pH 8 and 9 the diffusion coefficient is not constant due to nonlinear sorption and Equation 5.23 gave a poor estimate. In the Donnan diffusion model, the simplified estimation underestimates the diffusion rates at $\text{pH} > 7$ because of the additional flux caused by the electrostatic potential gradient. The higher surface potential caused by sorption of Sr^{2+} causes an electrostatic gradient towards the centre of the aggregate, which increases the diffusion rates of Sr^{2+} and H^+ in, and OH^- out of the aggregate.

An important result shown in Figure 5.5 is that the Donnan model predicts much lower diffusion rates than the free pore diffusion model (up to 4000 times lower at pH 5-6 for a maximum Donnan volume). This slow diffusion rate is directly related to the low Sr concentration in the Donnan phase (Fig. 5.4c). Diffusion is even slower for a smaller Donnan volume (up to 8000 times slower than free pore diffusion at pH 5-6), mainly because of the smaller pore volume that is available for diffusion. A 50% smaller Donnan volume results in a 50% reduction of the

apparent diffusion coefficient. At a low pH, the difference is a little larger because the Sr concentration in the smaller Donnan volume is slightly lower (Fig. 5.4c).

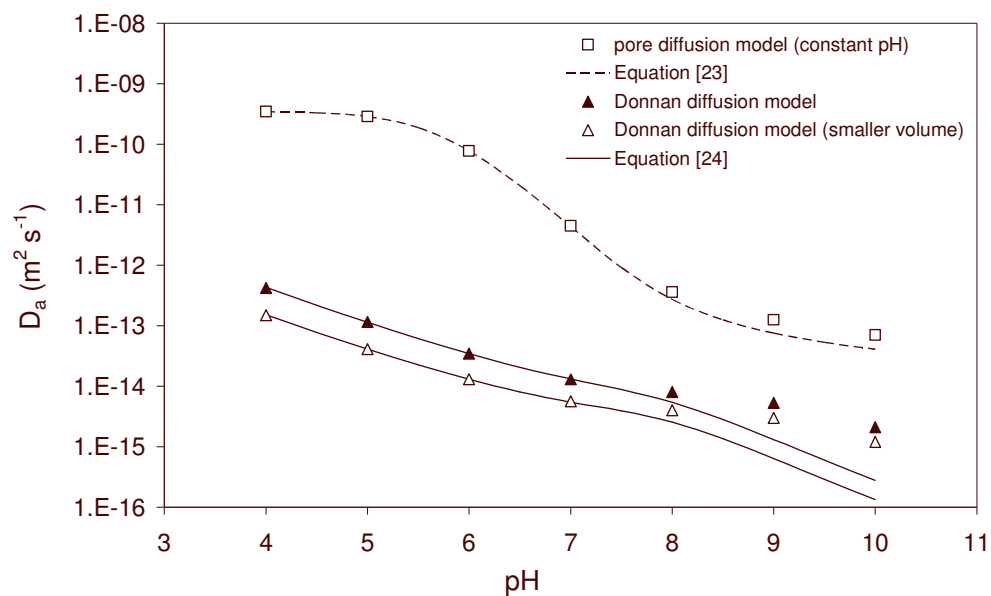


Figure 5.5. Apparent diffusion coefficients as a function of pH, derived from the simulations with the pore diffusion model at a constant pH, and with the Donnan diffusion model for a maximal Donnan volume and for half the pore volume. The lines show the estimations calculated with Equation 5.23 for pore diffusion and with Equation 5.24 for Donnan diffusion.

5. Sorption kinetics I. The Donnan diffusion model

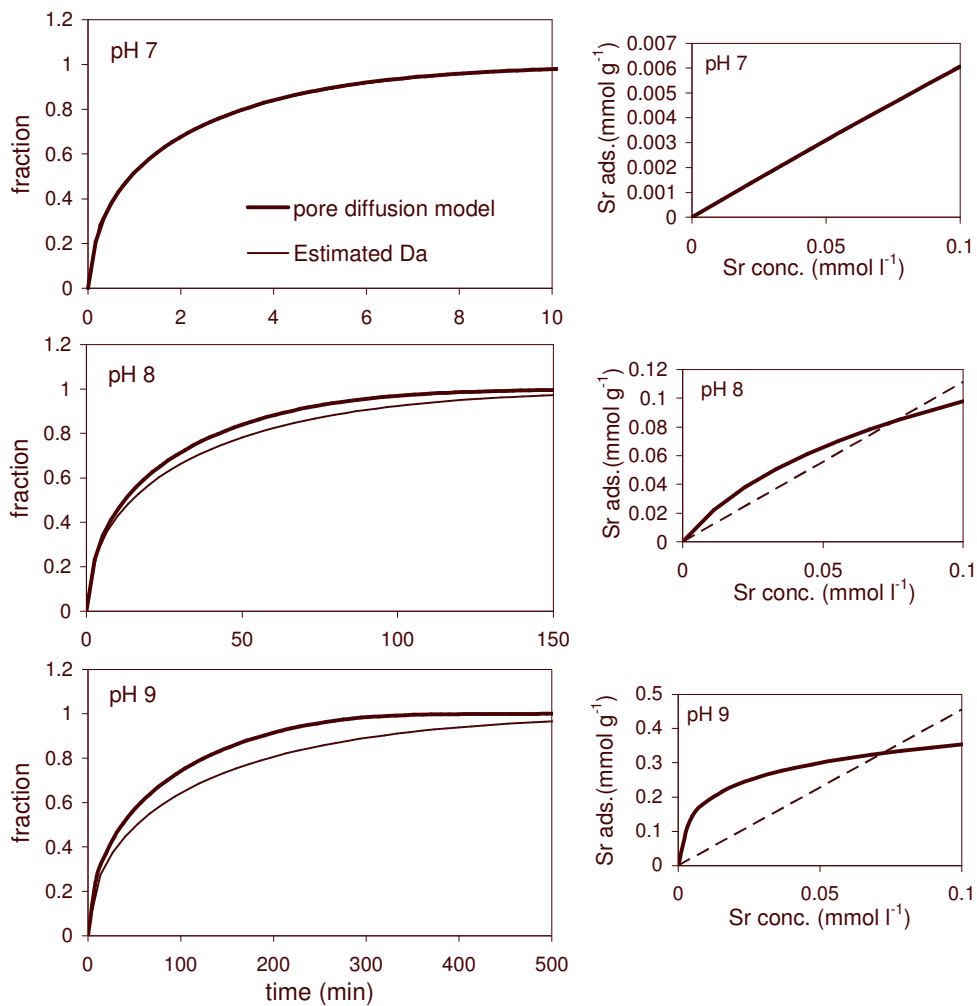


Figure 5.6. The effect of nonlinear sorption on the diffusion curves at pH 7, 8 and 9. Simulated pore diffusion at a constant pH (thick black line), and the diffusion rate estimated with the simplified analytical solution (D_a according to Equation 5.24 and plotted with Equation 5.20) (thin black line). The inserts on the right show the difference between the sorption isotherms at pH 7, 8 and 9 (solid line) and the linear approximation (dashed line).

5.3.3. Effects of pH on pore diffusion

The model simulations for both models were performed with a constant pH and with a variable pH. For a constant pH, the pH inside and outside the aggregate is set constant during the sorption and diffusion process. In the other simulations, the pH varies following proton desorption and diffusion, which is the way the pH would respond in most systems. We decided to show both results because in sorption-diffusion models, the pH is often assumed constant to simplify the calculations. Figure 5.7 shows the D_a values that followed from the simulations with both models with a constant pH or a variable pH. The results for pore diffusion at variable pH show that there is a significant pH effect at higher pH values (around pH 7 – 9). Figure 5.8 shows the diffusion curves that were found with the pore diffusion model at a constant and a variable pH. During Sr adsorption, proton desorption can cause a local decrease in pH. The pH subsequently recovers due to proton diffusion out of the aggregates and OH⁻ diffusion into the aggregates. The temporary decrease in pH reduces the affinity for Sr binding, slowing the diffusion of Sr into the aggregate. Sr sorption cannot be complete until the pH has recovered. The change in pH only influences the diffusion rate around pH 7 to 9. At pH 6 and lower, the amount of Sr sorption is very small, and therefore the change in pH and the effect on diffusion are not noticeable. At around pH 10, the pH recovers very quickly because of OH⁻ diffusion and, therefore, the Sr diffusion rate is not much affected. The recovery of pH is slow at pH 7 and 8 because of the low H⁺ and OH⁻ concentrations in the pores and high proton affinity. At pH 7, the recovery is so slow that the diffusion process could be interpreted as a two step process. As can be seen in Figure 5.8, the Sr diffusion curve at pH 7 levels off before reaching equilibrium sorption and only continues very slowly.

For the simulations with the Donnan model, the pH effect is different. At pH > 7 the adsorption of Sr²⁺ causes an electrostatic potential gradient that enhances Sr²⁺ diffusion into the aggregate and OH⁻ diffusion out of the aggregate. The diffusion rate of Sr is higher when the diffusion of OH⁻ is taken into account.

5. Sorption kinetics I. The Donnan diffusion model

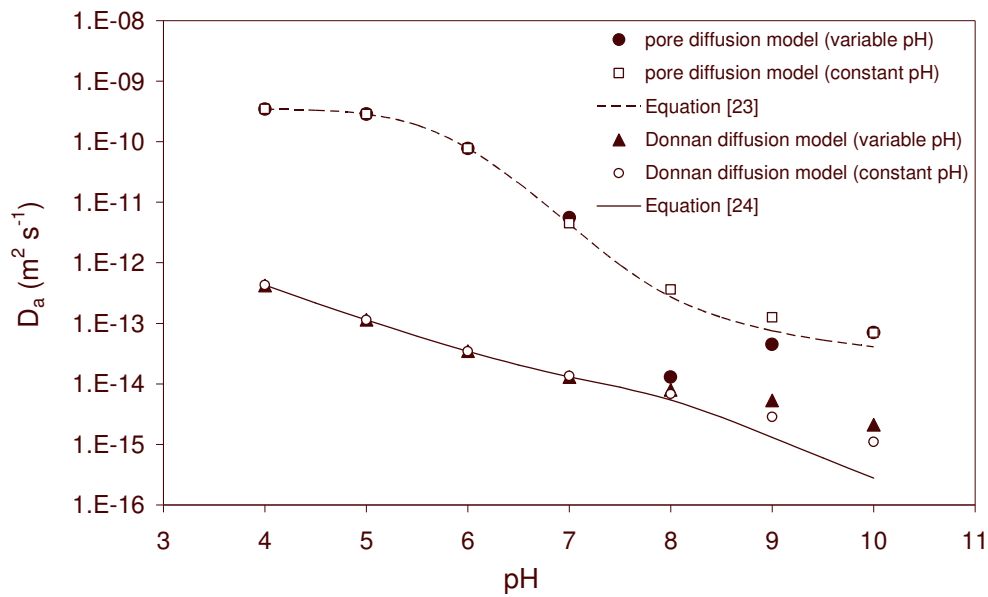


Figure 5.7. Apparent diffusion coefficients as a function of pH, derived from the simulations with the pore diffusion model and the Donnan diffusion model for constant pH and for variable pH (with H^+/OH^- diffusion). The lines show the estimations calculated with Equation 5.23 for pore diffusion and with Equation 5.24 for Donnan diffusion.

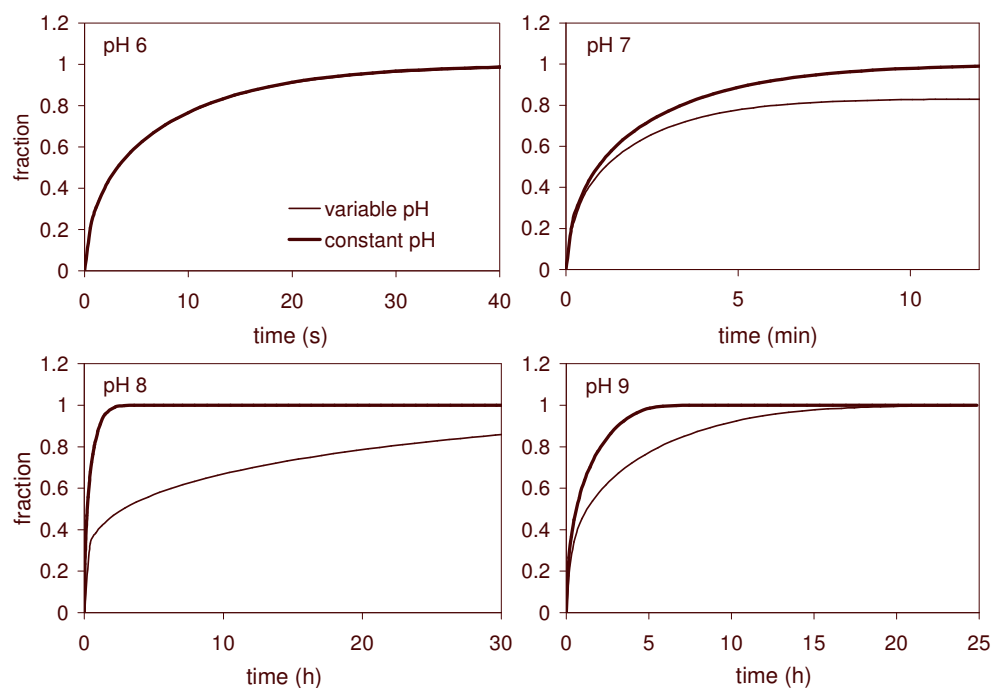


Figure 5.8. The effect of the change in pH during Sr sorption. The curves show the results of pore diffusion simulations with a variable pH (thin line) and with a constant pH (thick line).

5.4. Conclusions

The electrical potential caused by the surface charge of a hydroxide mineral can have a significant influence on the ion concentration in the pores of a hydroxide aggregate and, therefore, on the diffusion rate of an ion in the pore solution. With the Donnan electrostatic model, we showed that the concentration of an ion in the small pores of a mineral aggregate can be up to several thousand times lower than the concentration in the bulk solution. Because diffusion is driven by the concentration gradient in the pores, a very low pore concentration can cause an equivalent reduction in the diffusion rate. Other factors that influence the diffusion rate are the amount of sorption, the change in electrostatic potential caused by adsorption and the effective pore volume that is available for diffusion. The large difference between the apparent diffusion rates predicted by the two model approaches is, however, mainly caused by the low pore concentration predicted by the Donnan model.

5. Sorption kinetics I. The Donnan diffusion model

The Donnan diffusion model was implemented by adaptation of the CD-MUSIC model, by replacing the diffuse layer with a Donnan volume. It is necessary to use a surface complexation model that describes the electrostatic influences on sorption explicitly; otherwise it is not possible to calculate the electrostatic influence on diffusion.

Using a numerical scheme to calculate diffusion in time has the advantage that the influences of nonlinear sorption, and pH changes during Sr sorption, could be calculated simultaneously. The models showed that a temporary change in pH can alter the diffusion rate of Sr significantly. However, this effect is not so apparent for diffusion predicted by the Donnan model because the pH recovers faster through H^+/OH^- diffusion in the Donnan model than in the pore diffusion model. For Donnan diffusion, an apparent diffusion rate could be estimated using a simplified approximation (Equation 5.24), but only for the pH range where sorption does not create a significant change in surface potential.

6. Sorption kinetics of strontium in porous hydrous ferric oxide aggregates. II. Comparison of experimental results and model predictions

Annette Hofmann, Wendy van Beinum, Johannes C. L. Meeussen and
Ruben Kretzschmar

Colloid and Interface Science (2005), Vol. 283, pp. 29-40.

(experiments by A. Hofmann and modelling by W. van Beinum)

6. Sorption kinetics II. Experiments

Nomenclature

a	radius of the aggregate inner fraction (with Donnan diffusion)	m
$C_{D,i}$	concentration of ion i in the Donnan phase	mol m^{-3}
C_i	concentration of ion i in the inter-aggregate water	mol m^{-3}
D_i^0	diffusion coefficient of ion i	$\text{m}^2 \text{s}^{-1}$
F	Faraday constant	C mol^{-1}
f	volume fraction of outer pores to intra-aggregate pores	-
L	column length	mm or m
M_{am}	dry mass of HFO (at ambient conditions)	g
M_{HFO}	dry mass of HFO (dehydrated) in column	g
R	gas constant	$\text{J mol}^{-1} \text{K}^{-1}$
r	radial distance from aggregate center	m
r_0	aggregate radius	m
S_i	adsorbed amount of ion i	$\text{mol g}^{-1} \text{HFO}$
$S_{o,i}$	adsorbed amount of ion i in the outer aggregate	$\text{mol g}^{-1} \text{HFO}$
T	temperature	K
V_a	total wet volume of aggregates in column	mL
V_{inter}	inter-aggregate pore volume	mL
V_{intra}	intra-aggregate pore volume	mL
V_{mob}	mobile pore volume	mL
V_{tot}	total volume of the column	mL
x	distance	m
z_i	charge of ion i	
α_L	hydrodynamic dispersivity	mm or m
α_{num}	numerical dispersivity	mm or m
ρ_a	density of dry HFO aggregates	g m^{-3}
ρ_{am}	density of HFO (ambient conditions)	g cm^{-3}
ρ_{HFO}	density of HFO (dehydrated)	g cm^{-3}
ρ_{wet}	density of wet HFO aggregates	g cm^{-3}
τ^2	tortuosity correction factor	-
θ	volume fraction of the inter-aggregate pores	-
θ_a	wet aggregate porosity	-
v	average pore velocity in the inter-aggregate water	m s^{-1}
Φ_a	volume fraction of aggregates in the column system	-

Nomenclature (continued)

Ψ_D	electrical potential in the Donnan phase	V
$\Psi_{D,o}$	electrical potential in the Donnan phase of the outer fraction of the aggregate	V

6.1. Introduction

Hydrous ferric oxides (HFO) are important sorbents for trace metal cations and oxyanions in soils and aquatic environments (Dzombak and Morel, 1990; Cornell and Schwertmann, 1996). HFO consists of primary nano-particles with diameters between 2 and 5 nm and has an extremely large specific surface area in the order of $600 \text{ m}^2 \text{ g}^{-1}$ (Dzombak and Morel, 1990; Davis and Leckie, 1978; Roden and Zachara, 1996). Typically, the particles form porous aggregates with significant internal porosity (Hofmann et al., 2004; Stanjek and Weidler, 1992). Therefore, the kinetics of ion adsorption onto HFO is controlled by slow diffusion processes into small pores of HFO aggregates. The diffusion controlled kinetics of ion adsorption to HFO has been investigated for phosphate (Willett et al., 1988), arsenate (Fuller et al., 1993), strontium (Axe and Anderson, 1995), and some trace metal cations including Cd, Zn, Ni, Pb, Cu (Trivedi and Axe, 1999, 2000, 2001a; Axe and Trivedi, 2002; Scheinost et al., 2001). Most of these studies have been conducted using either freeze-dried (Willett et al., 1988; Scheinost et al., 2001) or freshly precipitated HFO suspensions (Fuller et al., 1993; Axe and Anderson, 1995; Trivedi and Axe, 1999, 2000, 2001a; Axe and Trivedi, 2002; Scheinost et al., 2001).

Axe and co-workers (Axe and Anderson, 1995, 1997; Trivedi and Axe, 1999, 2000, 2001b; Axe and Trivedi, 2002) described the adsorption kinetics of Sr, Cd, Zn, Ni by HFO, hydrous manganese oxide, and hydrous aluminium oxide using a surface diffusion model in which ions move along internal surfaces by hopping from one surface site to the next, depending on their activation energies. Theoretically, this type of diffusion is only significant for small pores with diameters below 2 nm. Investigations with compacted clays have indicated that surface diffusion may only be relevant in highly compacted systems. Otherwise, migration of charged species may occur predominantly by diffusion within the diffuse layer (Berry and Bond, 1992; Ochs et al., 1998, 2001; Oscarson, 1994; Sato et al., 1995).

6. Sorption kinetics II. Experiments

In Chapter 5, we presented an alternative pore diffusion model specific to pores of intermediate size, that are large enough to contain unbound water but small enough that the diffuse electric layers overlap inside the pores. The model uses a Donnan electrostatic model to calculate the pore solution chemistry. Ion diffusion in the pore water is calculated from the gradients in Donnan concentrations and Donnan potentials and is directly influenced by pH and sorption dependent surface charge. Surface chemical equilibria were described with a 1-pK basic Stern surface complexation model based on the CD-MUSIC model (Hiemstra et al., 1989; Hiemstra and Van Riemsdijk, 1996).

The objective of the present study was to validate the Donnan-diffusion model by investigating Sr adsorption and desorption by porous HFO aggregates. Sorption parameters and aggregate structural characteristics were all determined independently. Model predictions were compared with results of Sr transport experiments obtained with chromatographic columns packed with large HFO aggregates. The HFO aggregates, produced by a freezing and thawing method, had an average diameter of 235 μm , the internal pore size distribution was well characterized (Hofmann et al., 2004). Strontium was selected as sorbate because it has a rather simple aqueous chemistry and it has moderate adsorption affinity to HFO in the pH range of our experiments (pH 4-7).

6.2. Materials and Methods

6.2.1. Hydrous ferric oxide

Hydrous ferric oxide was synthesized following the method of Schwertmann and Cornell (1991) by titrating a 0.2 M $\text{Fe}(\text{NO}_3)_3$ solution with 1.0 M KOH to pH 8. The precipitated HFO gel was dialyzed for 10 days in deionized water to remove excess salts. The fresh HFO gel was then transformed into large, densely packed HFO aggregates by freezing and thawing. The method of preparation as well as the physical characterization of the HFO aggregates are presented in detail elsewhere (Hofmann et al., 2004). In summary, the wet HFO aggregates had a mean diameter of $235 \pm 35 \mu\text{m}$, a wet density of $1.8 \pm 0.06 \text{ g cm}^{-3}$, and an internal porosity of 0.73 ± 0.02 . A pore size analysis of the wet HFO aggregates by small angle neutron scattering (SANS) gave a number mean pore size of 2 nm, a minimum pore size of 0.5 nm and a maximum of 15 nm. On a volume basis, 74% of the pores are between 2 and 6 nm, 8% are smaller and about 18% are larger than this interval. X-ray diffraction analysis of the HFO confirmed that it was a 2-line ferrihydrite. In the present study, the crystallinity of the HFO was also monitored over the entire

duration of the experiments, which was up to 2 months. Sub-samples of HFO, taken at the beginning and at the end of each experiment, were freeze-dried and stored in a desiccator. X-ray diffraction measurements were conducted with a Scintag XDS2000, theta-theta diffractometer using Cu- $K\alpha$ radiation. The scan rate was $0.009^\circ \text{ s}^{-1}$. All samples showed the 2-line diffraction pattern characteristic of hydrous ferric oxide. No detectable mineral transformation occurred over the duration of our experiments. The dry density of the HFO aggregates was determined by pycnometry (Hofmann et al., 2004). The aggregates were first dried at 40°C for 48 hours. Oven drying did not alter the aggregate crystallinity as was shown by XRD control measurements. A weighed amount of about 1 g was then transferred to a 20 mL pycnometer vial which was filled with deionized water and equilibrated at 25°C . The weight differences of the vial with and without the HFO loaded allowed calculation of the HFO density. Because HFO was handled under ambient conditions, HFO surfaces were partially hydrated during the measurement. The HFO density determined by the pycnometer analysis is thus specific to the laboratory atmospheric conditions.

6.2.2. Proton and Sr sorption to HFO

Proton and Sr adsorption to HFO surfaces was studied using acid-base titration and batch sorption experiments, respectively. To minimize diffusion controlled kinetics and maximize surface accessibility for ion adsorption, the wet HFO aggregates were re-dispersed by gently crushing them in water with an agate mortar. The HFO particles were then suspended in deionised water and purged with nitrogen gas for 15 hours to remove adsorbed CO_2 . We assume that sorption on the dispersed HFO is fast and that equilibrium sorption was achieved during the experiments. The pH and ionic strength dependent protonation behaviour of the dispersed HFO was studied by potentiometric acid base titrations. The experimental set-up is described in detail elsewhere (Christl and Kretzschmar, 1999). Briefly, experiments were performed with a computer-controlled titration system (Kinniburgh et al., 1995) under thermostatic conditions at 25°C . The burettes were filled with CO_2 -free deionized water, 0.05 M HNO_3 (Titrisol, Merck), 2 M NaNO_3 , and NaOH of 0.05 M approximate concentration. For the base solution, a 10 M NaOH stock solution (Merck, p.a.) was diluted under N_2 -atmosphere to the appropriate concentration. The reagent solutions and the titration vessel were continuously purged with nitrogen gas to exclude CO_2 . Blank titrations of NaNO_3 electrolyte solutions permitted precise determination of the concentration of the base solution as well as the mean ion activity coefficient at each salt concentration. Acid and base titrations were performed consecutively at four constant ionic strengths (0.01,

6. Sorption kinetics II. Experiments

0.03, 0.1, 0.3 M NaNO₃) in a single batch of HFO suspension. Each addition of titrant was accompanied by addition of salt solution or water such that the ionic strength remained constant within 1% over each acid and base run. Titrations with HFO were performed using 100 mg of well dispersed and CO₂ free HFO in 50 mL of deionized and CO₂ free water. Forward and backward titrations for a given ionic strength gave identical results, except for a small hysteresis effect between pH 5 and 7 and around the point of zero charge (pH 8-9.5). The maximum amplitude of hysteresis effects was about 5% of the total charge interval. In this paper, we only report the averages of forward and backward titrations.

The pH and ionic strength dependent sorption of Sr²⁺ to HFO was investigated in batch equilibration experiments. The solid concentration for all samples was 5 g L⁻¹ of well dispersed and N₂-purged HFO. Series of 10 mL-batches were prepared with Sr concentrations of 10⁻⁴ or 10⁻³ M and ionic strengths of 0.01 or 0.1 M NaNO₃. In each series, μ L amounts of either 0.1 M HNO₃ or carbonate-free 0.1 M NaOH solutions were added to the samples to adjust the pH to values between pH 4 and 9. Samples were equilibrated for 48 hours with an end-over-end rotator, and then centrifuged at 2500 rpm for 15 minutes (Mistral 6000). The pH of the supernatant solutions was measured under N₂ atmosphere using a combination pH electrode, which was equilibrated for at least 30 minutes before the electrode readings were recorded. The supernatant was then passed through 0.025 μ m membrane filters (NC, Schleicher & Schuell) and acidified with 20 μ L of 0.1 M HNO₃. Dissolved Sr was analyzed by ICP-MS (Agilent 7500a). To determine the exact concentration of HFO in each sample, HFO was dissolved in 1-2 M HNO₃. Subsequently Fe was measured by atomic absorption spectrometry at 372 nm wavelength (Varian SpectrAA 220). For conversion between total iron and HFO, a weight ratio of 0.58 was used, which was derived from the ferrihydrite formula Fe₅HO₈.4H₂O (Towe and Bradley, 1967).

6.2.3. Surface complexation modeling

Acid-base titration and metal sorption data were modelled with the surface complexation model described in Chapter 5, based on the CD-MUSIC model (Hiemstra et al., 1989; Hiemstra and Van Riemsdijk, 1996). The model describes 1-pK protonation sites and basic Stern electrostatics with charge distribution (CD) between electrostatic planes. The relevant surface reactions are written as:





where $\equiv\text{XO}$ represents the reactive surface oxygen site.

In a 1-pK model, the pK of protonation (Equation 6.1) corresponds to the pristine point of zero charge (PPZC). The experimental acid-base titrations at different ionic strengths allowed determination of the point of zero salt effect, which was identified with the pH_{PPZC} (Lyklema, 1984; Schudel et al., 1997). The specific surface area of the wet HFO was assumed to be $600 \text{ m}^2\text{g}^{-1}$. This value lies between the specific surface area determined by N_2 gas adsorption, $380 \text{ m}^2\text{g}^{-1}$ (Hofmann et al., 2004) and the geometrical estimate, $750 \text{ m}^2\text{g}^{-1}$, which takes the HFO crystallite size and density into account. The surface area measured by N_2 gas adsorption is probably too small because of dehydration effects (Davis and Leckie, 1978; Hofmann et al., 2004). On the other hand, the calculated geometric surface area represents the theoretical maximum, which is probably too high. The value of $600 \text{ m}^2\text{g}^{-1}$ was thus taken as a realistic compromise.

In a first step, the acid-base titration data were modelled to obtain best-fit parameters for the Stern-layer capacitance, the site density and the ion pair formation constants for NO_3^- and Na^+ (for Equations 6.2 and 6.3). For the latter, symmetrical ion binding was assumed. In a second step, the Sr sorption isotherms were modelled by fitting the Sr surface complexation constant (for Equation 6.4) on the basis of the new protonation parameters. The distribution of Sr charges between the surface and the Stern plane was adjusted to obtain a good fit of the data. To fit the surface parameters the program ECOSAT, Version 4.7 (Keizer and Van Riemsdijk, 1998) was used in combination with the program FIT (Kinniburgh, 1993).

6. Sorption kinetics II. Experiments

Table 6.1. Parameters used to describe proton and Sr sorption to HFO with the 1-pK basic Stern model with charge distribution for Sr^{2+} and surface ion pair formation for Na^+ and NO_3^-

surface parameters	value	method
surface area	$600 \text{ m}^2 \text{ g}^{-1}$	estimate
site density	4 nm^{-2}	acid-base titration best fit
capacitance	1.07 F m^{-2}	acid-base titration best fit
$\log K_{\text{Na}}$	-1.5	acid-base titration best fit
$\log K_{\text{NO}_3}$	-1.5	acid-base titration, adjusted
pK H	8.7	acid-base titration
$\log K_{\text{Sr}}$	4.47	Sr adsorption experiments, best fit
charge distribution of the Sr surface complex	0-plane: 0.68 d-plane: 1.32	Sr adsorption experiments, best fit

6.2.4. Column experiments

The wet HFO aggregates were not resistant enough against mechanical forces to survive shaking in a batch reactor without generation of fine particles. Therefore, it was not possible to use batch experiments to study the uptake kinetics of Sr to the HFO aggregates. Instead, chromatographic flow-through column experiments were conducted, in which the HFO aggregates remain stationary and the solution flows through the inter-aggregate pores at a controlled flow rate.

Chromatographic glass columns (Omnifit) with 6.6 mm diameter were packed with 1.3 to 2.0 g of wet HFO aggregates. The resulting HFO columns were between 5.5 and 8 cm long. The exact column parameters for each experiment are provided in Table 6.2. Two HPLC pumps (Jasco Pu 980) were connected to the column inlet, delivering a pure background electrolyte solution and a Sr solution (with electrolyte), respectively. Inflowing solutions had been degassed. The remaining CO_2 partial pressure was calculated to be smaller 10^{-5} bar. A valve was used to switch between the two influent solutions without interrupting the flow. Both solutions were passed through a degasser (Erc 3315) prior to entering the pumps, which served to remove possible gas bubbles. The HFO columns were first adjusted to either pH 4.0 or pH 7.0 by leaching with 0.01 M NaNO_3 solution adjusted to the appropriate pH value. The flow rate was maintained at 0.2 mL min^{-1} . Equilibration of the HFO was continued until the pH value of the column effluent was equal to the pH of the influent solution. Both were monitored

with an online electrode (Hamilton minitrode). The equilibration of the HFO to pH 4 or 7 took between 15 days and 1 month. The stability of the HFO aggregates during flow through experiments was tested in preliminary experiments. Even when phosphate was introduced into the column, which is known to cause charge reversal at the Fe oxide surface, no particle mobilization or structural change in the HFO aggregates was observed.

After equilibrating the HFO to pH 4 or 7, an electrolyte solution containing 10^{-4} M Sr (added as $\text{Sr}(\text{NO}_3)_2$) was introduced at a constant flow rate of 0.2 mL min^{-1} . The column effluent was collected using an automated fraction collector and the solutions were analyzed for Sr by inductively coupled plasma mass spectrometry (ICP-MS, Agilent 7500a). The uptake of Sr by the HFO aggregates was followed for 40 and 210 hours for experiments at pH 4 and pH 7 respectively. Afterwards, a Sr desorption experiment was initiated by switching the influent back to the pure 0.01 M NaNO_3 background electrolyte solution. Sr desorption and diffusion out of the HFO aggregates was assessed over similar periods of time.

Table 6.2. Hydrodynamic and column parameters for the Sr transport experiments at pH 4 and 7

experiment	pH 4.0	pH 7.0
flow rate Q (mL min^{-1})	0.2	0.2
hydrodynamic dispersivity α_L (mm)	1.44 ± 0.2	1.44 ± 0.2
dry HFO (weighed at ambient conditions) M_{am} (g)	1.35	2.02
total column volume V_{tot} (mL)	1.81	2.68
total volume of wet aggregates V_a (mL)	1.16	1.73
inter-aggregate pore volume V_{inter} (mL)	0.65	0.95
intra-aggregate pore volume V_{intra} (mL)	0.85	1.27
f “outer pore fraction”	0.37	0.72
numerical dispersivity α_{num} (mm)	1.3	1.3
advection cells in series	20	20
aggregate concentric layers (for Donnan diffusion)	10	10

6. Sorption kinetics II. Experiments

6.2.5. Column geometry and hydrodynamic parameters

The inter- and intra-aggregate pore volumes of the columns were calculated from the column geometry, the weight of the column components, and the density of HFO aggregates (see Figure 6.1 for a schematic illustration). The total volume (V_{tot}) of the column is determined from the column length and diameter. At the end of the diffusion experiments, the HFO was retrieved from the column, dried at 40 °C for 48 hours, and weighed. The low drying temperature was used to prevent heat-induced mineral transformations. However, under these conditions hydration water is not completely removed from the HFO surface. To correct the total mass for the hydration effect, we used the equation:

$$M_{HFO} = M_{am} \frac{\rho_{HFO}}{\rho_{am}} \frac{(1 - \rho_{am})}{(1 - \rho_{HFO})} \quad [6.5]$$

where M_{am} is the mass of dried HFO weighed at ambient atmospheric conditions, $\rho_{am} = 3.17 \text{ g cm}^{-3}$ refers to the density as determined by pycnometry of this “ambient-dry” material. The mineral density of the dehydrated HFO, $\rho_{HFO} = 3.96 \text{ g cm}^{-3}$, was adopted from Towe and Bradley (1967). M_{HFO} is the equivalent mass of dehydrated HFO in the column.

The total volume of the wet aggregates, V_a , in the column is obtained from

$$V_a = M_{HFO} \left(\frac{\rho_{HFO} - 1}{(\rho_{wet} - 1) \rho_{HFO}} \right) \quad [6.6a]$$

$$\Phi_a = \frac{V_a}{V_{tot}} \quad [6.6b]$$

where $\rho_{wet} = 1.81 \text{ g cm}^{-3}$ is the bulk density of the wet aggregates (Hofmann et al., 2004), Φ_a is the volume fraction of aggregates in the system. The inter- and intra-aggregate pore volumes (V_{inter} , V_{intra}) are now easily obtained as

$$V_{inter} = V_{tot} - V_a \quad [6.7a]$$

$$\theta = \frac{V_{inter}}{V_{tot}} \quad [6.7b]$$

and

$$V_{intra} = M_{HFO} \left(\frac{\rho_{HFO} - \rho_{wet}}{(\rho_{wet} - 1) \rho_{HFO}} \right) \quad [6.8a]$$

$$\theta_a = \frac{V_{intra}}{V_a} \quad [6.8b]$$

where θ_a is the wet aggregate porosity.

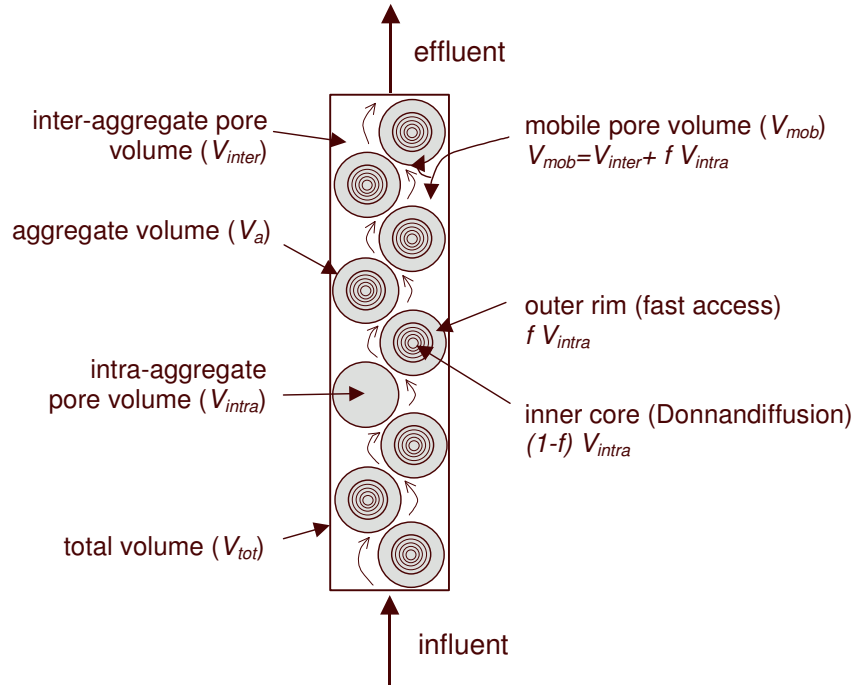


Figure 6.1. Schematic representation of the column filled with the HFO aggregates and illustrating the different types of pore volumes in this system.

When a tracer solution passes through the column, it displaces the solution present in the inter-aggregate pores. However, depending on the flow rate, the tracer flow may deviate from plug-flow due to (i) hydrodynamic dispersion, (ii) external film diffusion in a viscous layer around the aggregates, (iii) diffusion to intra-aggregate pores. The breakthrough curve of a tracer solution shows the replaced solution volume, called mobile pore volume (V_{mob}) in the following text. As the flow rate decreases, water film and intra-aggregate pores will be accessed by the tracer and V_{mob} will increase until a maximum volume is reached, which corresponds to the maximum accessible pore volume. To estimate the contribution of film- and intra-aggregate diffusion on the mobile pore volume, we conducted salt pulse experiments at varying flow-rates. A 95 μL injection loop was placed at the column inlet and filled with a NaNO_3 solution of 0.011 M, which is 10% above the background electrolyte. The pH was set to 7 equal to the equilibrium pH in the

6. Sorption kinetics II. Experiments

column. The salt pulses were injected at varying flow rates from 0.1 to 3 mL min⁻¹. They were recorded online with a conductivity meter (WTW LDM/S). The results (Fig. 6.2) showed that the replaced volume V_{mob} exceeded the inter-aggregate pore space at any flow rate. That indicates that part of the intra-aggregate pore space was accessed by salt diffusion during the residence time in the column, even at higher flow rates. The contribution of intra-aggregate diffusion suggests that diffusion into the aggregates was dominant relative to diffusion across the external water layer. The mobile pore volume increased with decreasing flow rate, which indicated that the fraction of intra-aggregate pores that were accessible depended on the residence time of the inflowing solution. However the maximum accessible pore volume was not reached within the selected range of flow rates.

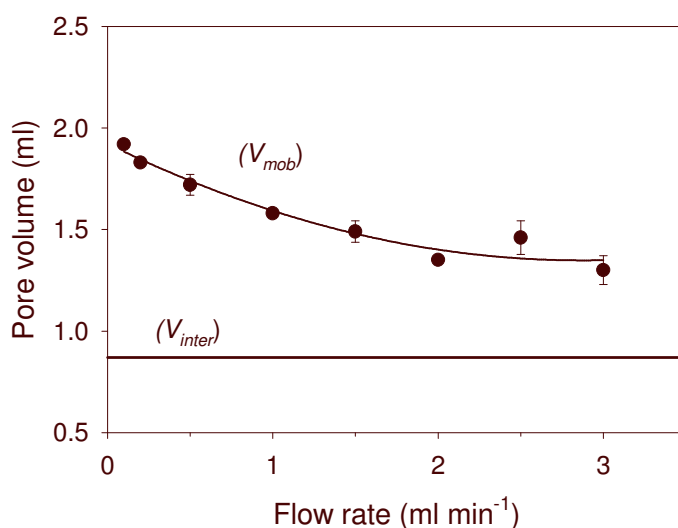


Figure 6.2. Salt-pulse experiments with 0.011 M NaNO₃ at pH 7 at varying flow rates. The column was filled with HFO aggregates and equilibrated at pH 7. The mobile pore volume (V_{mob}) corresponds to the volume eluted at the peak of the breakthrough pulse curve. The inter-aggregate pore volume (V_{inter}) was calculated from Equations 6.5 to 6.8.

In the Sr sorption experiments, we similarly used salt pulses to determine the mobile pore volume. Injection was at the same flow rate as the main experiment. The pH of the salt tracer solution was set equal to the background pH in the column. A salt pulse was recorded by conductivity at the beginning and at the end

of every sorption-diffusion experiment. The final measurement served to verify that pore-textural changes did not occur during the experiment.

The fraction f of the intra-aggregate volume that is accessible to a salt pulse under given experimental conditions is calculated with the help of the inter-aggregate (V_{inter}) and intra-aggregate (V_{intra}) pore volumes (Equations 6.6-6.8) and the experimentally determined mobile pore volume (V_{mob}):

$$f = \frac{(V_{mob} - V_{inter})}{V_{intra}} \quad [6.9]$$

It is assumed that the easily accessible pores correspond to the upper end of pore sizes in the HFO aggregates. Conceptually these larger pores are assumed to be located in the outer rim of the aggregate (Fig. 6.1).

Solute dispersion in the column system was estimated for the experiment at pH 4 with the broadening of the breakthrough curves of injected salt pulses. At pH 4, the fraction of intra-aggregate pores accessed by the salt pulse was small (see Results) so that the contribution of aggregate diffusion to the curve broadening was the smallest possible. The hydrodynamic dispersivity coefficient α_L determined as:

$$\alpha_L = \frac{\sigma^2}{2L} \quad [6.10]$$

where σ is the variance of the pulse curve and L the column length, amounted to 1.44 +/- 0.2 mm.

6.2.6. The Donnan diffusion model

For the interpretation of the experimental results, we used the Donnan diffusion model described in the previous paper (Chapter 5). To simulate the Sr column breakthrough curves, the model was extended to include mixing cells in series to describe advection in the column. In effect this corresponds to a two-region model with the aggregate inner pores being the immobile region. The mass balance for vertical transport is represented by:

$$\begin{aligned} \theta \frac{\partial C_i(x,t)}{\partial t} + f\phi_a \left(\rho_a \frac{\partial S_i(x,t)}{\partial t} + \theta_a \frac{\partial C_{D,i}(x,t)}{\partial t} \right) \\ = -\theta v \frac{\partial C_i(x,t)}{\partial x} + \theta v \alpha \frac{\partial^2 C_i(x,t)}{\partial x^2} - W_i(x,t) \end{aligned} \quad [6.11a]$$

6. Sorption kinetics II. Experiments

in which θ is the inter-aggregate porosity, C_i is the dissolved concentration of ion i in the inter-aggregate water (mol m^{-3}), Φ_a is the volume fraction of aggregates in the column, θ_a is the aggregate porosity and f is the fraction of outer pores, S_i is the adsorbed amount of ion i in the outer fraction of the aggregate (mol g^{-1} HFO), $C_{D,i}$ is the dissolved concentration of i in the Donnan volume of the outer fraction of the aggregate (mol m^{-3}) and $W_i(x,t)$ is a sink term for diffusion of ion i into the diffusion limited inner core of the aggregate. See Nomenclature list for definition of all other terms.

Free or weakly hindered pore diffusion and sorption in the outer rim of the aggregates are described in Equation 6.11a by local equilibrium in a Donnan phase. Because the outer pore volume fraction was determined at the same flow rate, pH and ionic strength as the corresponding sorption-diffusion experiment, the local equilibrium assumption is justified. In the model diffusion was restricted to the smaller aggregate pores located in the inner core. The mass balance for diffusion corresponds with Equation 5.7 (Chapter 5):

$$(1-f)\phi_a \left(\theta_a \frac{\partial C_{D,i}(r,t)}{\partial t} + \rho_a \frac{\partial S_i(r,t)}{\partial t} \right) = (1-f)\phi_a \left\{ \theta_a \tau^{-2} D_i^0 \left[\left(\frac{\partial^2 C_{D,i}(r,t)}{\partial r^2} + \frac{2}{r} \frac{\partial C_{D,i}(r,t)}{\partial r} \right) + z_i C_{D,i}(r,t) \frac{F}{RT} \left(\frac{\partial^2 \psi_D(r,t)}{\partial r^2} + \frac{2}{r} \frac{\partial \psi_D(r,t)}{\partial r} \right) \right] \right\} \quad [6.11b]$$

in which τ^{-2} is the tortuosity correction factor, D_i^0 is the diffusion coefficient in water of ion i (m^2s^{-1}), z_i is the charge of the ion and ψ_D is the electrical potential in the Donnan phase (V). For other terms, see Nomenclature list.

The two equations were solved simultaneously in a numerical finite difference scheme, with the following boundary conditions:

$$(i) \quad \frac{\partial C_D(r,t)}{\partial r} = 0; \quad \frac{\partial \psi_D(r,t)}{\partial r} = 0 \quad \text{for } r = 0 \text{ and } t \geq 0 \quad [6.11c]$$

The Donnan concentration of the outer fraction of the aggregates (C_D at $r = a$) is in equilibrium with the solution concentration in the inter-aggregate pore solution (C):

$$(ii) \quad C_{D,i}(r,t) = C_i(x,t) \exp\left(-z_i \frac{F}{RT} \psi_{D,o}(x,t)\right) \quad \text{for } r = a \text{ and } t \geq 0 \quad [6.11d]$$

where $\psi_{D,o}$ is the electrical potential in the Donnan phase of the outer fraction of the aggregates, a is the radius of the diffusion limited inner fraction of the aggregates.

In the numerical transcription of the Donnan diffusion model with advective transport, the advective fluid flow is one-dimensional, with a steady flow rate. The number of calculation cells (nodes) in the flow direction is set so that numerical dispersion in the model equals the hydrodynamic dispersion in the column (Van Ommen, 1985). With 20 cells and a calculation time step of 10 s, $\alpha_{num} = 1.3$ mm. The inter-aggregate pore volume is derived from Equation 6.7 and based on experimental data. In the numerical scheme, every calculation cell is linked with a row of 10 horizontally connected calculation cells that represent the inner fraction of the aggregates in the column. Diffusion within the aggregates is calculated similar as in the previous paper (Chapter 5), simultaneous with the vertical transport calculations.

6.3. Results

6.3.1. Proton and Strontium sorption

The results of potentiometric acid-base titrations of HFO are presented in Figure 6.3. The titration curves at different ionic strengths exhibit a common intersection point at pH 8.7, which is the point of zero salt effect (PZSE, (Sposito, 1989)). In Schudel et al. (1997), charging studies were conducted on hematite particles in NaNO_3 electrolyte. The isoelectric point obtained by electrophoretic mobility studies coincided with the PZSE obtained by potentiometric titrations, suggesting symmetrical electrolyte ion binding processes and supporting identification of pH_{PZSE} with pH_{PPZC} . We therefore assume that the PZSE in this study also coincides with the pristine point of zero charge (PPZC) of the HFO surfaces. The point is slightly higher than generally reported for HFO, which may be due to the exclusion of CO_2 in our titration system. Aging of HFO during dialysis and the treatment by freezing and thawing might also contribute to shifts in the surface charging behavior.

The lines in Figure 6.3 represent the best fit with the 1-pK basic Stern surface complexation model, resulting in model parameters reported in Table 6.1. The model gives a satisfactory description of the pH-dependent charging behavior of the HFO. The slight overestimate of surface charge at low pH and low ionic strength may be related to the effect of geometry on the surface potentials due to the small size and spherical shape of HFO crystallites.

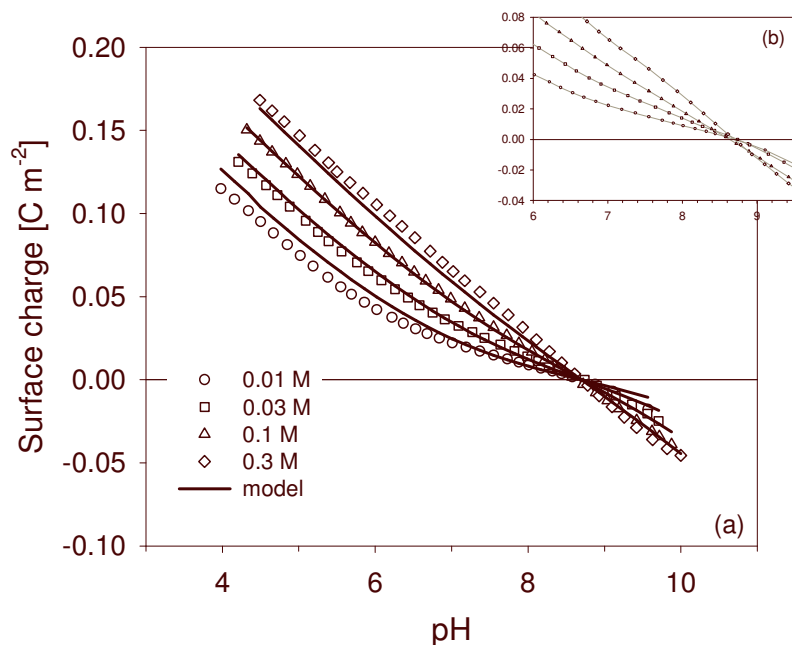


Figure 6.3. (a) Surface charge of the dispersed HFO aggregates determined by acid-base titrations at different ionic strength (0.01 M, 0.03 M, 0.1 M, 0.3 M NaNO₃). The experimental data (symbols) were fitted with a 1-pK basic Stern surface complexation model (continuous lines) including ion pair formation of Na⁺ and NO₃⁻ with surface hydroxyl groups. It is based on the CD-MUSIC model (Hiemstra *et al.*, 1989; Hiemstra and Van Riemsdijk, 1996), and is described in Chapter 5. (b) The inset gives a close-up view of the common intersection point. In (b) the dotted lines serve as eye-guides.

The pH-dependent adsorption of Sr by HFO is shown in Figure 6.4. Adsorption of Sr increased with increasing pH well below the PPZC of the HFO, the concentration of background electrolyte (0.01 or 0.1 M NaNO₃) had little effect on Sr sorption. The data were best modeled by defining a Sr surface complex (Equation 6.4) with charge distribution between the 0-plane and the d-plane. As compared to pure outer sphere complexation, allowing for charge distribution significantly improved the description of the pH dependence of Sr sorption. The fitted surface complexation parameters are listed in Table 6.1, and used in Figure 6.4 for the calculation of adsorption edges. Precipitation of SrCO₃ as an additional path of Sr uptake was excluded, because we excluded CO₂ during the experiments

so that the solutions were always under-saturated with respect to strontianite (SrCO_3).

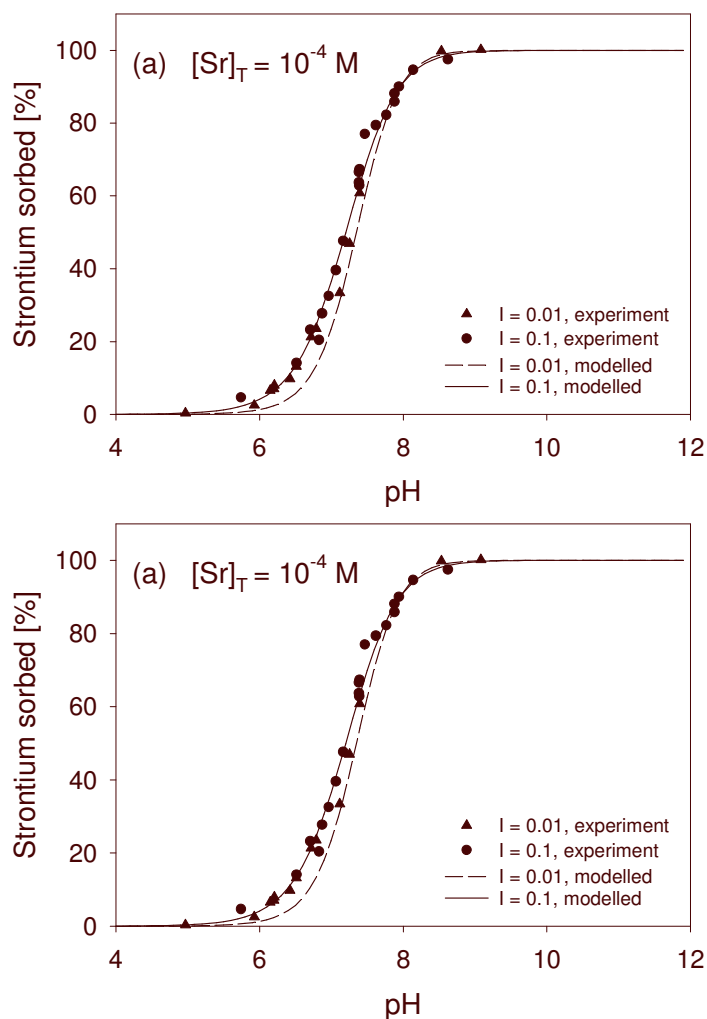


Figure 6.4. Strontium adsorption edges of re-dispersed HFO aggregates, as determined with 5 g L^{-1} HFO, total Sr concentrations of 10^{-4} M (a) and 10^{-3} M (b) and ionic strengths of 0.01 M and 0.1 M NaNO_3 . The model fit was done based on the 1-pK , basic Stern model and the protonation and ion pair parameters determined before. The best fit was obtained when charge distribution of the Sr ion between the 0-plane and d-plane was allowed.

6. Sorption kinetics II. Experiments

Synchrotron X-ray absorption fine structure (XAFS) spectroscopy has provided insights on Sr adsorption mechanisms on the surfaces of kaolinite, amorphous silica, and goethite (Sahai et al., 2000) and on hydrous ferric oxide (Axe et al., 1998). Results indicate that Sr generally adsorbs as a hydrated surface complex. Quantitative analyses indicated about 9 to 10 water ligands around the Sr^{2+} cation and an average Sr-O interatomic distance of 2.61 Å (Sahai et al., 2000). This is very close to the Sr-O distance of dilute Sr in aqueous solution (2.64 Å) and suggests the formation of outer-sphere surface complexes. The macroscopic data on Sr sorption to HFO in the present study and the model fit do not contradict the spectroscopic findings. The overlap of the sorption isotherms at different ionic strengths does not necessarily imply inner-sphere sorption (Lützenkirchen, 1997) as was suggested previously by Hayes and Leckie (Hayes and Leckie, 1987; Hayes et al., 1988). The modelled charge distribution of the Sr ion with 20% charge at the O-plane and 80% at the d-plane may be due to the discrete size of the Sr ion, as opposed to a point charge (Hiemstra and Van Riemsdijk, 1996).

6.3.2. Pore accessibility of the HFO aggregates

The salt pulse experiments showed that the volume replaced by the salt solution was larger than the theoretical inter-aggregate pore volume, but smaller than the total pore volume (inter- and intra-aggregate volume). Therefore a fraction of the intra-aggregate pore volume was accessible for the salt ions within the time that the salt pulse resided in the column.

It appeared from the salt pulses at different pH values that the accessible fraction of intra-aggregate pores varied with pH (Fig. 6.5b). At pH 4, the outer pore fraction corresponded to 37% of the intra-aggregate pores, whereas at pH 7, where surface protonation is low, 70-80% of the pores were freely accessible by the diffusing electrolyte ions. The size distribution of the pores in the wet HFO aggregate has been described by Hofmann et al. (2004). To estimate which fraction of pore sizes was accessed by the salt, we re-plotted the size distribution of the pores in the form of cumulative volume and surface distributions (Fig. 6.5a). Combining the cumulative volume distribution of the intra-aggregate pores as a function of pore size (Fig. 6.5a) with the fraction of outer pore volume obtained by the salt pulse experiments, we derived a lower pore size limit for the apparent free pore diffusion (Fig. 6.5b). At pH 4 only pores larger 4.4 nm would be easily accessible, at pH 7 this limit would reduce to 2.8 nm pore size.

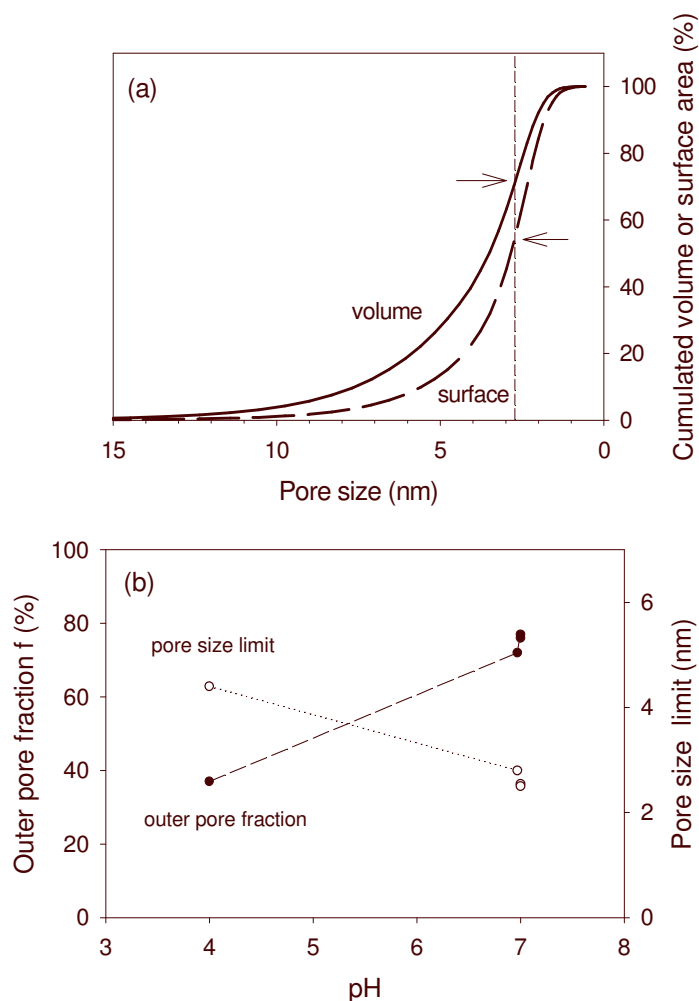


Figure 6.5. (a) Cumulative distribution of intra-aggregate pore volumes and surfaces as a function of pore size. The data were obtained by small angle neutron scattering (Hofmann et al., 2004). Arrows point to pores of 2.8 nm. They make up 72% of total volume but only 55% of total aggregate surface. (b) Fraction f of outer pores as a function of pH. The outer pore fraction is determined according to Equation 6.9 and corresponds to those intra-aggregate pores that are easily accessed during a salt pulse experiment (at 0.2 ml min^{-1}). Pores in the outer fraction are expected to be larger than the pore size limit shown. Lines serve as eye-guides.

6. Sorption kinetics II. Experiments

In the Donnan diffusion model (Chapter 5), we hypothesized that for small pores with overlapping electric diffuse layers, electrostatic constraint affects the ion diffusion rate. These pores make up the “inner-fraction”. At low surface potentials, the thickness of an electric diffuse layer can be estimated through the Debye-Hückel length (κ^{-1}). For an ionic strength of 0.01 M NaNO₃, κ^{-1} is 3 nm. In pores with diameters less than twice the Debye-Hückel length, that is in all pores smaller than 6 nm, substantial overlap of diffuse layers would occur. For the aggregates in this study, Donnan diffusion would be the appropriate model for 82% of the intra-aggregate pore volume. However, at the high surface potential of HFO, the Debye-Hückel length overestimates the diffuse layer thickness and overestimates the pore size in which overlap of diffuse layers takes place. It is therefore plausible that the inner pore fractions that were determined with the salt pulses, are significantly smaller than 82%.

6.3.3. Strontium breakthrough curves

Figure 6.6. shows the breakthrough curves for adsorption and desorption of Sr in a column packed with HFO aggregates adjusted to pH 4.0. At this low pH, adsorption of Sr to HFO is negligible (Fig. 6.4) and therefore no retardation is expected. The HFO surface is strongly protonated and positively charged (Fig. 6.3), which restrains Sr ions from diffusing into smaller pores. The salt pulse experiments indicate that only about 37% of the intra-aggregate porosity is accessible by free pore diffusion. The solid black line in Figure 6.6 shows the modeled breakthrough curves for Sr with 37% of the intra-aggregate pore volume accessible without electrostatic constraint. This describes the Sr breakthrough curves for adsorption and desorption very well. For comparison, the thin line shows the prediction when using the theoretical estimate of 18% outer-pore fraction (pore fraction $> 2\kappa^{-1}$). This does not give a good description of the experiment, indicating that the length of $2\kappa^{-1}$ overestimates the electrostatic constraint in the pores. The two remaining lines in Figure 6.6 show the extremes in which none or all aggregate pores are accessed by Sr. Neither of these two extremes permits an adequate description of the experimental data. Only the pore fraction estimated by the salt pulse gives an adequate description of the Sr breakthrough curve.

6. Sorption kinetics II. Experiments

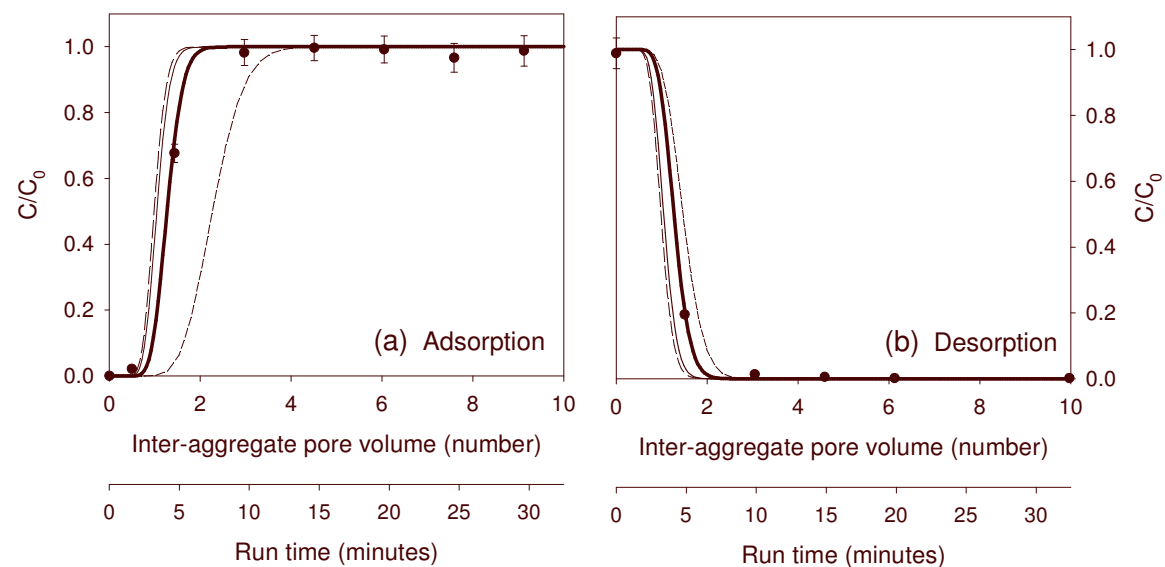


Figure 6.6. Strontium breakthrough curves at pH 4. Experimental data (\bullet) are best modeled with the Donnan diffusion model and an outer pore fraction of 37% (thick line). An outer-pore fraction of 18%, corresponding to all pores larger than 6 nm ($2\ \kappa^{-1}$), results in an earlier breakthrough (thin black line) and does not predict the data well. Models with no intra-aggregate diffusion (long-dashed line) and free pore diffusion in all intra-aggregate pores (short-dashed lines) do not predict the data either

6. Sorption kinetics II. Experiments

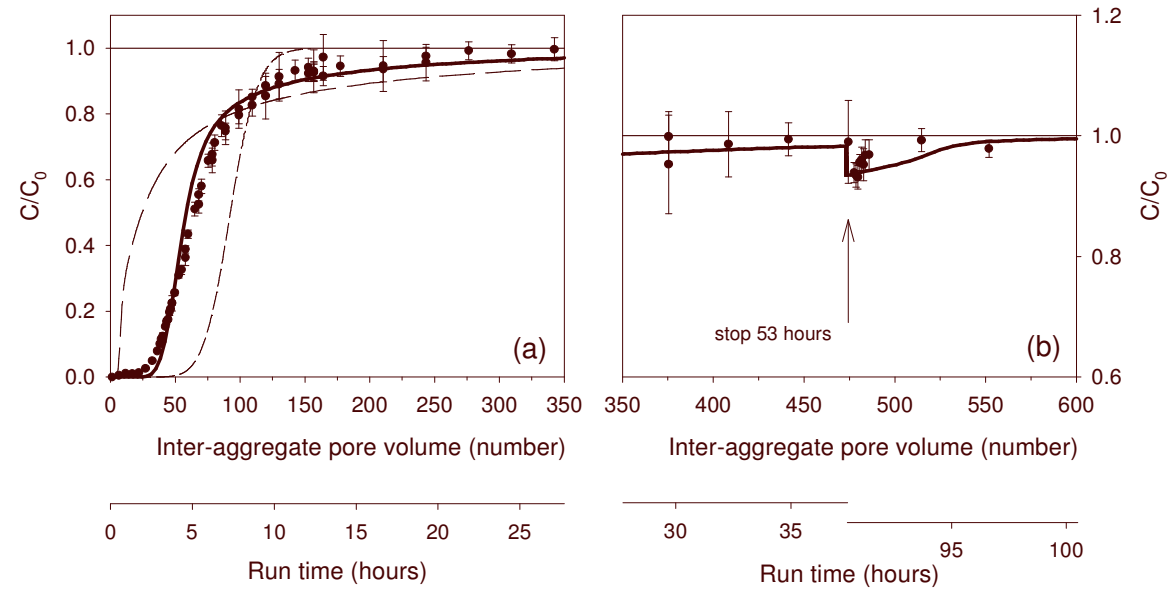


Figure 6.7. (a) Strontium adsorption data at pH 7 (●). In the model calculation with the Donnan diffusion model (thick line), an outer pore fraction of 72% was considered. The same calculation but with 18% outer pore fraction (long dashed line) underestimated the diffusion rate, whereas free pore diffusion in all intra-aggregate pores (short dashed line) overestimates the diffusion rate. (b) During interruption of flow (53 hours), Sr ions continue to diffuse into the aggregates, causing a concentration step.

The conditions drastically change at pH 7 (Fig. 6.7). At this pH, which is slightly below the PPZC of HFO, surface charging is lower and 72% of the aggregate pore volume is accessible by apparent free pore diffusion (Fig. 6.5b). This reduces the inner pore fraction to pores smaller than 2.8 nm. At pH 7, significant Sr uptake of $4.5 \cdot 10^{-6} \text{ mol g}^{-1}$ HFO was measured from the breakthrough curve. Good accessibility of a large portion of the pores and effective adsorption of Sr by HFO lead to considerable retardation of Sr. The first breakthrough of Sr was observed after about 20 pore volumes. The model prediction with 72% outer pore fraction (Fig. 6.7, thick solid line), is in good agreement with the experimental data and retardation of Sr is described correctly. In contrast, the theoretical estimate of the outer-pore fraction using the Debye-Hückel length does not allow a correct description of the experimental breakthrough curve. Retardation is underestimated by a factor 10. This discrepancy indicates that, even at pH 7, when surface potentials are lower, the pore size limit for Donnan-diffusion is much smaller than the assumed size of $2 \kappa^{-1}$.

The experimental breakthrough curve shows significant tailing (Fig. 6.7a). Sorption equilibrium was not yet reached after 350 pore volumes. This indicates that slow diffusion of Sr into the inner pore fraction of HFO aggregates was still continuing. The Donnan diffusion model fits the data very well, which supports the hypothesis that the electrostatic conditions in the inner fraction pores limit the diffusion rate, and that the Donnan model correctly predicts the sorption kinetics under these conditions. A further test of the validity of the model was performed with a flow interruption after 474 pore volumes (Fig. 6.7b). During the flow stop (53 hours), Sr in the mobile pores diffused to the intra-aggregate pores, thus decreasing the Sr concentration in the mobile solution. The concentration step appearing during the flow stop corresponded to a 7% decrease in Sr concentration and matched the experimental values. The good correspondence between model prediction and measurements adds evidence that the Donnan diffusion model correctly describes the diffusion rate in the small pores of the inner fraction. After 474 pore volumes the amount of adsorbed Sr corresponded to 85% of model predicted maximum adsorption at steady state. Uptake during stop would then mainly occur in the smallest pores, around or below 2 nm size. The Donnan diffusion model seems to hold for this strong spatial constriction.

After elution of 2000 pore volumes of Sr solution, the inflow was changed back to background electrolyte solution without Sr, causing Sr desorption and diffusion out of the aggregates. Figure 6.8 shows the results of this desorption experiment. Overall, the model prediction (Fig. 6.8) agrees fairly well with the experimental

6. Sorption kinetics II. Experiments

results, although some deviations remain. In the model, the effluent concentration remains unchanged for about 20 pore volumes before it starts to change significantly. However the Sr concentration in the desorption experiment dropped already after 4 pore volumes after switching to background electrolyte (Fig. 6.8). At 420 pore volumes, the experimental results indicate that 82% of the initially sorbed Sr had been eluted, while the model predicted 97%. Despite the lower predicted concentration of Sr remaining in the column, the predicted amount desorbed during the flow interruption is about three times higher than in the experiment. Both discrepancies between experimental and simulated curves indicate that the desorption reaction is somehow slowed down relative to predictions. Possibly desorption is not in local equilibrium and desorption kinetics are slower than adsorption kinetics.

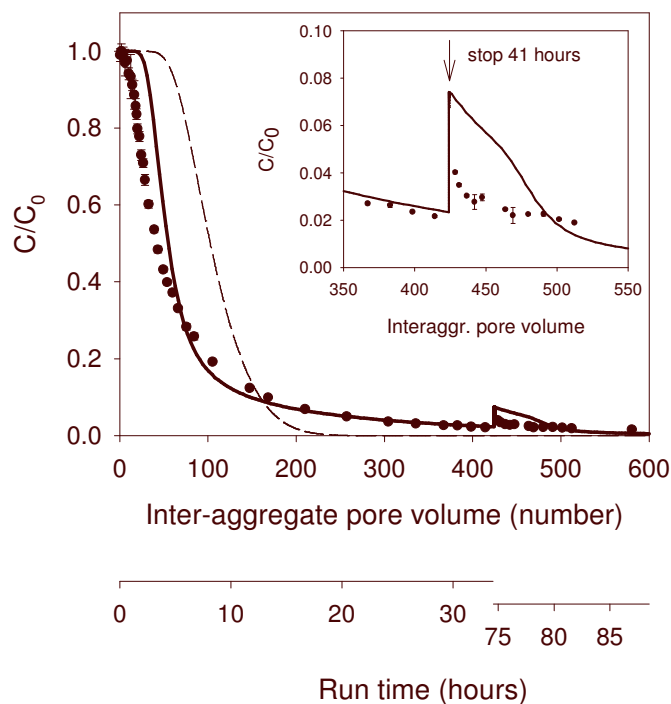


Figure 6.8. Strontium desorption data at pH 7(●) obtained after previous elution of 2000 pore volumes of Sr solution (Fig. 6.7). The thick line was calculated as in Fig. 6.7 using the Donnan diffusion model with an outer pore fraction of 72%. During the stop (41 h), Sr ions continue to diffuse out of the aggregates, thus increasing the Sr concentration in the mobile solution (inset). Free pore diffusion in all intra-aggregate pores (short dashes) is also shown.

6.4. Discussion

The Sr sorption experiments conducted in this study were designed to test the Donnan diffusion model developed in Chapter 5. The model is based on the theory that ion diffusion in small pores of oxide mineral aggregates is influenced by the variable chemical and electrical conditions in the pore. Experimental Sr breakthrough curves at pH 4 and pH 7 were successfully simulated, using a single set of independently determined sorption and textural parameters (Fig. 6.6 - 6.8 and Table 6.1). Only the inner/ outer pore fractions were determined specifically for each column. The good correspondence between experiment and model calculation confirmed that the Donnan diffusion model is suitable to predict slow diffusion in the nanometer size pores of the HFO aggregates. The pH dependent diffusion kinetics corresponded well with the observed changes in the breakthrough curves of the experiments at pH 4 and pH 7. Some disagreement was observed for Sr desorption at pH 7, however this might be related to factors independent of diffusion.

The Sr sorption experiments on HFO aggregates have provided insight into the range of pore sizes where Donnan diffusion is important. A very critical parameter for a good description of the sorption kinetics was a correct estimate of the outer- and inner-pore fractions. Comparison of these fractions with the pore size distribution (Fig. 6.5a) suggested that only pores smaller than 4.4 nm were governed by Donnan-diffusion at pH 4 and that this size limit decreased to 2.8 nm at pH 7. Initially, we had postulated that the validity of the Donnan-diffusion model was conditioned by the overlap of the electrical diffuse layers and was therefore dependent only on the ionic strength. However the results on pore accessibility presented in this study indicate that pH also influenced the fraction of pores in which Donnan diffusion is effective. The pH dependency suggests that the diffuse layers must overlap sufficiently so that the electric potential of the pore water, the Donnan potential, exceeds a given threshold value.

The lower limit of pore sizes where Donnan diffusion applies cannot be determined through the experiments conducted here. However the correct simulation of the stop and flow experiment at pH 7 conducted at a runtime of 37 hours when more than 85% of equilibrium Sr sorption had been achieved (Fig. 6.7b) suggested that pores of 2 nm or slightly below can still be modeled as Donnan-pores. From a geometric point of view, a lower limit between 1 nm and 2 nm seems plausible. Indeed the Stern layer of an oxide mineral can be as small as 0.28 nm, the size of one water molecule. The diameter of a hydrated Sr ion is about 0.62 nm (Robinson and Stokes, 1959) to 0.82 nm (Conway, 1981). Below the lower size limit of 1-2

6. Sorption kinetics II. Experiments

nm however, ion diffusion will be directly dependent on surface forces and surface diffusion could be the appropriate diffusion model.

The HFO aggregates used in this study were formed by a freeze and thaw technique (Hofmann et al., 2004) and were characterized by a majority of intermediate pore sizes: Pores in the range 2- 5 nm accounted for 65% of the total pore volume. Results in the present study showed that these aggregates were well suited to identify electrostatically constrained pore diffusion. Surface diffusion on the other hand was not specifically investigated on this material. However, since 8% of pore volume is contributed by pores of 2 nm or smaller (Fig. 6.5a), surface diffusion may contribute to some additional sorption. Based on the relation between pore volume and surface area, this contribution should however be less than 15% of the overall sorption (Fig. 6.5a). In contrast, Axe, Trivedi and co-workers (Axe and Anderson, 1995; Trivedi and Axe, 2000; 2001b) attributed a predominant role to surface diffusion in explaining the sorption kinetics onto hydrous oxides. Axe and Anderson (Axe and Anderson, 1995) investigated the sorption kinetics of Sr to fresh HFO aggregates under conditions of permanent mixing in a batch system. They showed that 60% of sorption sites were immediately accessible (“external sites”) whereas the remaining 40% of sites were situated “internally” and were reached via a slow diffusion process only. Under constant boundary conditions of 10^{-4} M Sr in the batch solution, it took about 50 days to reach sorption equilibrium at the internal sites. This slow process was attributed to surface diffusion. Pore diffusion was considered negligible in the hydrous oxide system. At pH 7, total Sr sorbed after 1 hour was $0.9 \cdot 10^{-4}$ mol g⁻¹ HFO and $1.48 \cdot 10^{-4}$ mol g⁻¹ after 50 days.

One major difference to our study is the Sr affinity to the HFO surface. At similar Sr²⁺ equilibrium concentration and pH, total Sr sorbed in our experiment was $4.5 \cdot 10^{-6}$ mol g⁻¹ HFO after 4 days contact time. This is 30 times less than what was measured in the study by Axe and Anderson (1995). The different sorption behavior of Sr to the HFO may be related to the freeze and thaw process used to form the dense HFO aggregates; however, also other differences in the HFO preparation method could have contributed to the different reactivity. Additionally, the thorough exclusion of CO₂ in our work might have influenced the sorption equilibrium. Regardless of the factors controlling surface reactivity, the fractions of easily accessible and inner sites were the same in Axe and Anderson’s and in our system. At pH 7 we found an outer pore fraction of 72%. Taking into account the relation between volumes and surfaces, this volume fraction corresponds to a surface fraction of 55% (Fig. 6.5a), which is very close to the fraction found by

Axe and Anderson (1995) and others (Fuller et al., 1993) at a pH of 7. Using the amount of Sr sorbed at immediately accessible sites to normalize Sr adsorption, sorption kinetics in both experiments can be compared (Fig. 6.9). For HFO aggregates produced by freeze and thaw, only 9 hours were needed to bind at internal sites an amount equivalent to 50% of the Sr sorbed at immediately accessible sites. For fresh HFO aggregates (Axe and Anderson, 1995), 20 days were necessary to reach this ratio. This major difference in the two sorption curves may however be attributed to retardation due to higher Sr-binding to the fresh HFO in Axe and Anderson's work. A priori it does not reflect a fundamental difference in the diffusion mechanisms.

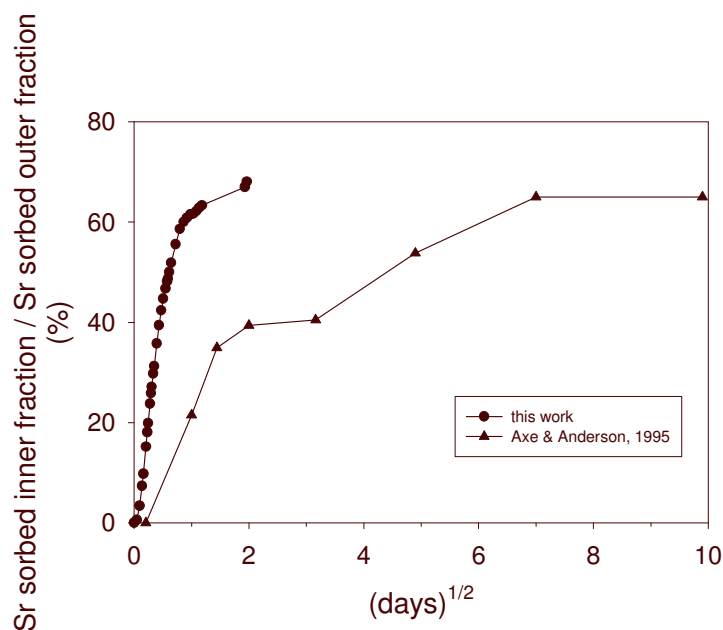


Figure 6.9. Comparison of Sr sorption to HFO in this study and in Axe and Anderson (Axe and Anderson, 1995). The curves show Sr sorbed at inner sites (inner-pore fraction in our study, “internal sites” in Axe and Anderson) relative to Sr sorbed at external sites (“outer pore fraction” in our study, external sites in Axe and Anderson). Sorption data are plotted as a function of time, visualizing the diffusion kinetics in the different HFO aggregates used.

6.5. Conclusion

The experiments conducted on diffusion and sorption of Sr by HFO aggregates and the simulation of the experiments by the Donnan diffusion model demonstrated that electrostatically constrained pore diffusion was important in pores of intermediate size, which are large enough to contain unbound water, but small enough that the diffuse electric layers overlap. The Donnan-diffusion model was appropriate to describe this process. The range of pore sizes where Donnan diffusion applied strongly depended on pH. Thus, this range is related to the thickness of the diffuse layers as well as to the level of the electrical potentials across the pore. For the HFO aggregates in this study, pores between 2 and 4.5 nm size were involved in Donnan diffusion.

So far we have studied Sr uptake at pH values below the pH_{ppzc} of HFO, under conditions where diffusion of a cation is slowed down by charge exclusion in the pores. The opposite condition, where the diffusing ions are attracted to the pores will need to be considered to further validate the model. Future studies might either investigate anion diffusion at a pH range below pH_{ppzc} or cation diffusion at pH values above pH_{ppzc} .

In analogy with the HFO formed by freezing and thawing, compression of other nano-particles at high pressure may typically produce dense materials with pores where Donnan diffusion is effective. In compacted bentonites, Ochs et al. (1998, 2001) modeled cation diffusion using an electrostatic diffusion model. Compacted materials may thus have strong potential for future application of the Donnan diffusion model. Its strength is that it automatically adapts diffusion kinetics and sorption affinities to chemical changes in the particle-solution aqueous system.

7. Epilogue

7.1. Modelling solute transport in soils

Transport of ions in soil is of mayor importance in determining the environmental risks of contaminants. The mobility of ions in soil is affected by a combination of physical and chemical processes. The physical processes convection and molecular diffusion determine the transport rate of dissolved ions, while chemical interaction between the dissolved ions and solid soil particles determines which fraction of the ions is mobile. Over recent years the mechanistic understanding of multicomponent interactions has increased significantly, and advanced models have been developed to describe these mechanisms. This has led to a better understanding of how different ions affect mutual binding behaviour in batch systems. Ions that do affect each others binding behaviour to soil solid particles also affect each other's mobility in a soil system.

In order to obtain a better understanding of the nature and magnitude of these interactions we combined chemical interaction modelling with a transport model for structured soil. Solute transport in structured soils, such as aggregated soils or cracked clay soils, is generally dominated by convection through cracks or large pores in between soil aggregates. The mobile-immobile transport model describes a soil with a mobile and an immobile water region. Ion transport takes place with water flow through the larger pores (the mobile region) and by diffusion into and out of an immobile water region, representing stagnant water inside the smaller pores. Numerical transport modelling in ORCHESTRA allowed us to explore the combination of complex chemistry with physical processes such as convection and diffusion. The ORCHESTRA software is organised in a unique way that does not limit the user to any predefined models, as it allows users to adapt existing models and to add new models to its model database. This includes chemical as well as transport models for which the layout and dimensions are completely user-definable.

A numerical model of multicomponent transport in a mobile-immobile flow system was evaluated and validated with an experimental system with well-defined chemical and physical properties. The use of a well-defined experimental system is essential to rigorously test the assumptions and theories that are embodied within the mechanistic model. The use of well-defined systems in combination with mechanistic modelling is therefore an effective approach for the development and validation of theories and for the improved understanding of chemical and physical processes.

7.2. Well-defined experimental systems

Soils are chemically and physically complex systems in which many processes occur simultaneously. Therefore, it is useful to study reactive transport processes in a simplified model system before trying to understand the processes that affect chemical behaviour in a complex natural system. By building up the experimental system from simpler to more realistic systems, fewer assumptions need to be made and theories about the mechanisms can be validated with more certainty. Artificial systems such as the gel-bead system described in Chapter 2 to 4 can give a lot of insight into chemical and physical processes. The use of alginate gel has several advantages. The gel mainly consists of water held together by a very open polymer structure. Small solutes can diffuse freely through the gel with virtually the same diffusion coefficient as diffusion in water. Particulate materials can be immobilised inside the gel to study chemical interactions with the particles. Here we demonstrate the immobilisation of goethite, but other small particles such as minerals and organic particles could be immobilised inside the gel. In this way the material becomes easier to handle for batch experiments and can be used in column experiments as demonstrated for goethite. The gel can also be used to encapsulate intact soil aggregates to protect them from falling apart during experiments.

In the first two articles of this thesis we demonstrated that the mobile-immobile transport model gave very accurate descriptions of ion transport in the gel-bead system (Chapter 2 and 3). Convection and diffusion of a non-reactive solute in a well-defined gel-bead system was evaluated and extended to reactive transport of protons. The physical dimensions and the chemistry of the system were uniform and well known. All information required for the modelling, such as the physical dimensions of the system and the chemistry of the gel matrix, were obtained from independent measurements. Transport as the result of a combination of convection, diffusion and chemical sorption was well simulated. The model simulated the influence of the flow rate on the breakthrough curves very well for the nonreactive and reactive solutes. The second article (Chapter 3) also showed the influence of competitive sorption for proton transport. Protons and calcium ions compete for binding onto the same reactive sites on the alginate polymer. Therefore a higher calcium concentration causes more calcium sorption and less proton sorption. As a result transport of protons through the column is less retarded and breakthrough takes place earlier in the presence of a higher calcium concentration. The effect was well simulated by the transport model. Additional model calculations showed that competition causes slightly more tailing due to a temporary delay in sorption

caused by a temporary increase in the concentration of the competing, desorbing, ion.

7.3. Solute transport in multicomponent systems

Transport becomes more difficult to predict when the systems become more complex and less well understood. Non-equilibrium transport of sulphate and chromate through a column with goethite in Chapter 4 was reasonably well simulated for transport of each ion on its own. The model was less successful in predicting the competitive effects during transport. The changes in pH caused by multicomponent sorption on the goethite surface were not described well, because of proton buffering by the gel matrix. Buffering from other sorbents is very likely to occur in natural soil systems that contain a cocktail of more and less reactive sorbents. The effect of competitive sorption was well described for chromate infiltration into a goethite column with sulphate, but not for sulphate infiltration into a column with chromate. Less chromate desorption occurred during sulphate infiltration than expected from the model calculations and from competition in batch experiments. A possible explanation for this discrepancy is that chromate desorption may not be instantaneous but relatively slow in comparison with the flow rate through the column. The model is based on a local equilibrium assumption (LEA) which implies that sorption and desorption are instantaneous when the solutes are near the goethite surface. Diffusion to and from the goethite inside the gel beads is the only rate limiting process in the model. It is possible that desorption of chromate from the goethite surface is a slow process in itself. The results for sulphate desorption following chromate infiltration showed that the effect of competition is far less pronounced in a nonequilibrium system than expected in an equilibrium system. The effect of competition was smaller for the same experiment at a higher flow rate.

7.4. The Donnan-diffusion model

Chapter 5 and 6 address strontium sorption in microscopic aggregates of hydrous ferric oxide (HFO). Sorption in HFO aggregates is a typical example for which modelling multicomponent sorption and diffusion can be applied. Strontium sorption is pH-dependent and influences the pH of the system by causing desorption of protons from the oxide surface. Therefore, to model strontium sorption one should account for sorption and diffusion rates of both ions. Diffusion inside microporous aggregates such as HFO is moreover influenced by the electrostatic behaviour of the oxide surfaces. At pH values below 8, the surfaces

7. Epilogue

are positively charged and due to the electrostatic potential the concentrations of positively charged ions are very low in the vicinity of the surface. The pore space inside the aggregates is strongly influenced by the internal surfaces and the diffusion of ions through the pore space is strongly affected. In Chapter 5 we suggested a mechanistic approach to account for the effect of the electrostatic potential on diffusion and sorption. The Donnan-diffusion model uses the Donnan electrostatic model that is part of the surface complexation model to estimate the concentration gradients and electrostatic gradients in the pores. This model is therefore a good example of the link between chemical and physical processes and the value of mechanistic modelling. Using a mechanistic model to describe the surface chemistry and sorption, the same electrostatic model could be employed to describe the diffusion rates in the pores.

The Donnan-diffusion model explained the very small diffusion coefficient for strontium in HFO that was reported in literature. The very low concentration of strontium in the Donnan pore space reduces the diffusion flux into the HFO particle. The model was also successful when extended to simulate strontium transport in a column with HFO in Chapter 6. The last chapter showed that it might be difficult to obtain parameters for a less well-understood system. The volume fraction of the pores that was subject to Donnan diffusion was estimated from salt exclusion during transport experiments with salt pulses, although this volume fraction varied with flow rate and pH. The transport model gave a good description of the strontium breakthrough curves at two pH values. However, the predictive value of the model is compromised by the assumptions made in the estimation of model parameters. Ideally, all parameters in a theoretical model would be measured independently to allow validation of the theory.

7.5. Conclusions

In summary, solute transport in well-defined systems can be accurately predicted by the combination of surface complexation models with transport modelling. Effects of non-linear sorption, concentration and pH-dependent transport, transport of protons, and competition with other ions, can all be predicted by combined modelling. However, we also learned that it is important to include all influencing processes in the model, including physical and chemical non-equilibrium, buffering by additional reactive surfaces and the sorption and transport of other solutes in the system. To predict transport in real soils is therefore a challenge.

We showed that the mobility of solutes in mobile-immobile transport systems is influenced by competitive sorption just as in equilibrium systems. Sorption of one

ion can cause desorption of a second ion, and a temporary increase in leaching of the second ion. The effect is however less pronounced than in equilibrium systems and the effect may be concealed by sorption and desorption from other surfaces (buffering) as we saw for competition between ions and protons.

The flow rate through the soil determines the time of breakthrough, but also the time available to reach equilibrium and therefore the shape of the breakthrough curve and extend of tailing. When sorption takes place inside aggregates, the time required to reach equilibrium is longer than for non-reactive ions, because more ions need to be migrated into the aggregate. Therefore strongly adsorbing ions show a stronger non-equilibrium effect than weakly adsorbing or non-reactive ions. Sorption inside microporous particles can be even slower because of the electrostatic potential caused by the charged surfaces. The concentration of oppositely charged ions inside the pores is several orders of magnitude smaller than the concentration outside the particle and the diffusion flux into the particle is very small, causing long time to reach equilibrium sorption. The effective diffusion coefficient is strongly dependent on the pH. The results indicate that a good understanding of the local chemistry is important to understand larger scale sorption and transport.

8. References

- Aguilella V.M., Mafé S. and Pellicer J. (1987) On the nature of the diffusion potential derived from Nerst-Planck flux equation by using the electroneutrality assumption. *Electrochimica Acta* 32 (3): 483-488.
- Appelo C.A.J. and Postma D. (1999) *Geochemistry, groundwater and pollution*; Balkema, Rotterdam.
- Atkinson R.J., Posner A.M. and Quirk J.P. (1967) Adsorption of potential-determining ions at the ferric oxide-aqueous electrolyte interface. *Journal of Physical Chemistry* 71: 550-558.
- Axe L. and Anderson P.R. (1995) Sr diffusion and reaction within Fe oxides - evaluation of the rate-limiting mechanism for sorption. *Journal of Colloid and Interface Science* 175 (1): 157-165.
- Axe L. and Anderson P.R. (1997) Experimental and theoretical diffusivities of Cd and Sr in hydrous ferric oxide. *Journal of Colloid and Interface Science* 185 (2): 436-448.
- Axe L., Bunker G.B., Anderson P.R. and Tyson T.A. (1998) An XAFS analysis of strontium at the hydrous ferric oxide surface. *Journal of Colloid and Interface Science* 199 (1): 44-52.
- Axe L. and Trivedi P. (2002) Intraparticle surface diffusion of metal contaminants and their attenuation in microporous amorphous Al, Fe, and Mn oxides. *Journal of Colloid and Interface Science* 247 (2): 259-265.
- Barrow N.J., Gerth J. and Brummer G.W. (1989) Reaction-kinetics of the adsorption and desorption of nickel, zinc and cadmium by goethite .2. Modeling the extent and rate of reaction. *Journal of Soil Science* 40 (2): 437-450.
- Berry J.A. and Bond K.A. (1992) Studies of the extent of surface-diffusion in the migration of radionuclides through geological-materials. *Radiochimica Acta* 58/59: 329-335.
- Bérubé Y.G., Onoda G.Y. and De Bruyn P.L. (1967) Proton adsorption at the ferric oxide/aqueous. solution interface. II. Analysis of kinetic data. *Surface Science* 8: 448.
- Brusseau M.L. and Rao P.S.C. (1990) Modeling solute transport in structured soils - A review. *Geoderma* 46: 169-192.

References

- Brusseau M.L. (1994) Transport of reactive contaminants in heterogeneous porous-media. *Reviews of Geophysics* 32 (3): 285-313.
- Christl I. and Kretzschmar R. (1999) Competitive sorption of copper and lead at the oxide-water interface: Implications for surface site density. *Geochimica et Cosmochimica Acta* 63 (19-20): 2929-2938 .
- Coats K.H. and Smith B.D. (1964) Dead-end pore volume and dispersion in porous media. *Society of Petroleum Engineers Journal* 4 (3): 73-84.
- Conway B. E. (1981) *Ionic hydration in chemistry and biophysics*; Elsevier, New York.
- Cornell R.M. and Schwertmann U. (1996) *The iron oxides*; VCH Verlagsgesellschaft mbH, Weinheim.
- Crank J. (1956) *The Mathematics of Diffusion*; Oxford University Press, London.
- Davis J.A. and Leckie J.O. (1978) Surface ionization and complexation at the oxide/water interface: II. Surface properties of amorphous iron oxyhydroxide and adsorption of metal ions. *Journal of Colloid and Interface Science* 67: 90-107.
- Davison W., Zhang H. and Grime G.W. (1994) Performance-characteristics of gel probes used for measuring the chemistry of pore waters. *Environmental Science and Technology* 28 (9): 1623-1632.
- De Smedt F. and Wierenga P.J. (1984) Solute transfer through columns of glass-beads. *Water Resources Research* 20 (2): 225-232.
- Deans H.A. and Rice U. (1963) A mathematical model for dispersion in the direction of flow in porous media. *Society of Petroleum Engineers Journal* 3 (3): 49-52.
- Dzombak D.A. and Morel F.M.M. (1990) *Surface complexation modeling; Hydrous ferric oxide*; John Wiley & Sons, New York.
- Fendorf S., Eick M.J., Grossl P. and Sparks D.L. (1997) Arsenate and chromate retention mechanisms on goethite. 1. Surface structure. *Environmental Science and Technology* 31 (2): 315-320.
- Fuller C.C., Davis J.A. and Waychunas G.A. (1993) Surface chemistry of ferrihydrite. *Geochimica et Cosmochimica Acta* 57 (10): 2271-2282.

- Gapon E.N. (1934) On the theory of exchange adsorption in soils. (in Russian). *Journal of General Chemistry (USSR)* 3 : 144-152.
- Gaston L.A. and Selim H.M. (1991) Predicting cation mobility in kaolinitic media based on exchange selectivities of kaolinite. *Soil Science Society of America Journal* 55 (5): 1255-1261.
- Geelhoed J.S., Hiemstra T. and Van Riemsdijk W.H. (1997) Phosphate and sulfate adsorption on goethite: Single anion and competitive adsorption. *Geochimica et Cosmochimica Acta* 61 (12): 2389-2396.
- Hatano R., Tomita A. and Sakuma T. (1993) Diffusion-processes in water-saturated spherical soil aggregates. *Soil Science and Plant Nutrition* 39 (2): 245-255.
- Hatzinger P.B. and Alexander M. (1997) Biodegradation of organic compounds sequestered in organic solids or in nanopores within silica particles. *Environmental Toxicology and Chemistry* 16: 2215-2221.
- Hayes K.F. and Leckie J.O. (1987) Modeling ionic-strength effects on cation adsorption at hydrous oxide-solution interfaces. *Journal of Colloid and Interface Science* 115 (2): 564-572.
- Hayes K.F., Papelis C. and Leckie J.O. (1988) Modeling ionic-strength effects on anion adsorption at hydrous oxide-solution interfaces. *Journal of Colloid and Interface Science* 125 (2): 717-726.
- Helfferich F. (1962) *Ion Exchange*; McGrawhill, New York.
- Hiemstra T., Van Riemsdijk W.H. and Bolt G.H. (1989) Multisite proton adsorption modeling at the solid-solution interface of (hydr)oxides - a new approach .1. Model description and evaluation of intrinsic reaction constants. *Journal of Colloid and Interface Science* 133 (1): 91-104.
- Hiemstra T. and Van Riemsdijk W.H. (1996) A surface structural approach to ion adsorption: The charge distribution (CD) model. *Journal of Colloid and Interface Science* 179 (2): 488-508.
- Hiemstra T. and Van Riemsdijk W.H. (1999) Surface structural ion adsorption modeling of competitive binding of oxyanions by metal (hydr)oxides. *Journal of Colloid and Interface Science* 210 (1): 182-193.
- Hofmann A., Pelletier M., Michot L., Stradner A., Schurtenberger P. and Kretzschmar R. (2004) Characterization of the pores in hydrous ferric oxide

References

- aggregates formed by freezing and thawing. *Journal of Colloid and Interface Science* 271 (1): 163-173.
- Jang L.K., Geesey G.G., Lopez S.L., Eastman S.L. and Wichlacz P.L. (1990) Use of a gel-forming biopolymer directly dispensed into a loop fluidized-bed reactor to recover dissolved copper. *Water Research* 24 (7): 889-897.
- Jang L.K., Nguyen D. and Geesey G.G. (1995) Effect of pH on the absorption of Cu(II) by alginate gel. *Water Research* 29 (1): 315-321.
- Jarvis N.J., Bergstrom L. and Dik P.E. (1991) Modeling water and solute transport in macroporous soil .2. Chloride breakthrough under nonsteady flow. *Journal of Soil Science* 42 (1): 71-81.
- Johnson R.M. and Pepperman A.B. (1998) Release of atrazine and alachlor from clay-oxamide controlled-release formulations. *Pesticide Science* 53: 233-240.
- Kärger J. and Ruthven D.M. (1992) *Diffusion in Zeolites and Other Micro-porous Solids*; John Wiley & Sons, New York.
- Kato H., Muroi M., Yamada N., Ishida H. and Sato H. (1995) Estimation of effective diffusivity in compacted bentonite. *Material Research Society Symposium Proceedings; Scientific basis for nuclear waste management XVIII* 353: 277-284.
- Keizer M.G. and Van Riemsdijk W.H. (1998) *ECOSAT Version 4.7*; Department Soil Sciences and Plant Nutrition, Wageningen University.
- Kinniburgh D.G. (1993) *FIT user guide*; British Geological Survey, NERC, Hydrogeological Series Technical Report WD/93/23.
- Kinniburgh D.G., Milne C.J. and Venema P. (1995) Design and construction of a personal-computer-based automatic titrator. *Soil Science Society of America Journal* 59 (2): 417-422.
- Kinniburgh D.G., Van Riemsdijk W.H., Koopal L.K., Borkovec M., Benedetti M.H. and Avena M.J. (1999) Ion binding to natural organic matter: competition, heterogeneity, stoichiometry and thermodynamic consistency. *Colloids and Surfaces A: Physicochemical and Engineering Aspects* 151 (1-2): 147-166.
- Koch S. and Fluhler H. (1994) Lateral solute mixing in homogeneous and layered sand columns. *Geoderma* 63 (2): 109-121.

- Koopal L.K., Van Riemsdijk W.H., De Wit J.C.M. and Benedetti M.F. (1994) Analytical isotherm equations for multicomponent adsorption to heterogeneous surfaces. *Journal of Colloid and Interface Science* 166: 51-60.
- Li Y. and Gregory S. (1974) Diffusion of ions in sea water and in deep-sea sediments. *Geochimica et Cosmochimica Acta* 38 (5): 703-714.
- Lützenkirchen J. (1997) Ionic strength effects on cation sorption to oxides: Macroscopic observations and their significance in microscopic interpretation. *Journal of Colloid and Interface Science* 195 (1): 149-155.
- Lützenkirchen J. (2001) Evaluation of experimental procedures and discussion of two different modelling approaches with respect to long-term kinetics of metal cation sorption onto (hydr)oxide surfaces. *Aquatic Geochemistry* 7 (3): 217-235.
- Lyklema J. (1984) Points of zero charge in the presence of specific adsorption. *Journal of Colloid and Interface Science* 99 (1): 109-117.
- Ma L.W. and Selim H.M. (1995) Transport of a nonreactive solute in soils - a 2-flow domain approach. *Soil Science* 159 (4): 224-234.
- Ma L.W. and Selim H.M. (1997) Physical nonequilibrium modeling approaches to solute transport in soils. *Advances in Agronomy* 58: 95-150.
- Manceau A. and Charlet L. (1994) The mechanism of selenate adsorption on goethite and hydrous ferric-oxide. *Journal of Colloid and Interface Science* 168 (1): 87-93.
- Mansell R.S., Bloom S.A., Selim H.M. and Rhue R.D. (1988) Simulated transport of multiple cations in soil using variable selectivity coefficients. *Soil Science Society of America Journal* 52 (6): 1533-1540.
- Marinsky J.A. and Ephraim J. (1986) A unified physicochemical description of the protonation and metal-ion complexation equilibria of natural organic-acids (humic and fulvic-acids) .1. Analysis of the influence of polyelectrolyte properties on protonation equilibria in ionic media - Fundamental concepts. *Environmental Science and Technology* 20 (4): 349-354.
- Martinsen A., Skjåk-Bræk G. and Smidsrød O. (1989) Alginate as immobilization material.1. Correlation between chemical and physical properties of alginate gel beads. *Biotechnology and Bioengineering* 33 (1): 79-89.

References

- Meeussen J.C.L., Scheidegger A., Hiemstra T., Van Riemsdijk W.H. and Borkovec M. (1996) Predicting multicomponent adsorption and transport of fluoride at variable pH in a goethite-silica sand system. *Environmental Science and Technology* 30 (2): 481-488.
- Meeussen J.C.L., Lumsdon D.G. and Meeussen V.C.S. (1996) An efficient object oriented approach for calculating chemical equilibria in combination with transport; In: *Hydroinformatics '96*; Balkema, Rotterdam.
- Meeussen J.C.L., Kleikemper J., Scheidegger A.M., Borkovec M., Paterson E., Van Riemsdijk W.H. and Sparks D.L. (1999) Multicomponent transport of sulfate in a goethite-silica sand system at variable pH and ionic strength. *Environmental Science and Technology* 33 (19), 3443-3450.
- Meeussen J.C.L. (2000) *ORCHESTRA*; <http://www.meeussen.nl/orchestra>
- Meeussen J.C.L. (2003) ORCHESTRA: An object-oriented framework for implementing chemical equilibrium models. *Environmental Science and Technology* 37 (6): 1175-1182.
- Mesure K. and Fish W. (1992) Chromate and oxalate adsorption on goethite .1. Calibration of surface complexation models. *Environmental Science and Technology* 26 (12): 2357-2364.
- Milne C.J., Kinniburgh D.G., De Wit J.C.M., Van Riemsdijk W.H. and Koopal L.K. (1995) Analysis of proton binding by a peat humic-acid using a simple electrostatic model. *Geochimica et Cosmochimica Acta* 59 (6): 1101-1112.
- Murphy J. and Riley J.P. (1962) A modified single solution method for the determination of phosphate in natural waters. *Analytica Chimica Acta* 27: 31-36.
- Nkedi-Kizza P., Rao P.S.C., Jessup R.E. and Davidson J.M. (1982) Ion-exchange and diffusive mass-transfer during miscible displacement through an aggregated oxisol. *Soil Science Society of America Journal* 46 (3): 471-476.
- Ochs M., Boonekamp M., Wanner H., Sato H. and Yui M. (1998) A quantitative model for ion diffusion in compacted bentonite. *Radiochimica Acta* 82: 437-443.
- Ochs M., Lothenbach B., Wanner H., Sato H. and Yui M. (2001) An integrated sorption-diffusion model for the calculation of consistent distribution and diffusion coefficients in compacted bentonite. *Journal of Contaminant Hydrology* 47 (2-4): 283-296.

- O'Reilly S.E., Strawn D.G. and Sparks D.L. (2001) Residence time effects on arsenate adsorption/desorption mechanisms on goethite. *Soil Science Society of America Journal* 65 (1): 67-77.
- Oscarson D.W. (1994) Surface-diffusion - is it an important transport mechanism in compacted clays. *Clays and Clay Minerals* 42 (5): 534-543.
- Parker J.C. and Valocchi A.J. (1986) Constraints on the validity of equilibrium and first-order kinetic transport models in structured soils. *Water Resources Research* 22: 399-407.
- Passioura J.B. (1971) Hydrodynamic dispersion in aggregated media .1. Theory. *Soil Science* 111: 339-344.
- Pefferkorn E. (1999) Polyacrylamide at solid/liquid interfaces. *Journal of Colloid and Interface Science* 216 (2): 197-220.
- Peryea F.J. and Kammereck R. (1997) Phosphate-enhanced movement of arsenic out of lead arsenate-contaminated topsoil and through uncontaminated subsoil. *Water Air and Soil Pollution* 93 (1-4): 243-254.
- Rao P.S.C., Jessup R.E., Rolston D.E., Davidson J.M. and Kilcrease D.P. (1980a) Experimental and mathematical description of nonadsorbed solute transfer by diffusion in spherical aggregates. *Soil Science Society of America Journal* 44: 684-688.
- Rao P.S.C., Rolston D.E., Jessup R.E. and Davidson J.M. (1980b) Solute transport in aggregated porous media: theoretical and experimental evaluation. *Soil Science Society of America Journal* 44 (6): 1139-1146.
- Rao P.S.C., Jessup R.E. and Addiscott T.M. (1982) Experimental and theoretical aspects of solute diffusion in spherical and nonspherical aggregates. *Soil Science* 133: 342-349.
- Rietra R.P.J.J., Hiemstra T. and Van Riemsdijk W.H. (1999a) The relationship between molecular structure and ion adsorption on variable charge minerals. *Geochimica et Cosmochimica Acta* 63 (19-20): 3009-3015.
- Rietra R.P.J.J., Hiemstra T. and Van Riemsdijk W.H. (1999b) Sulfate adsorption on goethite. *Journal of Colloid and Interface Science* 218 (2): 511-521.
- Robinson R.A. and Stokes R.H. (1959) *Electrolyte solutions*; Butterworths, London.

References

- Roden E.E. and Zachara J.M. (1996) Microbial reduction of crystalline iron(III) oxides: Influence of oxide surface area and potential for cell growth. *Environmental Science and Technology* 30 (5): 1618-1628.
- Rose D.A. and Passioura J.B. (1971) The analysis of experiments on hydrodynamic dispersion. *Soil Science* 111: 252-257.
- Sahai N., Carroll S.A., Roberts S. and O'Day P.A. (2000) X-ray absorption spectroscopy of strontium(II) coordination - II. Sorption and precipitation at kaolinite, amorphous silica, and goethite surfaces. *Journal of Colloid and Interface Science* 222 (2): 198-212.
- Sato H., Yui M. and Yoshikawa H. (1995) Diffusion behavior for Se and Zr in sodium-bentonite. *Material Research Society Symposium Proceedings; Scientific basis for nuclear waste management XVIII* 353: 269-276.
- Scheidegger A., B rgisser C.S., Borkovec M. and Sticher H. (1994) Convective-transport of acids and bases in porous-media. *Water Resources Research* 30 (11): 2937-2944.
- Scheinost A.C., Abend S., Pandya K.I. and Sparks D.L. (2001) Kinetic controls on Cu and Pb sorption by ferrihydrite. *Environmental Science and Technology* 35 (6): 1090-1096.
- Schudel M., Behrens S.H., Holthoff H., Kretzschmar R. and Borkovec M. (1997) Absolute aggregation rate constants of hematite particles in aqueous suspensions: A comparison of two different surface morphologies. *Journal of Colloid and Interface Science* 196 (2): 241-253.
- Schulin R., Papritz A., Fluhler H. and Selim H.M. (1989) Calcium and magnesium transport in aggregated soils at variable ionic-strength. *Geoderma* 44 (2-3): 129-141.
- Schwertmann U. and Cornell R.M. (1991) *Iron oxides in the laboratory*; VCH Verlagsgesellschaft, Weinheim.
- Seke M.D., Sandenbergh R.F. and Vegter N.M. (2000) Effects of the textural and surface properties of activated carbon on the adsorption of gold di-cyanide. *Minerals Engineering* 13 (5): 527-540.
- Selim H.M., Schulin R. and Fluhler H. (1987) Transport and ion-exchange of calcium and magnesium in an aggregated soil. *Soil Science Society of America Journal* 51 (4): 876-884.

- Selim H.M., Buchter B., Hinz C. and Ma L. (1992) Modeling the transport and retention of cadmium in soils - multireaction and multicomponent approaches. *Soil Science Society of America Journal* 56 (4): 1004-1015.
- Singh P., Kanwar R.S. and Thompson M.L. (1991) Measurement and characterization of macropores by using autocad and automatic image-analysis. *Journal of Environmental Quality* 20 (1): 289-294.
- Sparks D.L. (2000) New frontiers in elucidating the kinetics and mechanisms of metal and oxyanion sorption at the soil mineral/water interface. *Journal of Plant Nutrition and Soil Science* 163 (6): 563-570.
- Sposito G. (1989) *The chemistry of soils*; Oxford University Press, New York.
- Spurlock F.C., Huang K. and Van Genuchten M.Th. (1995) Isotherm nonlinearity and nonequilibrium sorption effects on transport of fenuron and monuron in soil columns. *Environmental Science and Technology* 29 (4): 1000-1007.
- Stanjek H. and Weidler P.G. (1992) The effect of dry heating on the chemistry, surface-area, and oxalate solubility of synthetic 2-line and 6-line ferrihydrites. *Clay Minerals* 27 (4): 397-412.
- Strawn D.G., Scheidegger A.M. and Sparks D.L. (1998) Kinetics and mechanisms of Pb(II) sorption and desorption at the aluminum oxide water interface. *Environmental Science and Technology* 32 (17): 2596-2601.
- Swift G. (2002) Acrylic (and Methacrylic) Acid Polymers. In: *Encyclopedia of Polymer Science and Technology*; John Wiley & Sons, New York.
- Tanaka H., Matsumura M. and Veliky I.A. (1984) Diffusion characteristics of substrates in Ca-alginate beads. *Biotechnology and Bioengineering* 26: 53-58.
- Technicon Instruments Co. Ltd. (1987) *Technicon TrAAcs 800; Industrial Method No: 333-86E*.
- Towe K.M. and Bradley W.F. (1967) Mineralogical constitution of colloidal "hydrous ferric oxides". *Journal of Colloid and Interface Science* 24: 384-392.
- Trivedi P. and Axe L. (1999) A comparison of strontium sorption to hydrous aluminum, iron, and manganese oxides. *Journal of Colloid and Interface Science* 218 (2): 554-563.
- Trivedi P. and Axe L. (2000) Modeling Cd and Zn sorption to hydrous metal oxides. *Environmental Science and Technology* 34 (11): 2215-2223.

References

- Trivedi P. and Axe L. (2001a) Predicting divalent metal sorption to hydrous Al, Fe, and Mn oxides. *Environmental Science and Technology* 35 (9): 1779-1784.
- Trivedi P. and Axe L. (2001b) Ni and Zn sorption to amorphous versus crystalline iron oxides: Macroscopic studies. *Journal of Colloid and Interface Science* 244 (2): 221-229.
- Tuwiner S.B. (1962) *Diffusion and membrane technology*; Reinhold Publishing Cooperation, New York.
- Van Genuchten M.T. and Wierenga P.J. (1976) Mass transfer studies in sorbing porous media. 1. Analytical solutions. *Soil Science Society of America Journal* 40: 473-480.
- Van Genuchten M.T. and Dalton F.N. (1986) Models for simulating salt movement in aggregated field soils. *Geoderma* 38: 165-183.
- Van Ommen H.C. (1985) The mixing-cell concept applied to transport of non-reactive and reactive components in soils and groundwater. *Journal of Hydrology* 78 (3-4): 201-213.
- Villalobos M., Trotz M.A. and Leckie J.O. (2001) Surface complexation modeling of carbonate effects on the adsorption of Cr(VI), Pb(II), and U(VI) on goethite. *Environmental Science and Technology* 35 (19): 3849-3856.
- Waltham C.A. and Eick M.J. (2002) Kinetics of arsenic adsorption on goethite in the presence of sorbed silicic acid. *Soil Science Society of America Journal* 66 (3): 818-825.
- Waychunas G.A., Rea B.A., Fuller C.C. and Davis J.A. (1993) Surface-chemistry of ferrihydrite .1. EXAFS studies of the geometry of coprecipitated and adsorbed arsenate. *Geochimica et Cosmochimica Acta* 57 (10): 2251-2269.
- Westall J. and Hohl H. (1980) A comparison of electrostatic models for the oxide/solution interface. *Advances in Colloid and Interface Science* 12: 265-294
- Willett I.R., Chartes C.J. and Nguyen T.T. (1988) Migration of phosphate into aggregated particles of ferrihydrite. *Journal of Soil Science* 39 (2): 275-282.
- Zachara J.M., Girvin D.C., Schmidt R.L. and Resch C.T. (1987) Chromate adsorption on amorphous iron oxyhydroxide in the presence of major groundwater ions. *Environmental Science and Technology* 21 (6): 589-594.

Appendix 1. Proton sorption by calcium alginate beads

To measure proton sorption by alginate gel between pH 7 and 3.5, acid titrations were performed on alginate beads at different CaCl_2 concentrations. The results were used to validate the use of the Gapon ionexchange model and to fit the exchange constant.

Preparation of the beads

New alginate beads were prepared from 5% alginate solution, by dripping into a 0.2 M CaCl_2 solution. The average amount of gel solution per bead was 44.03 mg, containing 0.2187 mg alginate per bead. After gelation (approx. one hour), the gel beads were kept in 0.2 M CaCl_2 solution for at least 24 hours before rinsing and equilibration with the desired CaCl_2 concentration. During equilibration, the CaCl_2 solution was replaced by fresh solution several times. The final bead size ranged from 2.5 to 3 mm, depending on the CaCl_2 concentration they are kept in.

Ionexchange model

Ionexchange of protons against Ca-ions on the alginate sites was described by the Gapon equation (Chapter 3). The amount of protons bound (mol g^{-1} alginate) is described by:

$$\text{SH} = S_t \frac{K (\text{Ca}^{2+})^{-1/2} (\text{H}^+)}{1 + K (\text{Ca}^{2+})^{-1/2} (\text{H}^+)} \quad [\text{A1.1}]$$

in which (Ca^{2+}) and (H^+) are the activities of calcium and protons (mol L^{-1}), K is the exchange constant, and S_t is the site concentration (mol g^{-1} alginate).

S_t was estimated from the molecular weight of the alginate monomers ($M=198$), assuming that every uronate residue in alginate contains one sorption site, which gives $S_t = 5.05 \cdot 10^{-3} \text{ mol g}^{-1}$. The value of K was obtained from the titration results.

Titration

Acid titrations were performed by stepwise adding small volumes of HCl to 100 mL CaCl_2 solution containing an amount of beads. The pH was stepwise decreased from pH 7 to 3.5. After every addition, the solution with beads was stirred for 90 minutes before measuring the equilibrium pH. The number of beads and the concentration of the acid solution was varied between the experiments (Table A1), to maintain an almost constant Ca concentration and ionic strength during the

titrations. After every titration the calcium concentration in the batch was measured and the calcium activity was calculated using the Davies equation (Equation 3.5).

Blank titrations were performed with the same solutions, but without beads, and with 5 minutes between additions and measurements. The pH electrode was calibrated before every experiment with buffers at pH 4 and 7. The titrations were performed in an airtight container and N₂ gas was purged through the system to keep CO₂ out.

Table A1. Experimental conditions during acid-base titrations

no.	number of beads	HCl (mol L ⁻¹)	temperature (°C)	CaCl ₂ (mol L ⁻¹)	I (mol L ⁻¹)	Ca ²⁺ activity (mol L ⁻¹)
1	825	0.020	20.6	0.0098	0.029	0.0051
2	250	0.010	20.9	0.0045	0.014	0.0028
3	240	0.005	20.1	0.0021	0.0064	0.0015
4	100	0.005	20.9	0.00094	0.0028	0.00074

Results

The proton activities that were measured during blank titrations were plotted against the added amount of protons divided by the solution volume, to obtain the activity correction factor from the slope. The resulting factor was then used to calculate the proton concentration from the pH for every step of the bead titration. Proton sorption by the beads was calculated from the difference between the added amount of protons and the amount measured in solution. The sorbed amount at the beginning of the titration (pH 6-7) was assumed zero. The results are plotted against the proton activity in Figure 3.1 (Chapter 3). The figure also shows the sorption curves calculated with the Gapon model. The exchange constant K was visually fitted to the sorption data of all four experiments, resulting in K=25.

Appendix 2. Derivation of multicomponent diffusion equation

To remain electrical neutrality throughout the solution during diffusion, different ions have to diffuse simultaneously. Movement of cations in one direction requires movement of anions in opposite direction or movement of cations in the same direction. In case of co-diffusion of a cation and an anion, the faster ion will drag the slower ion with it, and conversely the faster ion will be slowed down by an electrostatic potential, until the movement of the two ions is the same (Tuwiner, 1962). The slightest deviation from electroneutrality results in a very strong electric field which prevents further accumulation of net charge (Helfferich, 1962).

The total force acting upon the ions is caused by the composite of the chemical potential caused by a concentration gradient and the electric potential. The resulting flux (J_i in $\text{mol m}^{-2}\text{s}^{-1}$) can be described with the Nernst-Planck equation:

$$J_i = -D_i \frac{dC_i}{dx} - D_i z_i C_i \frac{F}{RT} \frac{dE}{dx} \quad [\text{A2.1}]$$

In case of anions, z has a negative value and the electrostatic force works in the same direction as the potential increases. In case of cations, z is positive and the force acts in the opposite direction of the increasing potential. The Nernst-Planck equation was derived for ideal solutions, in which the effects of activity coefficients were not included. The equation applies whenever an electric field exists, either externally generated or by diffusion of ions (Helfferich, 1962).

If we allow no separation of electric charge during diffusion, the sum of equivalent fluxes should be zero:

$$\sum_j z_j J_j = 0 \quad [\text{A2.2}]$$

If we combine Equation A2.1 and Equation A2.2 we find for the electrical gradient (Aguilella et al., 1987):

$$\frac{dE}{dx} = - \frac{\sum_j D_j z_j \frac{dC_j}{dx}}{\sum_j D_j z_j^2 C_j} \frac{RT}{F} \quad [\text{A2.3}]$$

Appendix 2

Substitution of Equation A2.3 for dE/dx into Equation A2.1 results in a flux expressed solely as a function of concentration gradients (Aguilella et al., 1987):

$$J_i = -D_i \frac{dC_i}{dx} + D_i z_i C_i \frac{\sum_j D_j z_j \frac{dC_j}{dx}}{\sum_j D_j z_j^2 C_j} \quad [\text{A2.4}]$$

Summary

The mobility of contaminants in soil is an important factor in determining their ability to spread into the wider environment. For non-volatile substances, transport within the soil is generally dominated by transport of dissolved fractions in the soil water phase, via either diffusion or convection. During this process the mobility of reactive ions is strongly affected by adsorption. Adsorption processes regulate the distribution of ions over an immobile fraction that is attached to soil particles and a mobile fraction that is present in the soil water phase, and therefore determine which fraction of ions is available for transport via the water phase.

In structured soil the conditions are more complex as water flow is not homogeneous. The flow of water is fast through cracks and macropores in between soil peds and aggregates, but at the same time a significant part of the soil water can be stagnant inside the smaller pores inside peds and aggregates. In order to reach adsorbing particles inside the peds and aggregates, ions have to diffuse through the smaller pores inside the aggregates or soil peds. Depending on the size of the aggregates, this can cause a significant delay in sorption and a marked different behaviour from the instantaneous equilibrium assumption that is usually adhered to for homogeneous systems. The effect this has on ion transport is referred to as physical nonequilibrium.

Adsorption of ions onto charged surfaces in soil is a complex process. Soils are multicomponent systems in which the behaviour of contaminant ions is influenced by other ions, for example through competitive sorption. Recent developments in surface complexation models start to become increasingly successful in accounting for competitive effects during sorption.

This thesis addresses the combination of multicomponent chemistry, diffusion-limited sorption and transport. Transport and sorption processes were studied in flow experiments with well-defined artificial model systems and by computer modelling. The modelling was stepwise validated against experimental results. An artificial flow system was developed in the first part of this thesis by gradually increasing the complexity of the system from non-reactive transport to multicomponent reactive transport. The model progressed accordingly by including the relevant sorption models into the transport model. The model simulations were then used to evaluate the effects of multicomponent chemistry on transport.

The initial flow system was prepared from a column filled with spherical gel beads made from alginate gel. The gel acts as a stagnant water phase, in which ions can

Summary

only move by diffusion. Transport through the column with gel beads was modelled with a two-region transport model. An immobile region represented the solution inside the beads and an immobile region represented the flowing solution in between the beads. Ion transport was modelled by convection in the mobile region and by diffusion in the immobile region. First, diffusion of nitrate and phosphate out of the gel beads was measured in a batch system. The model predicted the release of ions from the gel beads accurately using reported diffusion coefficients for diffusion of the ions in water. Leaching of nitrate through a bead filled column was measured at different flow rates. The concentration in the effluent was plotted against time to give breakthrough curves. The breakthrough curves predicted by the model matched the measurements accurately.

The next experiments evaluated proton transport through a column with alginate gel beads. Proton sorption on alginate occurs by ion-exchange with the calcium ions that cross-link the alginate polymer structure. The sorption parameters were measured separately in acid-base titrations of the gel at different calcium levels. The ion-exchange model was incorporated in the two-region transport model. The combined model described the proton leaching curves at different calcium concentrations very well. The results showed the combined effects of nonlinear sorption and competition, which added to the effects of physical nonequilibrium.

The third set of experiments considered sulphate and chromate sorption and transport in a column with goethite. Column experiments were performed with goethite embedded in polyacrylamide gel beads. The two-region transport model was combined with a surface complexation model to predict reactive transport in the goethite-gel bead system. Chromate and sulphate breakthrough curves were measured in a set of transport experiments, along with corresponding changes in the effluent pH. Model parameters for the surface complexation model were obtained from literature data and sorption measurements. The model predicted the breakthrough curves well for transport of chromate and sulphate in separate column experiments. However, the model overestimated the pH changes in the effluent, possibly because of proton buffering by the polyacrylamide gel. The effect of competitive sorption on transport was examined in experiments with both anions present. The model predicted the effect of competition very well in a system initially equilibrated with sulphate, followed by infiltration with chromate. However, when sulphate was infiltrated after equilibration with chromate, chromate desorption and sulphate adsorption were clearly underestimated by the transport model. The exchange between the more strongly bound chromate and the

sulphate added subsequently may be too slow to cause a substantial chromate peak in the effluent.

The second part of the thesis applied multicomponent chemistry and transport modelling to strontium sorption in microscopic aggregates of hydrous ferric oxide (HFO). Previous studies found that it takes days to months to reach equilibrium sorption probably due to slow diffusion into the porous particles. A novel mechanistic approach was suggested to explain slow diffusion into the small aggregates. A model was developed that relates diffusion to the electrostatic potential inside the aggregate pores. At pH values below 8, the surfaces are positively charged which causes an electrostatic potential that stretches across the whole pore diameter. Positively charged ions such as strontium are repulsed and remain at very low concentrations in the pore space. Here a Donnan electrostatic model was used to calculate the electrostatic potential inside the pores based on the assumption that the potential gradients in the small pores are overlapping. The electrostatic model is directly linked to the surface complexation model (CD-MUSIC) that describes the surface charge dependent on protonation of the surface groups and adsorption of counter ions and strontium. Strontium sorption is pH-dependent and in its turn influences the local pH inside the aggregates by causing desorption of protons from the oxide surface. Therefore the model accounts for sorption and diffusion of both ions. Diffusion is calculated from the local concentrations and electrostatic gradient in the pores using the Nernst-Planck diffusion equation. The diffusion flux of strontium is small at the low concentrations in the pores. The time it takes to reach equilibrium is strongly dependent on pH which determines the amount of strontium sorption, but above all, the mineral charge and the repulsion from the pores. The Donnan-diffusion model was compared with non-electrostatic pore diffusion, which does not take electrostatic interactions into account. The Donnan model predicts very low concentrations of strontium in the pores and diffusion rates that are up to 8000 times lower than predicted with a non-electrostatic model.

The Donnan-diffusion model was validated against strontium transport in a column of hydrous ferric oxide. Microscopic aggregates of hydrous ferric oxide (230 nm) were prepared by freezing and thawing ferrihydrite. The resulting aggregates have pores with a number-average size of 2 nm and a size distribution ranging from 1 to 12 nm. The surface complexation parameters were assessed by acid-base titrations and strontium sorption experiments. Strontium transport in the columns was measured at pH 4 and 7. The Sr breakthrough curves showed that sorption was virtually instantaneous on part of the hydrous ferric oxide. Instantaneous sorption

Summary

was explained by unrestrained diffusion in the largest pore fraction of the aggregate pores. The accessible pore fraction was determined by salt pulses and was found to be dependent on pH. Taking the fast accessible pore fraction into account in the transport simulations, the model matched the experimental breakthrough curves well at both pH values.

This thesis demonstrates that the combination of multicomponent chemistry, diffusion-limited sorption and transport can be modelled by combining mechanistic process descriptions. There were often more influencing factors than initially anticipated, even in relatively simple systems. Nevertheless, mechanistic modelling provides valuable insights into the processes that are involved in multicomponent transport in soil systems.

Samenvatting

De mobiliteit van stoffen in de bodem bepaalt in belangrijke mate hoe deze zich in geval van bodemverontreiniging in het milieu kunnen verspreiden. Voor niet-vluchtige stoffen, vindt verspreiding in de bodem voornamelijk plaats door transport van opgeloste fracties in de waterfase, via diffusie dan wel convectie. In dit proces wordt de mobiliteit van stoffen sterk bepaald door de concentraties in de waterfase en door de verdeling van een stof over de mobiele waterfase en een immobiele fractie die aan bodemdeeltjes is gebonden. Voor reactieve stoffen wordt deze verdeling in het algemeen bepaald door niet-lineaire adsorptieprocessen. Hierdoor spelen adsorptieprocessen dus een cruciale rol bij mobiliteit van stoffen in de bodem.

In gestructureerde bodems, waar de stroming van het water niet homogeen is, ontstaan locale verschillen in chemische en fysische condities (heterogeniteit). De stroming van water is sneller via krimpscheuren en macroporiën tussen de bodemklompen en aggregaten. Tegelijkertijd kan een significant deel van het bodemwater voorkomen als stagnant water binnenin de kleinere poriën in de aggregaten waar de meeste adsorberende oppervlakken aanwezig zijn. Om adsorberende oppervlakken te bereiken, moeten ionen dan via de kleinere poriën de aggregaten in diffunderen. Afhankelijk van de grootte van de aggregaten kan dit al snel een significante vertraging in adsorptie veroorzaken en een duidelijk verschillend gedrag veroorzaken ten opzichte van de veronderstelling van adsorptie-evenwicht die normaal gesproken voor homogene systemen gehanteerd. Het effect dat dit heeft op ionentransport wordt ook wel physical nonequilibrium (fysisch niet-evenwicht) genoemd.

Adsorptie van ionen aan geladen oppervlakken is een complex proces. Bodems zijn multicomponent systemen waarin het gedrag van ionen worden beïnvloed door andere ionen, bijvoorbeeld door competitieve adsorptie. Recent ontwikkelde oppervlakte-complexatiemodellen worden steeds beter in het beschrijven van deze competitieve effecten tijdens adsorptie. Dit proefschrift behandelt de combinatie van multicomponent chemie, diffusiegelimiteerde adsorptie en transport. De processen met betrekking tot transport en adsorptie werden bestudeerd in kolomexperimenten met goed gedefinieerde (kunstmatige model) systemen, en met computermodellen. Deze modellen werden stapsgewijs gevalideerd aan de hand van experimenten. In het eerste gedeelte van dit proefschrift werd een kunstmatig experimenteel kolomsysteem ontwikkeld, waarbij de complexiteit van het systeem geleidelijk aan werd opgebouwd, van niet-reactief transport tot multicomponent

reactief transport. Het model werd evenzo stapsgewijs ontwikkeld door het transportmodel uit te breiden met de relevante adsorptiemodellen. De modelsimulaties werden daarna gebruikt om de effecten van multicomponent chemie op transport te bepalen.

Het eerste proefsysteem werd gemaakt van een kolom gevuld met bolletjes van alginate gel. De gel fungeert als een stagnante waterfase waarin ionen zich alleen door diffusie kunnen verplaatsten. Transport door de kolom met gel bolletjes werd gemodelleerd met het twee-zone transport model: Een immobiele zone stelt de oplossing in de bolletjes voor en een mobiele zone stelt de oplossing voor die tussen de bolletjes stroomt. Ionentransport werd gemodelleerd door convectie in de mobiele zone en door diffusie in de immobiele zone. Om te beginnen werd de diffusie van nitraat en fosfaat uit de bolletjes gemeten in een batchsysteem. Het model voorspelt het vrijkomen van ionen uit de gelbolletjes nauwkeurig met behulp van de diffusiecoëfficiënten voor diffusie van de ionen in water. Uitspoeling van nitraat uit een met bolletjes gevulde kolom werd gemeten bij verschillende stroomsnelheden. De doorbraakcurven werden verkregen door het uitzetten van de concentratie in het effluent tegen de tijd. De door het model voorspelde doorbraakcurven toonden een goede gelijkensis met de gemeten curven.

In de daaropvolgende experimenten werd het transport van protonen door een kolom met alginate bolletjes bestudeerd. Proton adsorptie aan alginate vindt plaats door ionenwisseling met de calciumionen die de polymeerstructuur van het alginate verbinden (cross-linkage). De adsorptieparameters werden onafhankelijk gemeten in zuur-base titraties van de gel bij verschillende calciumniveaus. Het transportmodel werd gecombineerd met het ionenwisselingsmodel. Het gecombineerde model beschrijft de uitspoelingscurven van de protonen bij verschillende calciumconcentraties erg goed. Het resultaat laat de gecombineerde effecten van niet-lineair adsorptie en competitie zien die bijdragen aan het effect van fysisch niet-evenwicht.

De derde set van experimenten richtte zich op adsorptie en transport van sulfaat en chromaat in een kolom met goethiet. Kolomexperimenten werden uitgevoerd met goethiet dat met polyacrylamide was vermengd tot gelbolletjes. Het twee-zone transport model werd gecombineerd met een oppervlaktecomplexatiemodel (CD-MUSIC) om reactief transport in het systeem met goethiet en gelbolletjes te voorspellen. De doorbraakcurven van chromaat en sulfaat werden gemeten in een set van transportexperimenten, samen met de overeenkomstige veranderingen van de pH in het effluent. Modelparameters voor het oppervlaktecomplexatiemodel werden verkregen van literatuurgegevens en adsorptiemetingen. Het model gaf een

goede voorspelling van de doorbraakcurven voor chromaat en sulfaat in twee onafhankelijke kolomexperimenten. Het model voorspelt te hoge veranderingen van de pH in het effluent, mogelijk door protonbuffering door de polyacrylamide gel. Het effect van competitieve adsorptie op transport werd bestudeerd in experimenten waarbij beide anionen aanwezig waren. Het model voorspelde het effect van competitie erg goed in een systeem dat eerst met sulfaat op evenwicht werd gebracht en daarna met chromaat werd geïnfiltreerd. Maar chromaat desorptie en sulfaat adsorptie werden duidelijk onderschat in een systeem dat met chromaat op evenwicht werd gebracht en daarna met sulfaat werd geïnfiltreerd. Uitwisseling tussen het sterker gebonden chromaat en het sulfaat dat later werd toegevoegd is mogelijk te langzaam om een duidelijke chromaatpiek te veroorzaken in het effluent.

Het tweede deel van het proefschrift past multicomponent chemie en transport modellering toe op de adsorptie van strontium in microaggregaten van HFO (hydrous ferric oxide). Eerdere studies ondervonden dat het dagen tot maanden duurt voor het adsorptie maximum is bereikt, waarschijnlijk door langzame diffusie het poreuze deeltje in. Een nieuwe methode werd voorgesteld om langzame diffusie in oxidedeeltjes mechanistisch te verklaren. Een model werd ontwikkeld dat de diffusie relateert aan de elektrostatische potentiaal in de poriën van het aggregaat. Bij een pH lager dan pH 8 zijn de oppervlakken van het oxide positief geladen. Dit veroorzaakt een elektrostatische potentiaal die zich over het gehele volume van de porie uitstrekt. Positief geladen ionen zoals strontium worden afgestoten en verblijven daardoor met een heel lage concentratie in het poriewater. We gebruikten we het Donnan-model om de elektrostatische potentiaal in de poriën te berekenen, ervan uitgaande dat de potentiaalgradiënten in de poriën elkaar overlappen en dat de potentiaal daardoor bij benadering constant is over de gehele poriebreedte. Het elektrostatische model is direct gebonden aan het oppervlakte-complexatiemodel (CD-MUSIC) dat de oppervlaktelading van het oxide beschrijft als functie van de protonatie van de oppervlaktegroepen en de adsorptie van strontium- en zoutionen. Adsorptie van strontium is afhankelijk van de pH en beïnvloedt op zijn beurt de lokale pH binnen in de aggregaten door desorptie van protonen te veroorzaken. Daarom neemt het model adsorptie en diffusie van beide ionen in beschouwing. Diffusie werd berekend van de lokale concentratie en van de elektrostatische gradiënt met behulp van de Nernst-Planck diffusievergelijking. De diffusieflux van strontium is laag bij een lage concentratie in de poriën. De tijd die het kost om evenwicht te bereiken is sterk afhankelijk van de pH (die de strontiumsorptie bepaalt) maar bovendien van de oppervlaktelading van het oxide en de mate van afstoting uit de poriën. Het Donnan-diffusiemodel werd vergeleken

Samenvatting

met een model voor diffusie in poriën dat geen elektrostatistische interacties in beschouwing neemt. Het Donnan-model voorspelde erg lage concentraties van strontium in de poriën en diffusiesnelheden die tot 800 keer lager zijn dan voorspeld met het niet-elektrostatistische model.

Het Donnan-diffusie model werd gevalideerd met metingen van strontiumtransport in een kolom met HFO. Microscopische aggregaten van HFO (230 nm diameter) werden bereid door vriezen en ontdooien van een ferrihydriet suspensie. De resulterende aggregaten hebben poriën met een gemiddelde grootte van 2 nm en een grootte verdeling van 1 tot 12 nm. De oppervlaktecomplexatieparameters werden bepaald door zuurbasis titraties en strontium adsorptie experimenten. Strontium transport in de kolom werd gemeten bij pH 4 en 7. De doorbraakcurven van het strontium lieten zien dat adsorptie aan een deel van het HFO ogenschijnlijk meteen plaats vindt. Instantane adsorptie werd verklaard door ongehinderde diffusie in een fractie grotere poriën. De poriefraction die meteen toegankelijk is voor adsorptie bleek afhankelijk van de pH en werd daarom bepaald door kolomexperimenten met zoutpulsen bij verschillende pH's. Door in de transportsimulaties rekening te houden met de snel toegankelijke poriefraction kon het model de experimentele doorbraakcurven goed beschrijven bij beide pH waarden.

Dit proefschrift laat zien dat de combinatie van multicomponentchemie, diffusiegeïmiteerde adsorptie en transport gemodelleerd kan worden door het combineren van de mechanistische procesbeschrijvingen. Zelfs in relatief simpele systemen waren er vaak meerdere beïnvloedende factoren dan eerst verwacht werd. Desondanks gaf de mechanistische aanpak waardevolle inzichten in de processen die betrokken zijn bij multicomponenttransport in bodemsystemen.

Curriculum Vitae

Gerdientje Wendelmoet (Wendy) van Beinum werd op 27 augustus 1972 geboren te Groenlo in de Achterhoek (GLD). In 1988 behaalde zij haar MAVO diploma aan de Wilhelmina MAVO te Eibergen. Vervolgens behaalde zij in 1990 haar HAVO diploma en in 1992 haar VWO diploma aan het Marianum te Groenlo. Van 1992 tot september 1997 studeerde ze Milieuhygiëne aan Wageningen Universiteit met als specialisatie Bodemkwaliteit. De studie werd afgerond met een stage bij het Macaulay Instituut in Aberdeen (Schotland). Na haar afstuderen keerde Wendy terug naar het Macaulay Instituut waar ze van januari 1998 tot november 2002 onderzoek deed naar het modelleren van adsorptie en transport van opgeloste stoffen in de bodem. In januari 2007 is dit promotieonderzoek afgerond met de verdediging van dit proefschrift.

Van november 2002 tot november 2004 was Wendy werkzaam aan Cranfield University in Silsoe, Engeland. Daar deed zij onderzoek naar adsorptie en afbraak van bestrijdingsmiddelen in de bodem. Sinds november 2004 is zij werkzaam bij het Central Science Laboratory in York, waar zij onderzoek doet naar het gedrag van bestrijdingsmiddelen in de bodem en het modelleren van transport ten behoeve van de risicobeoordeling van bestrijdingsmiddelen in het milieu.

Publications

Transport of ions in physically heterogeneous systems; convection and diffusion in a column filled with alginate gel beads, predicted by a two-region model. *W. van Beinum, J.C.L. Meeussen, A.C. Edwards, W.H. van Riemsdijk*. Water Research 34 (2000), Issue 7, pp. 2043-2050.

Modeling transport of protons and calcium ions in an alginate gel bead system: The effects of physical nonequilibrium and nonlinear competitive sorption. *W. van Beinum, J.C.L. Meeussen, W.H. van Riemsdijk*. Environmental Science and Technology 34 (2000), Issue 23, pp. 4902-4907.

Diffusion-limited Sr sorption by hydrous ferric oxide aggregates: Influence of pore sizes. *A. Hofmann, W. van Beinum, J.C.L. Meeussen, R. Kretzschmar*. Geochimica et Cosmochimica Acta 68 (2004), Issue 11, Supplement 1, pp. A223-A223.

Sorption kinetics of strontium in porous hydrous ferric oxide aggregates I. The Donnan diffusion model. *W. van Beinum, A. Hofmann, J.C.L. Meeussen, R. Kretzschmar*. Journal of Colloid and Interface Science 283 (2005), Issue 1, pp. 18-28.

- Sorption kinetics of strontium in porous hydrous ferric oxide aggregates II. Comparison of experimental results and model predictions. *A. Hofmann, W. van Beinum, J.C.L. Meeussen, R. Kretzschmar*. *Journal of Colloid and Interface Science* 283 (2005), Issue 1, pp. 29-40.
- Influence of kinetic sorption and diffusion on pesticide movement through aggregated soils. *S. Beulke, C.D. Brown, C.J. Fryer and W. van Beinum*. *Chemosphere* 57 (2004), pp. 481-490.
- Determination of time-dependent partition coefficients for several pesticides using diffusion theory. *F.G. Renaud, P.B. Leeds-Harrison, C.D. Brown, W. van Beinum*. *Chemosphere* 57 (2004), pp. 1525-1535.
- Evaluation of simplifying assumptions on pesticide degradation in soil. *S. Beulke, W. van Beinum, C.D. Brown, M. Mitchell, A. Walker*. *Journal of Environmental Quality* 34 (2005), pp 1933-1943.
- Pesticide sorption and diffusion in natural clay loam aggregates. *W. van Beinum, S. Beulke, C.D. Brown*. *Journal of Agriculture and Food Chemistry* 53 (2005), pp 9146-9154.
- Pesticide sorption and desorption by lignin described by an intra-particle diffusion model. *W. van Beinum, S. Beulke, C.D. Brown*. *Environmental Science and Technology* 40 (2006), pp 494-500.
- Verification and intercomparison of reactive transport codes to describe root-uptake. *B. Nowack, K. U. Mayer, S. E. Oswald, W. van Beinum, C. A. J. Appelo, D. Jacques, P. Seuntjens, F. Gérard, B. Jaillard, A. Schnepf, T. Roose*. *Plant Soil* 285 (2006), pp 305–321
- Competitive sorption and diffusion of chromate and sulphate in a flow system with goethite in gel beads. *W. van Beinum, J.C.L. Meeussen, W.H. van Riemsdijk*. *Journal of Contaminant Hydrology* 86 (2006) pp 262-278.
- Lysimeter experiment to investigate the influence of diffusion-limited sorption on pesticide availability for leaching. *W. van Beinum, S. Beulke, C.J. Fryer, C.D. Brown*. *Journal of Agriculture and Food Chemistry* 54 (2006), pp 9152 -9159.

Final word

It has been nine years since I arrived in Aberdeen as a fresh postgraduate. I quickly felt at home at the Macaulay Institute. The staff were really friendly and always willing to help out when I was looking for equipment or advice. We also had a lot of fun. There was a large group of chummy national and international students and there was always a ceilidh to visit or a hill to climb.

The research kicked off well too. I was excited about the early version of ORCHESTRA and both Hans and I were very pleased that we could model the first lab results so well. In fact, the model matched the data so well that I had to convince people that the data in my graphs were real lab data! But when the work progressed, the lab work became more challenging and the gel beads did not always behave as expected. But nothing could spoil Hans' optimism and we always found an answer.

Jeanine arrived in our team not long after I started and with her and David we formed a little group of ORCHESTRA enthusiasts. Jeanine kept me going with her bicycle repair skills and reliable supply of biscuits and advice, and we became good friends. The collaboration with Annette was a welcome variation from the work with the gel beads. It was exiting to see how the modelling in ORCHESTRA could be used to describe more realistic systems. I enjoyed working with Annette and the way we managed to communicate our ideas by email, often with many equations and diagrams.

After almost 5 years of working with the lovely Macaulay people my time had come to say goodbye. With my laptop, suitcase and bicycle on the train I set off for my new job at Cranfield University. Even though pesticide behaviour in soil was a new area for me, the work with gel beads and ORCHESTRA turned out to be very useful. Little by little I continued writing the last parts of this thesis and, thanks to my great colleagues Sabine and Colin, I managed to find the time to do so.

I would like to thank the many people who have given me help or advice along the way. Willem, thank you for your valuable ideas and advice. Thank you, Hans, for passing on your enthusiasm for modelling and for the many opportunities you have given me to develop my skills. Thanks also to everybody else who made the time in Aberdeen such a great experience. And finally many thanks to everyone who has encouraged me to complete!

This research was funded by the Macaulay Development Trust
Printer: Ponsen en Looijen BV Wageningen
Cover design: Ponsen en Looijen BV Wageningen

